Local Buckling of Steel Multi-Sided Tube Sections

Zannatul Mawa Dalia

A Thesis in
The Department of
Building, Civil and Environmental Engineering

Presented in Partial Fulfillment of the Requirements
for the Degree of Master of Applied Science (Civil Engineering)
at Concordia University, Montreal, Quebec, Canada

July 2020

CONCORDIA UNIVERSITY

School of Graduate Studies

This is to certify that the thesis prepared

By: Zannatul Mawa Dalia

Entitled: Local Buckling of Steel Multi-Sided Tube Sections

and submitted in partial fulfillment of the requirements for the degree of

Master of Applied Science (Civil Engineering)

complies with the regulations of the University and meets the accepted standards with respect to originality and quality.

Signed by the final Examining Committee:

Dr. Lucia Tirca	Chair
Dr. Akshay Kumar Rathore	Examiner External (to program)
Dr. Emre Erkmen	Examiner
Dr. Anjan Bhowmick	Supervisor

Approved by Dr. Michelle Nokken, GPD
Department of Building, Civil and Environmental Engineering

Dr. Mourad Debbabi, Interim Dean
Gina Cody School of Engineering and Computer Science

Date

Abstract

Local Buckling of Steel Multi-Sided Tube Sections

Zannatul Mawa Dalia

Multi-sided steel tubular sections are commonly used in many structures such as road side light posts, road signposts, transmission and telecommunication towers, etc. These sections are generally subjected to axial compression, pure bending, combined bending and compression, or torsion. From the design point of view, it is very important to make sure that these thin-walled sections do not buckle locally before reaching their capacity. Current AASHTO 2015 standard for Structural Supports for Highway Signs, Luminaires, and Traffic Signals provides width-thickness limits to check for local buckling of Octagonal (8-sides), Dodecagonal (12-sides) and Hexadecagonal (16-sides) steel tube sections when they are subjected to axial compression and bending. The new Canadian steel standard, CAN/CSA S16-19 has recently adopted the same slenderness limit for compact multi-sided tube sections as suggested in AASHTO. While AASHTO recommends the same width-thickness limit for all the three multi-sided sections when they are compact, the requirements for non-compact sections are different for different sections. ASCE/SEI 48-11 provides limits for the non-compact sections, which are very close to the non-compact limits of AASHTO. Although many structures now use these multi-sided sections, no study has been conducted to evaluate AASHTO slenderness limits of these thin-walled sections. In addition, no study is currently available on local buckling of multi-sided sections subjected to bending and axial compression. Thus, a detailed study is required to investigate the local buckling behavior of multi-sided steel tube sections and evaluate these limits. This thesis presents a finite element (FE) analysis based study of local buckling of multi-sided steel tubular

sections. A nonlinear finite element model is developed for this study and validated against experimental results from stub column tests of 8, 12, and 16-sided cross-sections. The FE model is further validated against experimental test results of 16-sided cross-sections subjected to pure bending. The validated FE model is then used to analyze a series of multi-sided steel tubular sections subjected to axial compression, pure bending, combined bending and compression, and pure torsion. Three different geometry, namely, eight, twelve, and sixteen-sided polygonal sections are considered. FE analyses show that AASHTO provided compact limit for members under flexure might need to be revised. However, AASHTO provided non-compact limits are quite relaxed for the sections subjected to pure bending. Based on FE results, revised compact and non-compact limits have been proposed for Octagonal, Dodecagonal, and Hexadecagonal sections subjected to flexure. Moreover, FE analyses indicate that the non-compact limit of the Hexadecagonal section can also be used for the other two sections under axial compression. Furthermore, FE results are used to evaluate capacity equations provided in different standards (*i.e.,* AASHTO, ASCE/SEI 48-11, Eurocode 3, and EN 50341-1) for multi-sided tubes subjected to different loading conditions. FE analyses show that while AASHTO provides a pretty good prediction for the Octagonal and Dodecagonal sections under combined bending and compression, it overestimates the capacities of several selected Hexadecagonal sections. It is also observed that torsional capacities for the Octagonal and Dodecagonal sections are predicted well for the compact sections in AASHTO and ASCE/SEI 48-11 and for a large number of selected Hexadecagonal compact sections, both codes are predicting higher torsional resistance.

ACKNOWLEDGMENTS

It is a great pleasure to express my gratitude to numerous people who helped me in many ways throughout these two years to complete my degree. Without their help and assistance, it would have been impossible to complete my thesis.

First and foremost, praises and thanks to the Almighty God, for His showers of blessings upon me, the strength, peace of mind, and good health in order to finish my research.

I would like to express my deep and sincere gratitude to my supervisor Dr. Anjan Bhowmick for giving me the opportunity to do this research and providing invaluable guidance and support throughout this research. It has been a privilege and honor to work with him and learn so many things from him. Besides, I am extremely grateful to Gina Cody School of Engineering and Computer Science, Concordia University, Montreal, Canada and the Natural Sciences and Engineering Research Council of Canada for funding this research project. I would gratefully acknowledge Dr. Gilbert Y. Grondin for his valuable suggestions in this research.

Special thanks go to my colleagues and friends, especially Farhan Ahmed Chowdhury, Saikat Bagchi, and Masoud Mohammadzadeh, for their support and encouragement during my studies.

I am extremely thankful to my parents, my sister, and my in-law's family, for their immense support, sacrifice, and lifelong encouragement to accomplish many of my academic and personal goals. Finally, I would like to thank my husband, Faruk Ahmed Sakib, who is always by my side when I needed him the most and helped me a lot in doing my research.

CONTENTS

LIST OF FIGURES

LIST OF TABLES

List of Symbols

A	Cross-sectional Area
A_{EFF}	Effective Cross-sectional Area
A_g	Gross Cross-sectional Area
B	Moment Magnification Factor
b	Element Width of Multi-sided Tube According to AASHTO
b'	Width of Mid-surface of Multi-sided Tubes
b_{eff}	Effective Element Width
C_t	Torsional Constant
c	Distance from Neutral Axis to Extreme Fiber
c_x	Distance from Y–Y Axis to Point Where Stress is Checked
c_y	Distance from X–X Axis to Point Where Stress is Checked
D	Mid-surface Distance from Flat Side to Flat Side of Multi-sided Tubes
D'	Outside Distance from Flat Side to Flat Side of Multi-Sided Tubes
D"	Flexural Rigidity
E	Modulus of Elasticity
F_{cr}	Critical Buckling Stress
F_e	Euler Stress
F_{nt}	Nominal Torsional Stress
F_t	Tensile Stress Permitted
F_y	Yield Stress
F_u	Ultimate Stress
f	Buckling Stress

H	Plate Buckling Co-efficient for Shear Stress
I	Moment of Inertia
I_x	Moment of Inertia about X–X Axis
I_y	Moment of Inertia about Y–Y Axis
J	Torsional Constant of Cross-Section
K	Effective Length Factor
k	Plate Buckling Co-efficient
K_p	Shape Factor
k_t	Stress Concentration Factor
L	Member Length
M_{cr}	Critical Bending Moment
M_y	Yield Moment
M_n	Nominal Bending Strength
M_p	Plastic Moment
M_r	Factored Flexural Resistance
M_u	Factored Bending Moment
M_x	Bending Moment about X–X Axis
$M_{y'}$	Bending Moment about Y–Y Axis
n	Number of Sides of Multi-sided Tube
n'	Ratio of the Inside-Corner Radius to Wall Thickness
P_{cr}	Critical Compressive Strength
P_e	Euler Elastic Buckling Capacity
P_{nc}	Nominal Compressive Strength

P_r	Minimum nominal compressive strength or tensile strength
P_u	Factored Axial Load
Q	Local Buckling Adjustment Factor
Q'	Moment of Section about Neutral Axis
R	Plate Width-Thickness Parameter
R'	Radius Measured to the Mid-thickness of the wall
r	Radius of Gyration
r_b	Inside Bend Radius
S	Elastic Section Modulus
S_{eff}	Effective Section Modulus
T_n	Nominal Torsion Strength
T_r	Factored Torsional Resistance
T_u	Factored Torque
t	Wall Thickness
V_r	Factored Shear Resistance
V_u	Factored Shear
w	Flat Width of Multi-sided Tube
Z	Plastic Section Modulus
σ	Uniform Longitudinal Compressive Stress
σ_{cr}	Elastic Plate Buckling Stress
σ_{cyl}	Collapse Capacity of Cylinder
τ	Uniform Longitudinal Shear Stress
ν	Poison's Ratio

Θ	Bending Axis Angle
β	Circumradius over Thickness Ratio
λ	Width-Thickness Ratio
λ_p	Width-Thickness Ratio at Compact Limit
λ_r	Width-Thickness Ratio at Non-compact Limit
λ_{max}	Maximum Width-Thickness Ratio
ρ	Reduction Factor for Plate Buckling
ψ	Stress Ratio

List of Abbreviations

AASHTO	American Association of State Highway and Transportation Officials
ASCE	American Society of Civil Engineers
CSA	Canadian Standards Association
FE	Finite Element
FEA	Finite Element Analysis
GBT	Generalized Beam Theory
LPF	Load Proportionality Factor
LRFD	Load Resistance Factor Design
RCPS	Regular Convex Polygonal Sections
SEI	Structural Engineering Institute

Chapter 1 Introduction

1.1 General

Multi-sided tube sections are hollow sections having a polygonal cross-section. These thin-walled sections are used in many structures like overhead road signpost, light post, traffic signal, transmission pole, etc. Multi-sided poles are used to avoid land usage and to attain an unobtrusive appearance. They have become a popular form of construction due to having the freedom of designs for steel shapes. Figure 1.1 shows the use of multi-sided steel tube sections in various structures.

(a)

(b)

(c)

Figure 1.1: Use of multi-sided steel tubular sections as (a) Transmission Pole (https://www.novapole.com/product-details-86-dead-end-transmission-pole), (b) Light Post (https://www.ecvv.com/product/1000088796.html), and (c) Signpost (https://www.novapole.com/product-details-82-ferry-toll-booth-double-arm-sign-bridge)

Multi-sided tube sections may have a different number of sides. However, Octagonal (8-sides), Dodecagonal (12-sides), and Hexadecagonal (16-sides) steel tube sections are commonly used. Following Figure 1.2 shows the cross-section of Octagonal, Dodecagonal, and Hexadecagonal steel tube sections.

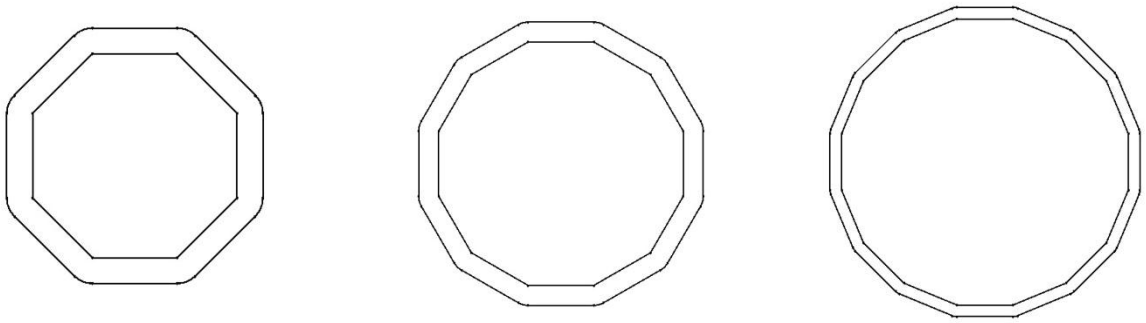

(a) (b) (c)

Figure 1.2: Cross-section of (a) Octagonal, (b) Dodecagonal and (c) Hexadecagonal steel tube section

Structures like overhead road signpost, light post, traffic signal post, transmission pole, etc. are generally subjected to axial compression, pure bending, combined bending and compression, or torsion. These thin-walled sections tend to buckle locally if proper width-thickness ratios are not maintained. Local buckling of multi-sided tube section must be prevented so that the member can reach its capacity. This will ensure the adequate service life of the structure.

There have been some studies on the local buckling behavior of multi-sided steel tube sections under various loading conditions. Wittrick and Curzon (1968) developed a "Stability Function" based theoretical method to establish criteria for local buckling analyses of polygonal tubular sections subjected to combined compression and torsion and reported the critical combination of compression and torsion for three and four-sided polygonal tube sections. Aoki et al. (1991) experimentally investigated the local buckling behavior of polygonal steel sections of four to eight sides under compression. Teng et al. (1999) studied the elastic local buckling behavior of columns having polygonal cross-sections (4- to 8- sided) under uniform axial compression or bending by using the finite strip method and reported plate buckling coefficients (k-values) for different slenderness ratios. Godat et al. (2012) conducted an experimental study to investigate elastoplastic local buckling behavior of thin-walled tubes having polygonal cross-sections (i.e., 8-, 12-, and 16-sided) under concentric compression. Critical local buckling stress has been observed for different plate width-thickness ratios. Bräutigam et al. (2017) experimentally and numerically investigated the bending behavior of sixteen (16) sided polygonal tubular steel sections under pure bending and combined bending and torsion. Their study indicated that bending moment capacity for the compact section could be more than the yield moment capacity.

Current AASHTO (AASHTO 2015) has provided width-thickness limits for eight, twelve, and sixteen-sided polygonal steel sections. In AASHTO, the width-thickness requirements for

compact sections for all three multi-sided sections subjected to bending are considered the same as that for flanges of rectangular HSS sections, which is $1.12\sqrt{\frac{E}{F_y}}$. The new Canadian steel standard, CAN/CSA S16-19 has also adopted the same slenderness limit for compact multi-sided tube sections as suggested in AASHTO. While AASHTO recommends the same width-thickness limit for all the three multi-sided sections when they are compact, the requirements for non-compact sections subjected to flexure are different for different sections, a recommendation not yet supported by any research. ASCE/SEI-48-11 provides design equations for local buckling capacities of eight, twelve, and sixteen-sided polygonal steel sections of the transmission line. Eurocode 3 (EN 1-1, 2005, EN 1-3, 2006, EN 1-5, 2006) has design equation for plate elements. A multi-sided steel tubular section can be considered as a collection of individual longitudinal plate strips to find the resistance using Eurocode 3.

1.2 Motivation of this research

The new Canadian steel standard, CAN/CSA S16-19 has adopted the same slenderness limit for compact multi-sided tube sections, as suggested in AASHTO (AASHTO 2015). Current AASHTO has recommended same compact limit for all three multi-sided sections (*i.e.* 8-, 12- and 16- sided) subjected to bending and considered same as that for flanges of rectangular HSS sections, which is $1.12\sqrt{\frac{E}{F_y}}$. However, the requirements for non-compact sections subjected to flexure are different for different sections. To the best of author's knowledge, no study has been conducted to evaluate the width-thickness limits in AAHSTO. Besides, current AASHTO does not provide any width-thickness limits for local buckling of multi-sided tube sections subjected to combined bending and compression. Multi-sided tube sections commonly subjected to combined bending and compression, it is extremely important to investigate whether the same

width-thickness limits as for bending can also be applied for combined bending and compression. Currently, no study is available for the behavior of multi-sided tube sections subjected to combined bending and compression and a very limited study is available on the behavior of sections under torsion.

1.3 Research objectives

The main objective of this research is to investigate the local buckling behavior of multi-sided steel tube sections under different loading conditions and to evaluate the slenderness limits provided in the existing standards. Towards this goal, the principal objectives of this research are as follows:

- To investigate the local buckling behavior of multi-sided steel tube sections (*i.e.,* eight (08), twelve (12), and sixteen (16) sided) subjected to axial compression, pure bending, combined bending and compression.
- To evaluate the width-thickness limits provided by AASHTO for compact and non-compact multi-sided tube sections.
- If required, to propose width-thickness limits for compact and non-compact multi-sided tube sections for different loading conditions.
- To evaluate the capacity equations provided in different standards (*i.e.,* AASHTO, ASCE/SEI-48-11, Eurocode 3, and EN 50341-1) for multi-sided tubes subjected to different loading conditions (axial compression, pure bending, combined bending and compression, and pure torsion).

1.4 Outline of the research

Chapter 1 presents a short background of multi-sided steel tube sections. The research need and research objectives are also briefly discussed in this chapter.

Chapter 2 presents the literature review conducted for this research. A detailed review of previous studies on local buckling of multi-sided steel tube sections is done in this chapter. It also presents the summary of the design provisions of multi-sided steel tube sections in different standards.

Chapter 3 presents the details of finite element modelling techniques. It also discusses the assumptions made in modelling. The selection of element type, mesh configuration, material properties, boundary conditions, and application of load have been discussed in detail. Moreover, it presents the validation of the finite element (FE) models against experimental test results available in the literature.

Chapter 4 discusses the local buckling behavior of the multi-sided tube under axial compression and pure bending. Details of the geometry selected for the FE models are presented in this chapter. Finally, this chapter presents the FE results of models subjected to axial compression and pure bending, along with the comparison of results with existing standards.

Chapter 5 presents the behavior of the multi-sided tube subjected to combined bending and compression and pure torsion. It consists of the FE results of models under combined bending and compression and pure torsion followed by the comparison of results with existing standards.

Chapter 6 concludes the thesis with a summary and presents conclusions accumulated throughout the whole study, along with recommendations for future studies.

Chapter 6 is followed by appendices, which include geometric property tables, calculation of yield moment and plastic moment capacity, FE results, and resistances according to different standards.

Chapter 2 Literature Review

2.1 Introduction

The strength of steel members may be compromised by buckling. There are two main modes of buckling failure of steel members (*i.e.*, local buckling and global buckling). Cross-sections of steel shapes can be made of number of thin plates. When the cross-section is subjected to large compression or shear, thin plates made up the cross-section may buckle before the member's full capacity is reached, if thin plates are too slender. This phenomenon of buckling is known as local buckling failure. On contrary, the member cross-section is not deformed in global buckling mode. The longitudinal axis of the member will be buckled or distorted in case of global buckling failure, whereas, longitudinal axis of the member will not be distorted in local buckling failure. Figure 2.1 shows the local and global buckling of structural steel shapes.

(a) Local buckling failure

(a) Global buckling failure

Figure 2.1: (a) Local buckling (https://www.bgstructuralengineering.com/BGSCM13/BGSCM006/stl6.jpg) and (b) Global buckling (http://www.ssrcweb.org/tag/volume-4/) failure mode of steel

This research only focuses on the local buckling behaviour of multi-sided steel tube sections. The literature review in this chapter consists of two main sections. A detailed review of previous studies on local buckling of multi-sided steel tube sections has been discussed in the next section 2.2, while section 2.3 presents the summary of multi-sided steel tube section design provisions in different standards. Finally, a summary of the literature review and the need for the research has been presented in section 2.4.

2.2 Review of studies on local buckling of multi-sided steel tube sections

The following subsections briefly discuss the basic plate buckling problem and existing studies on local buckling behavior of multi-sided steel tube sections subjected to different loading conditions.

Elastic buckling of plates under uniaxial compression

Bryan (1891) gave the solution to the most basic form of plate buckling problem, which is simply supported flat plate under uniaxial compression. The energy method was used to analyze the problem. It was assumed that the deflected surface of the buckled plate could be represented by a double Fourier series. However, Timoshenko used a different method to solve this plate buckling problem. He assumed that plate buckles in the form of several half sinusoidal waves in the direction of compression. The problem was discussed in some standard textbooks, such as Timoshenko and Gere (1961). The elastic plate buckling stress (σ_{cr}) is expressed as the following equation.

$$\sigma_{cr} = \frac{k\pi^2 E}{12(1-\nu^2)\left(\frac{b}{t}\right)^2} \quad (2.1)$$

where, k is the plate buckling coefficient determined by theoretical critical-load analysis and is a function of plate geometry and boundary conditions; E, ν, b and t are the modulus of elasticity, poison's ratio, plate width, and plate thickness, respectively. For the simply supported plate, a k value of 4.0 can be used. Apart from simply supported plates, several studies have been undertaken to find values of k for different geometry, loading, and support conditions.

Wittrick and Curzon (1968)

The authors developed a "Stability Function" based theoretical method to generate criteria for the local buckling analysis of polygonal tubular sections subjected to combined compression and torsion. For polygonal sections with three and four numbers of sides, a critical combination of compression and torsion was found, and interaction diagrams were developed. Results were presented in terms of plate buckling coefficient k and H for compressive and shear stress, respectively. k and H were defined as follows-

$$k = \frac{\sigma b^2 t}{\pi^2 D''} \tag{2.2}$$

$$H = \frac{\tau b^2 t}{\pi^2 D''} \tag{2.3}$$

where, σ, τ, b, t, D" is uniform longitudinal compressive stress, shear stress, the width of the wall, wall thickness, and flexural rigidity, respectively.

For both equilateral triangular tube and square (or rhombic) tube, critical values of k and H were presented for critical modes for combined compression and torsion. The following figure shows the interaction diagram developed for the triangular and square (or rhombic) tube.

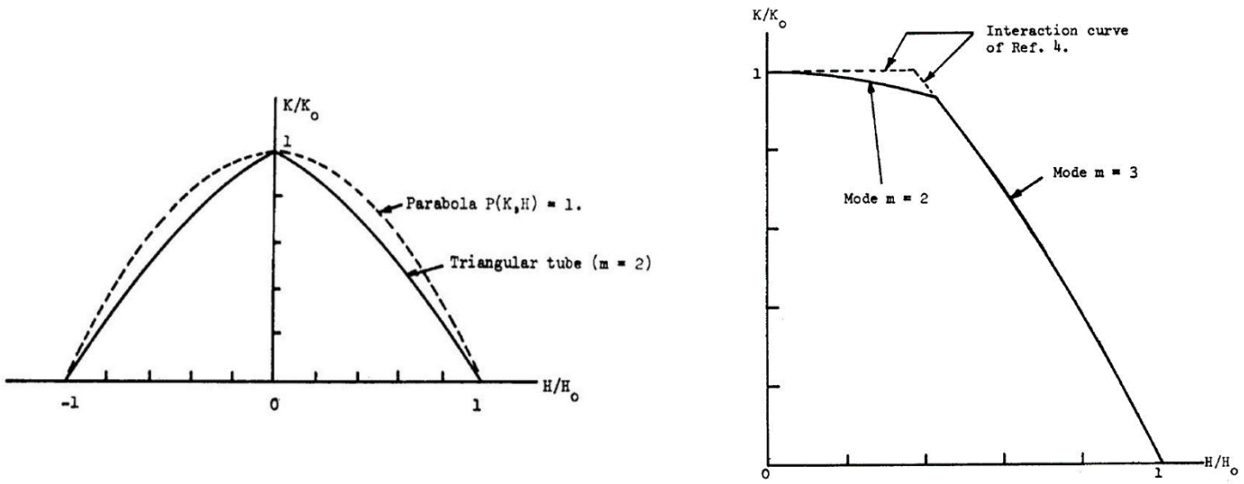

Figure 2.2: Interaction curves for (a) triangular and (b) square (or rhombic) tubes (Wittrick and Curzon, 1968)

In the interaction diagram, k_o and H_o indicate the maximum value of k and H for pure compression and pure torsional loading conditions, respectively. For triangular tube k_o and H_o were found to be 4.7077 and 5.5341, respectively. Moreover, for the square (or rhombic) tubes, k_o and H_o were 4.0 and 5.3395, respectively. In the case of pure compression, each wall of square (or rhombic) tubes behaved like a simply supported plate.

Bulson (1969)

The author conducted a compression test to observe the behavior of thin-walled tubes made with a number of flat plates. The number of sides of the specimen was chosen even numbers ranging from four (04) to forty (40). Tests were undertaken for thin-walled cylindrical tubular shapes also. For all the specimens, equal perimeter, cross-sectional area, and length were considered. Furthermore, three different thicknesses were considered for each polygonal profile. The author observed the change in maximum strength and failure mode with the change in the number of sides. It was reported that the capacity of tubular sections having a number of sides up to eighteen (18) could be found from the following theoretical formula, which is based on the elastic critical buckling stress and equivalent width concept.

$$\frac{F_{cr}}{\sigma_{cyl}} = \frac{n}{0.66}\left(\frac{F_y}{E}\right)^{\frac{1}{2}} \tag{2.4}$$

where, σ_{cyl} is collapse capacity of a cylinder having the same perimeter and thickness as multi-sided section

For the sections having eighteen (18) or more number of sides, capacity can be represented by the strength of the cylindrical tubular section having equal perimeter and thickness. Furthermore, it was reported that the failure mode of sections having twenty-two (22) or more sides resemble cylindrical failure mode.

Avent and Robinson (1976)

The authors investigated the elastic buckling behavior of folded plate columns having polygonal cross-sections. Elastic stability analysis of thin-walled polygonal columns was conducted by expanding nodal displacements into the Fourier series. Stability equations were used to develop buckling curves for polygonal sections having a different number of sides. These buckling curves

provided the buckling coefficient (k) for different aspect ratios. For short columns, buckling curves provided local plate buckling, whereas, buckling curve segments for long columns indicated Euler column buckling. Buckling curves were developed for axially loaded columns having a simply supported end condition.

It was concluded that Euler column buckling and classical plate buckling formula performs well in many cases. However, polygonal sections having an odd number of sides showed higher local buckling capacity than the classical plate buckling formula. Polygonal sections having the number of sides increased to sixteen (16), behave more like ideal cylindrical hollow sections.

Aoki et al. (1991)

Aoki et al. investigated the local buckling behavior of polygonal steel columns experimentally. Short columns having five different polygonal cross-sections (*i.e.*, four to eight sides) were used to sustain uniform compression under fixed end condition. Fabrication of the specimens was conducted by welding two half-sections made of folded steel plates. One Octagonal specimen was fabricated by welding eight flat plates to compare between welded and folded specimens. Each specimen had a nominal thickness of 4.5 mm, and one to four different width-thickness ratios of the component plate of each cross-sectional profile was used. A total of fifteen (15) numbers of specimens, each having a length of 1500 mm, were tested under compression. Two diaphragms were placed at the two ends of each specimen, and the distance between diaphragms was 1200 mm. From the tensile coupon test, average Yield Strength (F_y) and Young's Modulus (E) were found to be 289 N/mm^2 and 215 KN/mm^{2,} respectively. Residual stress was measured prior to the compression test, and maximum compressive residual stress found to be varied from $0.25F_y$ to $0.3F_y$ and $0.22F_y$ to $0.5F_y$ for rectangular section and all other sections respectively.

Furthermore, initial imperfection was measured, and the mean value was found to be 1.21 mm, which is 1/1000 of plate length.

From the compression tests, longitudinal stress-strain curves were obtained and presented in the study. For all the specimens, local buckling at the component plate was observed. This paper proposed an empirical formula to find the local buckling capacity of polygonal steel section as follows-

$$\frac{F_{cr}}{F_y} = 1.35 - 0.55\,R \qquad (R > 0.636) \tag{2.5}$$

where,

$$R = \sqrt{F_y/\sigma_{cr}} \tag{2.6}$$

and σ_{cr} can be found using Equation 2.1 for k=4.0

It has been concluded that, in the case of local buckling of component plates, polygonal short columns under compression perform better than box sections in terms of ultimate strength.

Migita and Fukumoto (1997)

In this paper, the authors conducted experimental and analytical methods to observe the elastoplastic local buckling behavior of thin-walled sections having a polygonal cross-section. The authors investigated the average buckling stress of polygonal sections for different aspect ratios, bent angle, width-thickness parameter, number of sides, and buckling modes. At first, local buckling behavior was investigated analytically by a computer program developed by Nishimura et al. (1990) for various bent angles and aspect ratios. Analytical models consisted of folded plate structures with two-component plates and regular polygonal shapes. Bent angles of folded plate structures varied from 10° to 180° Analytical models with polygonal shapes had

odd-sided sections having five and seven number of sides and even-sided sections having four to twenty-four (24) numbers of sides. A total of seventeen (17) specimen having five different polygonal cross-sections (*i.e.,* rectangular, pentagonal, hexagonal, heptagonal, and octagonal shapes) were tested to failure under axial compression.

From the analytical and experimental results, the authors concluded that average buckling stress was found to be minimal for aspect ratio between 0.5 and 0.7. For the folded plate structures, buckling stress was noticed to remain constant for bent angles between 60° to 170° and lower stresses for bent angle less than 60° as compared to sections having bent angles between 60° to 170°. A discontinuity in average buckling stress was observed for the bent angle between 170° to 180°. For the polygonal sections having the number of sides twenty-two (22) or less, it was found that local buckling strength can be express by one single equation. However, polygonal sections having more than 22 sides behave more like a cylindrical section. It was also found that polygonal sections having a different number of sides and same width-thickness parameter (R) has a small difference in buckling capacity.

Based on the analytical and experimental results, the authors proposed two formulas to find the local buckling strength of polygonal sections as follows. The first and second equation represents the lower and mean strength curve, respectively.

$$\frac{F_{cr}}{F_y} = \begin{cases} 1 & (\mathrm{R} \leq 0.44) \\ \dfrac{0.67}{\mathrm{R}^{0.5}} & (0.44 < \mathrm{R} \leq 1.3) \end{cases} \tag{2.7}$$

$$\frac{F_{cr}}{F_y} = \begin{cases} 1 & (\mathrm{R} \leq 0.67) \\ \dfrac{0.74}{\mathrm{R}^{0.75}} & (0.67 < \mathrm{R} \leq 1.3) \end{cases} \tag{2.8}$$

Teng et al. (1999)

This paper has studied the elastic local buckling behavior of columns having polygonal cross-sections under uniform axial compression or bending by using the finite strip method. Five different polygonal cross-sections (*i.e.,* Square, Pentagon, Hexagon, Heptagon, and Octagon), each having thirteen (13) different width-thickness ratios (minimum of 10 to a maximum of 252) were considered in the study. For each width-thickness ratio, the cross-sectional area was kept constant for all the five polygonal profiles. The authors used the finite strip method based program to find the local buckling capacity. In this study, elastic local buckling capacity is presented in terms of the dimensionless plate buckling coefficient (k).

For each plate slenderness ratio (width-thickness ratio), the plate buckling coefficient (k) was found for columns under uniform axial compression. It was found that sections having an even number of sides (*i.e.,* 4, 6, and 8 sides) have nearly the same local buckling capacity for slenderness ratio more than fifty (50). Odd sided sections (*i.e.,* 5 and 7 sides) have a higher capacity as compared to even sided sections. For all the sections, it was found that the buckling stress coefficient starts to reduce when the slenderness ratio is decreased less than fifty (50). Figure 2.3 shows the local buckling modes of polygonal sections under axial compression.

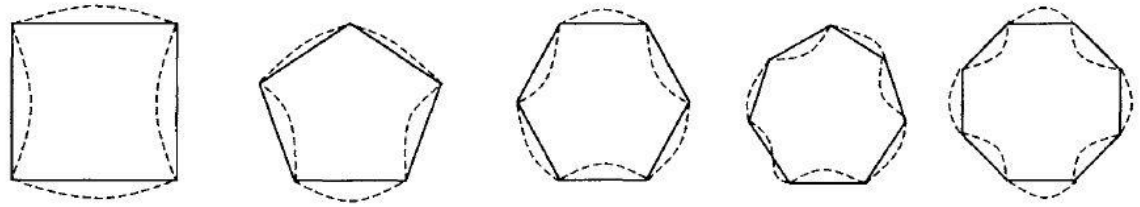

Figure 2.3: Local buckling modes of polygonal sections under axial compression (Teng et al. 1999)

The critical buckling capacity of polygonal sections under bending was found from the lowest value of capacity found by applying bending about the positive and negative x-axis and y-axis. It

was found that the pentagonal section reaches the highest bending capacity followed by heptagonal, square, hexagonal, and octagonal section. A comparison between local buckling capacity under axial compression and bending showed that all the sections under bending could reach around twenty-five (25) percent more resistance as compared to the sections under axial compression. Figure 2.4 shows the local buckling modes of polygonal sections under bending.

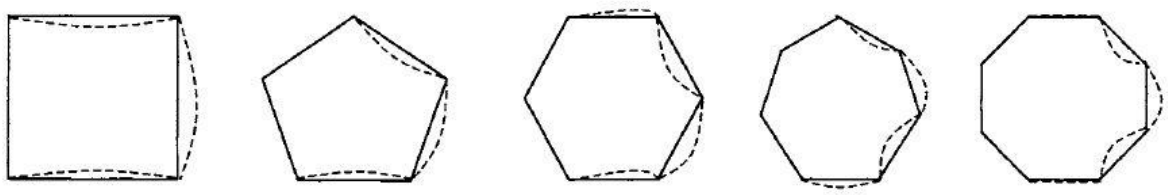

Figure 2.4: Local buckling modes of polygonal sections under bending (Teng et al. 1999)

Godat et al. (2012)

The authors undertook an experimental test to observe elasto-plastic local buckling behavior of thin-walled tubes having polygonal cross-sections. Thin-walled stub columns having three different polygonal profiles (*i.e.,* Octagonal, Dodecagonal, and Hexadecagonal) were tested under concentric compression. For each polygonal profile, two width-thickness ratios were considered, and a total of six stub columns were tested. These ratios were chosen in such a range to eliminate global buckling and observe elasto-plastic local buckling behavior. For each specimen, two half-sections made of the folded plate were combined together by welding to get a polygonal tubular section. Each specimen had one diaphragm at each end to reduce the end effect. All the columns had a nominal height of 780mm. Moreover, the mechanical properties of steel and geometric imperfection were measured prior to the experiment and reported in the paper. For the entire specimens, the end condition was kept simply supported, and radial movement was restraint.

Compression test results were reported in the paper as the critical buckling load, critical buckling stress, and strain. From the stress-strain diagram, it was observed that all the polygonal sections except one Hexadecagonal section had identical ascending and descending pattern of the stress-strain curve. Furthermore, the influence of the number of sides was investigated and reported to be insignificant when local buckling capacity is considered for constant plate width-thickness ratio. It was also found that critical local buckling stress has an inverse relation with the plate width-thickness ratio.

For all the specimens, local buckling was found to be located close to the end of the column. The failure mode of octagonal shapes was such that neighboring plates buckle in the opposite direction (*i.e.,* inward and outward direction), which resemble a typical pattern of local buckling in polygonal sections with even number of sides. However, both Hexadecagonal sections and one Dodecagonal section failed in such a mode, which is close to cylindrical buckling mode, indicating a higher number of faces buckle more like a cylindrical hollow section.

The results of this paper were compared with some previous studies, ASCE/SEI 48-11 and Eurocode 3. A new design equation was established by modifying Loove's design equation (Loove, 1996) to determine the local buckling capacity of the thin-walled polygonal tubular column under concentric compression. Following equation shows the design equation proposed by the authors-

$$F_{cr} = F_y \left(1 + R^{2N}\right)^{\left(-\frac{1}{N}\right)} \tag{2.9}$$

Where N value was found by regression analysis and proposed to be taken as 2.0. The following Figure 2.5 shows the experimental results of twenty-two (22) polygonal tubular sections of this

paper, including test results from previous literature, design equation of ASCE/SEI 48-11 and Eurocode 3 along with the proposed design equation by the authors.

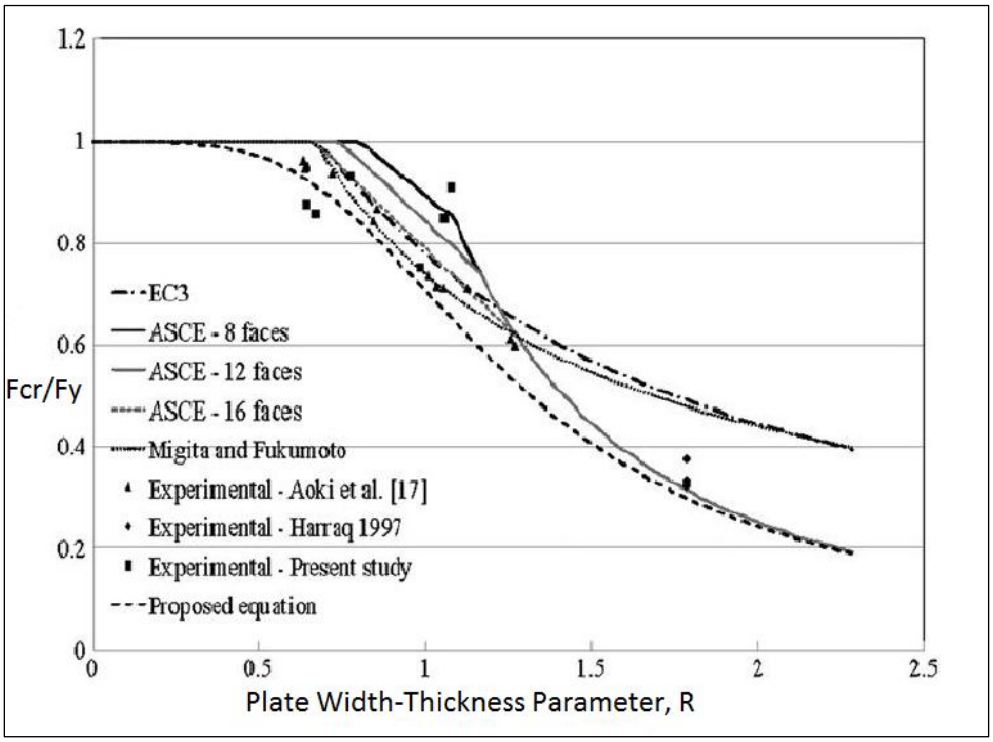

Figure 2.5: Comparison of test results with existing literature (Godat et al. 2012)

Gonçalves and Camotim (2013)

The authors investigated the elastic buckling behavior of the tubular section having regular polygonal cross-section by focusing on local, cross-section extensional, distortional, and multi-mode buckling under uniform compression. Generalized Beam Theory (GBT) has been deployed in a specialized form to exclusively use for Regular Convex Polygonal Sections (RCPS). To check the validity of GBT, Finite Strip Analysis was employed. At first, pure local buckling, cross-section extensional buckling and distortional buckling behavior were implemented independently. Then multi-mode buckling behavior was addressed for RCPS.

For pure local buckling, it was found that sections having an even number of sides would buckle in such a manner that adjacent sides will buckle in opposite directions (*i.e.,* inward and outward). Furthermore, the minimum critical buckling stress of an even-sided section can be predicted by the familiar equation of critical elastic plate buckling using buckling coefficient, k=4. For the odd-sided sections (i.e., 3, 5, and 7 sided), k-values were reported to be falling with an increase in the number of sides and approach 4.0 for both GBT and Finite Strip Analysis. However, buckling modes were found to be dissimilar for the two methods due to the reason of not uniquely defined.

Cross-section (in-plane) extensional buckling behavior was observed, and minimum buckling stress was reported in the paper for polygonal sections having a different number of sides. From the paper, it is observed that cross-section extensional buckling stress has an inverse relation with the number of sides. Moreover, this decrease in stress is very significant for sections having a number of sides up to ten (10). However, for sections having a number of sides fifteen or more shows a similar capacity. Distortional buckling stress was reported for the different number of sides for different mode pairs.

Moreover, a comparison was made between pure local buckling, cross-section extensional buckling and distortional buckling. It was reported that distortional buckling stress is always lower than cross-section extensional buckling stress. The comparison showed that local buckling becomes governing as compared to distortional buckling when circumradius over thickness ratio (β) is increased, though the transformation value of β is high for an increasing number of sides. Finally, multi-mode buckling was analyzed. It was reported that GBT yields accurate results for two modes, namely distortional mode and associated shear mode.

Gonçalves and Camotim (2013)

The authors investigated the buckling behavior of polygonal tubular sections subjected to bending or torsion by using Generalized Beam Theory (GBT). Finite Element Models were also developed to validate the results. Local buckling behavior of polygonal tubular sections subjected to bending was investigated by observing the effect of the bending axis angle. Figure 2.6 and Figure 2.7 shows the variation of critical buckling coefficient (k) and bending moment (M_{cr}) with the bending axis angle (Θ).

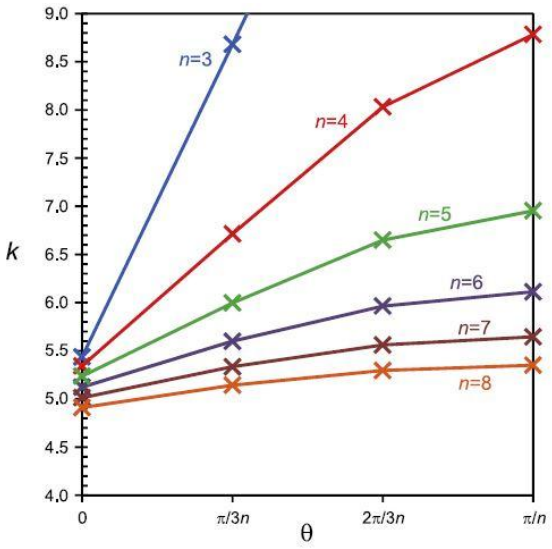

Figure 2.6: Critical buckling coefficient Vs. bending axis angle graph (Gonçalves and Camotim, 2013)

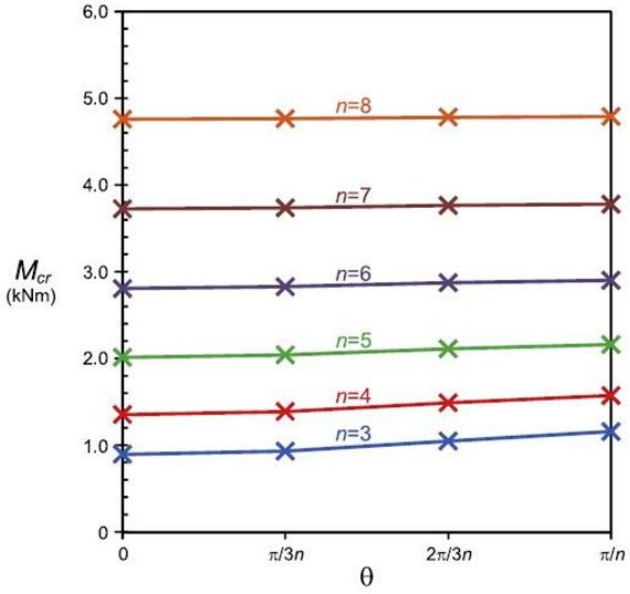

Figure 2.7: Critical bending moment Vs. bending axis angle graph (Gonçalves and Camotim, 2013)

Figure 2.6 shows that k increases with an increase in Θ; however, the effect of Θ becomes negligible for sections having more number of sides. On the other hand, Figure 2.7 indicates a slight variation of bending moment with increasing Θ. For the sections having a higher number of sides, non-null wall junction displacements were found.

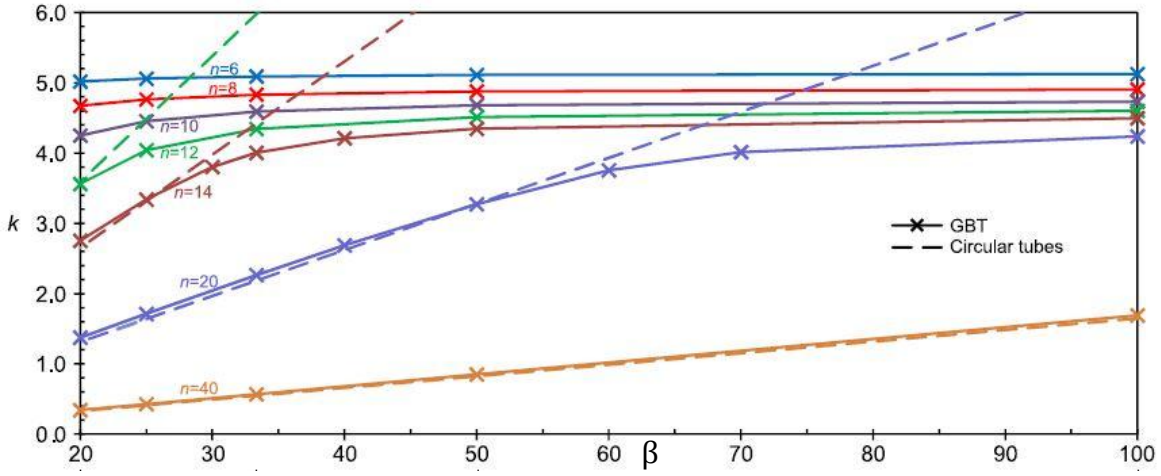

Figure 2.8: Buckling coefficient (k) Vs. circumradius over thickness ratio (β) graph for sections subjected to bending (Gonçalves and Camotim, 2013)

Figure 2.8 shows that k value increases with increasing β value and remains constant when mode change occurs (*i.e.,* becomes plate-like mode). The increase in k value with increasing β value is insignificant for sections having a number of sides ten (10) or less. However, this change in k value is significant for sections having a number of sides more than ten (10).

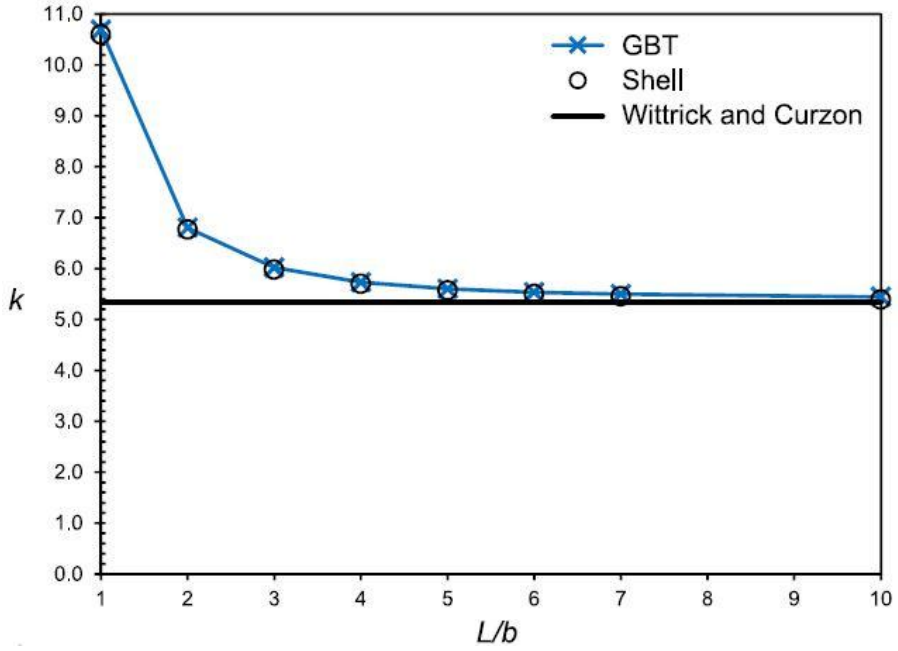

Figure 2.9: Buckling coefficient Vs. width to length ratio for sections subjected to torsion and having a number of sides n=4 (Gonçalves and Camotim, 2013)

For the sections subjected to torsion, local buckling, distortional buckling, and local-distortional buckling modes were observed by the authors. Figure 2.9 shows that k-value for local buckling decreases with increasing member length until a horizontal plateau is reached. This study provides minimum k-values for local buckling for a different number of sides for width to member length ratio of 10.

Reinke et al. (2014)

The authors investigated the bending behavior of polygonal hollow sections to find the inconsistency in available design procedures for polygonal steel poles having a higher number of

sides and cylindrical steel poles. European design code EN 50341-1 provides bending moment capacity for different polygonal sections and cylindrical steel poles. Design curves provided in EN 50341-1 for the polygonal section are based on the Plate buckling plate strip concept. However, design curves for cylindrical sections are based on experimental results. Authors intended to find the transition point where polygonal sections with a higher number of sides behave like cylindrical sections.

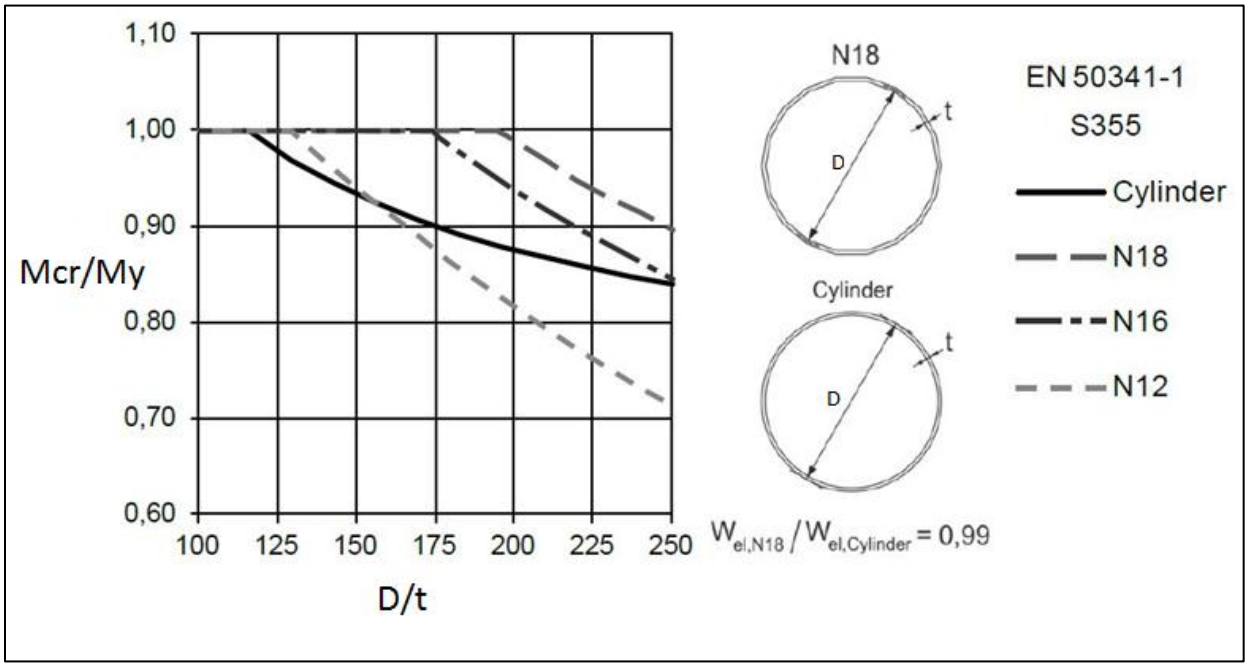

Figure 2.10: Normalized bending moment capacity M_{cr}/M_y for polygonal and cylindrical sections according to EN 50341-1 (Reinke et al. 2014)

Experimental tests were conducted to observe the bending behavior of full-scale specimens with a polygonal cross-section (*i.e.,* 6, 12, and 24 sided) and cylindrical sections. The entire specimen had an identical length and slenderness ratio (D/t). Experimental results indicated higher bending capacity is associated with a higher number of sides. Moreover, Finite Element Models were developed to investigate the bending capacity of polygonal sections having an arbitrary number

of sides. A substitute imperfection approach based on the data found from the experiment was assigned to get a realistic imperfection.

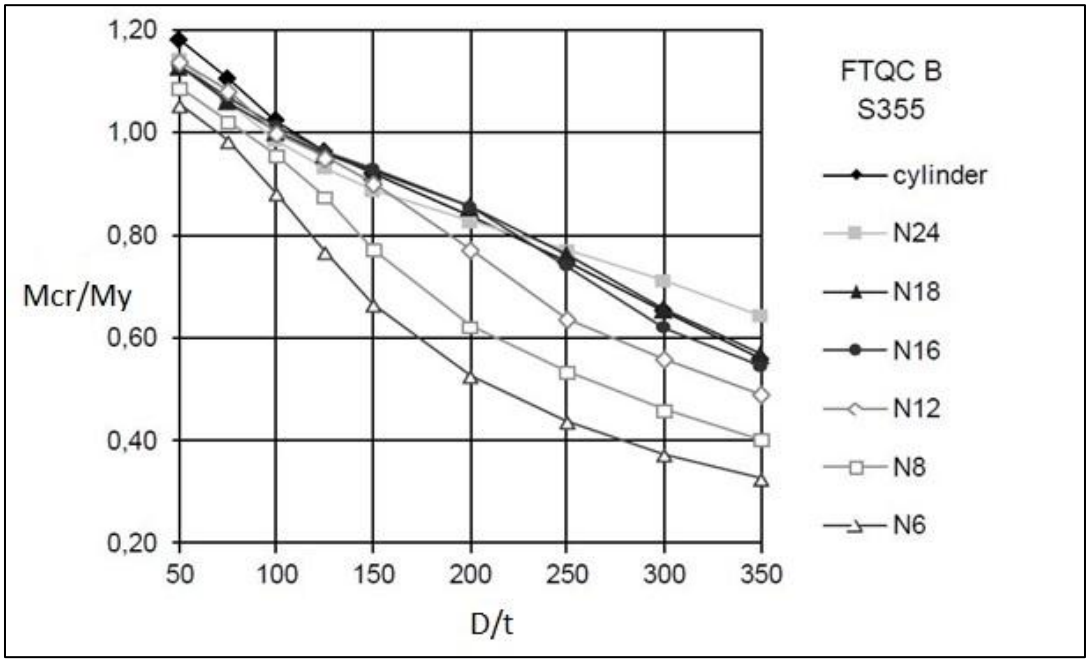

Figure 2.11: Normalized bending moment capacity M_{cr}/M_y Vs. slenderness D/t for steel poles with the polygonal and cylindrical section (Reinke et al. 2014)

Results indicated that polygonal sections having the number of sides sixteen (16) or more behave like cylindrical sections (*i.e.,* shell buckling behavior). Finally, it was concluded that current design regulations for polygonal steel poles do not fully reflect the actual influence of geometric imperfection and shell-like behavior.

Bräutigam et al. (2017)

Authors investigated the bending behavior of sixteen (16) sided polygonal tubular steel sections to properly identify the ultimate bending capacity of polygonal tubular sections and to reflect the proper transition between plastic bending moment capacities and limit state of buckling. This paper summarized different design rules for bending capacity from different codes. European design rules EN 50341-1 for electrical lines only considers the elastic bending moment capacity,

whereas Eurocode 3 considers the plastic bending moment. However, there is a sudden drop of resistance when the class of the section is changed from 2 to 3. Another European standard EN 40-3-3, for octagonal or circular lighting columns, is based on the plastic moment.

Authors tested nine (09) specimens of sixteen-sided tubular sections having two different classes (*i.e.,* Class 1 and Class 4) under pure bending and combined bending and torsion. For all the specimens, an identical span of 8 meters was used. Numerical analysis was conducted using ANSYS. To incorporate imperfection in the model Substitute imperfection approach was used. Experimental and numerical results, along with different codes were plotted in the same graph to make comparisons. The following figure shows the graphical comparison by plotting normalized bending capacity (M_{cr}/ M_y) against slenderness ratio w/t. In the figure, experimental specimens under pure bending are denoted by V1, V2, V5, and V6, whereas specimens under combined bending and torsion are denoted by V3, V4, V7, V8, and V9.

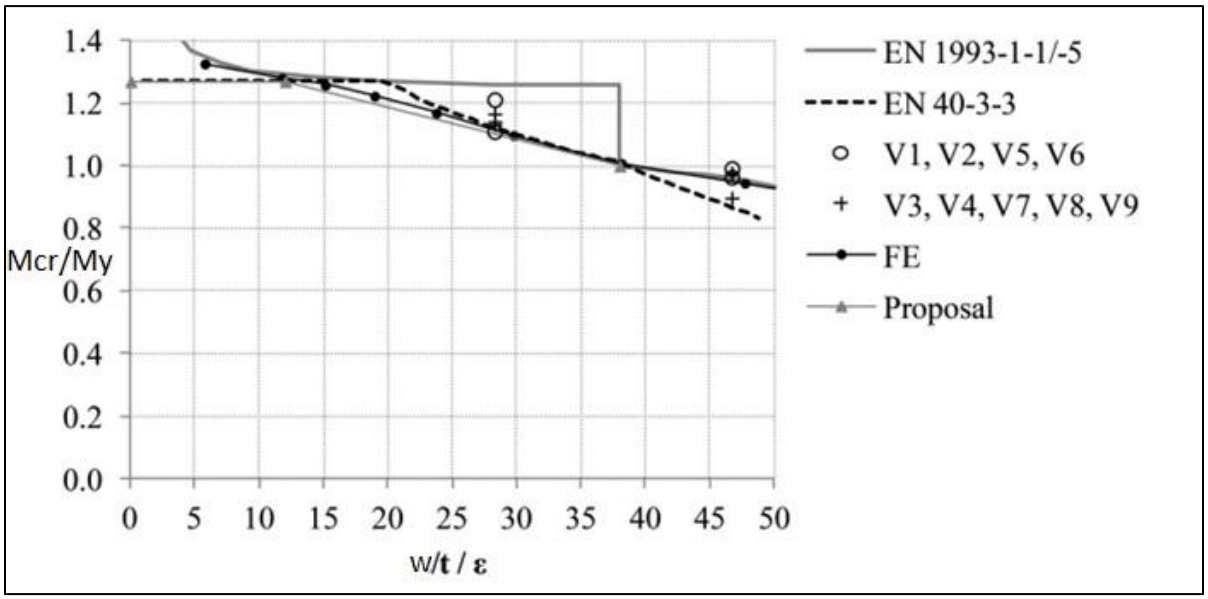

Figure 2.12: Normalized bending moment capacity M_{cr}/M_y Vs. slenderness ratio w/t/ε (Bräutigam et al. 2017)

Results suggest that the sudden step in the resistance curve is overestimating the bending capacity in EC3. Furthermore, experimental and numerical results indicate that bending moment capacity can be more than the elastic bending moment capacity for the compact sections. However, it might not be appropriate to use full plastic moment capacity.

Martins et al. (2018)

The authors investigated the post-buckling behavior of regular convex polygonal cross-sections (RCPS) columns in local and distortional buckling modes. Specialized Generalized Beam Theory (GBT) has been employed to extract the post-buckling behavior of columns. For comparison purposes, ABAQUS finite element models were developed.

Whether the governing post-buckling behavior will be local or distortional depends on the geometric parameters (*i.e.*, Circumradius over Thickness Ratio, β, and Number of Sides, n). For a specific n value, columns having high β value would buckle in local buckling mode, whereas the low value of β value will result in distortional buckling mode.

Different combination of local to distortional buckling load ratio was considered to observe its effect post-buckling behavior. Moreover, several amplitudes of initial geometric imperfection were taken into consideration to reveal their influence on the results. For local buckling modes, it was found that distinct initial geometrical amplitudes only influence the initial post-buckling stages, and equilibrium paths merge as the applied load increases. Results showed that RCPS columns pure local post-buckling behavior is immensely stable. However, RCPS column pure distortional post-buckling behavior indicates somewhat instability. Furthermore, the RCPS column show complex post-buckling behavior after the peak load has been reached. Moreover, RCPS column local-distortional post-buckling behavior was also found slightly unstable.

2.3 Design provisions of different standards

Current AASHTO (AASHTO 2015) has provided width-thickness limits for eight, twelve, and sixteen-sided polygonal steel sections. While AASHTO recommends the same width-thickness limit for all the three sections when they are compact, the requirements are different for non-compact sections. Moreover, AASHTO defined the capacities of multi-sided tubular sections subjected to compression, tension, bending, shear, and combined forces. ASCE/SEI-48-11 provides design equations for local buckling capacity of eight, twelve, and sixteen-sided polygonal steel sections of the transmission line. Eurocode 3 (EN 1-1, 2005, EN 1-3, 2006, EN 1-5, 2006) has design equation for plate elements. In this study, multi-sided steel tubular section has been considered as a collection of individual longitudinal plate strips to find the resistance using Eurocode 3. The design concept of Eurocode 3 is adopted by the European design rules for overhead power lines (EN 50341-1, 2012); however, overlooking plastic reserves. All the polygonal tubular steel sections have been classified as either class 3 or class 4 sections.

2.3.1 AASHTO 2015

"AASHTO-LRFD Specifications for Structural Supports for Highway Signs, Luminaires, and Traffic Signals" has provided design guidelines for multi-sided steel tubular sections (AASHTO 2015). AASHTO has specified width-thickness ratio limits for Octagonal, Dodecagonal, and Hexadecagonal sections. The minimum values of different geometric parameters are also mentioned in AASHTO. Moreover, AASHTO defined the capacities of multi-sided tubular sections subjected to compression, tension, bending, shear, and combined forces.

2.3.1.1 Width-thickness ratios for multi-sided tubular sections

AASHTO has provided width-thickness ratio limits for the Compact section, Non-compact sections, and maximum limit. If the width-thickness ratios of any compression element section

exceed the non-compact limiting value, λ_r, the section is classified as a slender element section. Table 2.1 shows the width-thickness ratio limits proved by AASHTO. It is also mentioned that flexural members may be subjected to local buckling if the width-thickness ratio is more than the compact limit (λ_p). However, compression members may face local buckling if the width-thickness ratio exceeds the non-compact limit (λ_r).

Table 2.1: Width-thickness ratios for multi-sided tubular sections (AASHTO 2015)

Shape	Ratio	λ_p	λ_r	λ_{max}
Octagonal (8 sided)	b/t	$1.12\sqrt{E/Fy}$	$1.53\sqrt{E/Fy}$	$2.14\sqrt{E/Fy}$
Dodecagonal (12 Sided)	b/t	$1.12\sqrt{E/Fy}$	$1.41\sqrt{E/Fy}$	$2.14\sqrt{E/Fy}$
Hexadecagonal (16 Sided)	b/t	$1.12\sqrt{E/Fy}$	$1.26\sqrt{E/Fy}$	$2.14\sqrt{E/Fy}$

2.3.1.2 Element width of the multi-sided tubular section

AASHTO has provided equation to determine the element width (b) of multi-sided tubular sections. The element width of multi-sided tubular sections can be found using the following equation.

$$b = tan\left(\frac{180}{n}\right)[D' - 2t - minimum(2r_b, 8t)] \quad (2.10)$$

Where,

b= Element width of multi-sided tube

t= wall thickness of the multi-sided tube

D'= Outside distance from flat side to flat side of multi-sided tubes

n= number of sides of multi-sided tubes

r_b= inside bend radius of a plate

and $(\frac{180}{n})$ is in degrees

2.3.1.3 General dimensions

According to AASHTO, the minimum thickness of material for main supporting members of steel truss-type supports should be 4.55 mm. Moreover, the minimum thickness of material for all members of pole-type supports and truss-type luminaire arms shall be 3.175mm.

The minimum number of sides (n) of multi-sided tubular sections should be as shown in Table 2.2. Furthermore, it should have a minimum internal bend radius (r_b) of five times tube wall thickness or 25.4 mm, whichever is larger.

Table 2.2: Minimum number of sides of multi-sided tubes (AASHTO 2015)

Outside Distance from Flat Side to Flat Side of Multisided Tubes (D') (mm)	Minimum Number of Sides (n)
D'≤ 330	8 sides
330 < D' ≤ 711	12 sides
711< D' ≤ 1270	16 sides

2.3.1.4 Nominal bending strength for multi-sided tubular members

According to AASHTO, multi-sided tubular sections having compact, non-compact, and slender elements should have nominal bending moment capacity, as shown in Table 2.3. However, the nominal bending strength for multi-sided tubes shall not exceed the nominal bending strength for round tubes of equivalent diameter.

Table 2.3: Nominal bending strength for multi-sided tubular members (AASHTO 2015)

Shape	Compact	Non-Compact	Slender
	$\lambda \leq \lambda_p$	$\lambda_p < \lambda \leq \lambda_r$	$\lambda > \lambda_r$
Octagonal	$M_n = M_p = Z_x \times F_y$	$M_n = M_p[1.5 - \frac{0.45\left(\frac{b}{t}\right)}{\sqrt{E/Fy}}]$	$M_n = M_p[1.14 - \frac{0.22\left(\frac{b}{t}\right)}{\sqrt{E/Fy}}]$
Dodecagonal	$M_n = M_p = Z_x \times F_y$	$M_n = M_p[1.77 - \frac{0.69\left(\frac{b}{t}\right)}{\sqrt{E/Fy}}]$	$M_n = M_p[1.15 - \frac{0.25\left(\frac{b}{t}\right)}{\sqrt{E/Fy}}]$
Hexadecagonal	$M_n = M_p = Z_x \times F_y$	$M_n = M_p[2.59 - \frac{1.43\left(\frac{b}{t}\right)}{\sqrt{E/Fy}}]$	$M_n = M_p[1.12 - \frac{0.26\left(\frac{b}{t}\right)}{\sqrt{E/Fy}}]$

2.3.1.5 Nominal compressive strength for the multi-sided tubular member

According to AASHTO, nominal compressive strength (P_{nc}) of a multi-sided tubular column shall be calculated using Equation 2.11 to 2.15 (AASHTO 2015).

$$P_{nc} = A_g F_{cr} \tag{2.11}$$

When, $\frac{KL}{r} \leq 4.71\sqrt{\frac{E}{QFy}}$, here, K and r indicates effective length factor and radius of gyration respectively

$$F_{cr} = Q(0.658)^{\left(\frac{QFy}{Fe}\right)}F_y \tag{2.12}$$

When, $\frac{KL}{r} > 4.71\sqrt{\frac{E}{QFy}}$

$$F_{cr} = 0.877F_e \tag{2.13}$$

Where,

$$Fe = \frac{\pi^2 E}{(kL/r)^2} \tag{2.14}$$

If $\lambda \leq \lambda_r$, Q=1

If $\lambda > \lambda_r$, $Q = A_{EFF}/A_g$, where, A_{EFF} is calculated from the sum of parts using effective widths, b_e

$$b_e = 1.92t\sqrt{\frac{E}{f}}\left[1 - \frac{0.34}{\frac{b}{t}}\sqrt{\frac{E}{f}}\right] \leq b \tag{2.15}$$

where, f = F_{cr} using Q=1

2.3.1.6 Nominal torsion strength for the multi-sided tubular member

According to AASHTO, nominal torsional strength (T_n) shall be computed using the following equations.

$$T_n = C_t\, F_{nt} \tag{2.16}$$

where,

T_n = nominal torsion strength, and

C_t = the torsional constant

The nominal torsional stress capacity for multi-sided tubular shapes shall be:

$$F_{nt} = 0.6\, F_y \tag{2.17}$$

Torsional Constant C_t shall be computed by using Table 2.4.

Table 2.4: Torsional constant for stress computation (AASHTO 2015)

	Octagonal	Dodecagonal	Hexadecagonal
Torsional Constant (C_t) for stress computation	$\frac{6.63R'^2t}{k_t}$	$\frac{6.43R'^2t}{k_t}$	$\frac{6.37R'^2t}{k_t}$

In Table 2.4 k_t indicates the stress concentration factor and it should be determined using the following equation.

$$k_t = \frac{t}{R'}\left[\frac{\frac{R'}{n't} - \frac{1}{2}\left(1 + \frac{n'+1}{n'}\right)}{ln\left(\frac{n'+1}{n'}\right)}\right] + \frac{n't}{R'} \geq 1 \quad (2.18)$$

where (consistent units):

k_t = stress concentration factor

t = wall thickness

R' = radius measured to the mid-thickness of the wall

n′ = ratio of the inside-corner radius to wall thickness

2.3.1.7 Multi-sided tubular member under combined forces

If the multi-sided tubular member is subjected to combined bending, axial compression or tension, shear, and torsion, it should be such proportioned that the following criterion is met.

$$\frac{P_u}{P_r} + \frac{BM_u}{M_r} + (\frac{V_u}{V_r} + \frac{T_u}{T_r})^2 \leq 1.0 \quad (2.19)$$

where,

P_u= factored axial load

P_r= minimum nominal compressive strength or tensile strength

B= moment magnification factor

M_u= factored bending moment

M_r= factored flexural resistance

V_u= factored shear

V_r= factored shear resistance

T_u= factored torque

T_r= factored torsional resistance

If $T_u/T_r \leq 0.20$, torsional and shear effects can be ignored.

when $\frac{\mathrm{Pu}}{\mathrm{Pr}} \geq 0.2$

$$\frac{P_u}{P_r} + \frac{8}{9}\frac{BM_u}{M_r} \leq 1.0 \tag{2.20}$$

when $\frac{\mathrm{Pu}}{\mathrm{Pr}} < 0.2$

$$\frac{P_u}{2P_r} + \frac{BM_u}{M_r} \leq 1.0 \tag{2.21}$$

When the member is in compression, moment magnification factor (B) for the prismatic member shall be computed using the following equation,

$$B = \frac{1}{1 - \frac{Pu}{Pe}} \tag{2.22}$$

where, $\mathrm{Pe} = \frac{\pi^2 \mathrm{EAg}}{\left(\frac{\mathrm{kL}}{\mathrm{r}}\right)^2}$

When the member is in tension, B=1.

2.3.2 ASCE/SEI-48-11

ASCE/SEI-48-11 has provided design equations for the local buckling capacity of multi-sided steel tubular columns. ASCE/SEI-48-11 relies on the effective stress concept supported by the total cross-section. It has provided different equations depending on the number of sides of multi-sided tubes and width-thickness ratio. ASCE/SEI-48-11 has similar definition of element

width (b) as AASHTO. It provides design provisions for multi-sided tubes subjected to compression, tension, bending, shear, and combined forces.

2.3.2.1 Multi-sided tubes under axial compression

Table 2.5 shows the design equations for the local buckling capacity of multi-sided tubes under axial compression. In Table 2.5, F_{cr} indicates compressive stress permitted and ϕ=6.9 and Ω= 2.62 for F_y and F_{cr} in MPa.

Table 2.5: ASCE/SEI-48-11 design equations for local buckling capacity of the multi-sided tubular column

No of Faces	Bend Angle (Degree)	Limit	Compressive Resistance Permitted, F_{cr}
4,6 or 8	≥45	$b/t \leq 260\Omega/\sqrt{F_y}$	$F_{cr} = F_y$
		$260\Omega/\sqrt{F_y} < b/t \leq 351\Omega/\sqrt{F_y}$	$F_{cr} = 1.42F_y(1 - 0.00114\frac{1}{\Omega}\sqrt{F_y}\frac{b}{t})$
		$b/t > 351\Omega/\sqrt{F_y}$	$F_{cr} = 104980\phi/\left(\frac{b}{t}\right)^2$
12	30	$b/t \leq 240\Omega/\sqrt{F_y}$	$F_{cr} = F_y$
		$240\Omega/\sqrt{F_y} < b/t \leq 374\Omega/\sqrt{F_y}$	$F_{cr} = 1.45F_y(1 - 0.00129\frac{1}{\Omega}\sqrt{F_y}\frac{b}{t})$
		$b/t > 374\Omega/\sqrt{F_y}$	$F_{cr} = 104980\phi/\left(\frac{b}{t}\right)^2$
16	22.5	$b/t \leq 215\Omega/\sqrt{F_y}$	$F_{cr} = F_y$
		$215\Omega/\sqrt{F_y} < b/t \leq 412\Omega/\sqrt{F_y}$	$F_{cr} = 1.42F_y(1 - 0.00137\frac{1}{\Omega}\sqrt{F_y}\frac{b}{t})$
		$b/t > 412\Omega/\sqrt{F_y}$	$F_{cr} = 104980\phi/\left(\frac{b}{t}\right)^2$

2.3.2.2 Multi-sided tubes under bending

According to ASCE/SEI-48-11, the stress resulting from bending shall not exceed either of the following

$$\frac{M_n c}{I} \leq \mathrm{F_t} \tag{2.23}$$

Or

$$\frac{M_n c}{I} \leq \mathrm{F_{cr}} \tag{2.24}$$

where

M_n= nominal bending moment

c = distance from neutral axis to extreme fiber

I = moment of inertia

F_t = tensile stress permitted and

F_{cr} = compressive stress permitted

The tensile stress permitted (F_t) can be found from either of the following, whichever is smaller:

$$F_t = F_y \; or \; 0.83 \; F_u \tag{2.25}$$

2.3.2.3 Multi-sided tubes under shear

According to ASCE/SEI-48-11, the shear stress resulting from applied shear forces, torsional shear, or a combination of the two shall satisfy the following equation:

$$\frac{V_u Q'}{Ib} + \frac{T_u c}{J} \leq F_v \quad (2.26)$$

$$F_v = 0.58\, F_y \quad (2.27)$$

where,

V_u = factored shear

Q' = moment of section about neutral axis

I = moment of inertia

b = 2 times wall thickness (t)

T_u = factored torque

c = distance from neutral axis to point where stress is checked and

J = torsional constant of cross-section

F_v = shear stress permitted; and

F_y = specified minimum yield stress

Table 2.6: Maximum value of $\frac{c}{J}$ according to ASCE/SEI-48-11

	Octagonal	Dodecagonal	Hexadecagonal
Max. $\frac{c}{J}$	$\frac{0.603 \times (D+t)}{D^3 \times t}$	$\frac{0.622 \times (D+t)}{D^3 \times t}$	$\frac{0.628 \times (D+t)}{D^3 \times t}$

In Table 2.6, D indicates mid-surface distance from flat side to flat side of multi-sided tubes, and t indicates tube wall thickness.

2.3.2.4 Multi-sided tubes under combined forces

According to ASCE/SEI-48-11, the stress resulting from the combined stress at any point on the cross-section shall not exceed the following

$$\left[\left(\frac{P_u}{A}+\frac{M_x c_y}{I_x}+\frac{M_{y'} c_x}{I_y}\right)^2+3\left(\frac{V_u Q'}{It}+\frac{T_u c}{J}\right)^2\right]^{1/2} \leq \mathrm{F_t}\ or\ \mathrm{F_{cr}} \tag{2.28}$$

where,

F_{cr} = compressive stress permitted

F_t = tensile stress permitted

P_u= factored axial load

A = cross-sectional area

M_x = bending moment about X–X axis

$M_{y'}$ = bending moment about Y–Y axis

I_x = moment of inertia about X–X axis

I_y = moment of inertia about Y–Y axis

c_x = distance from Y–Y axis to point where stress is checked

c_y = distance from X–X axis to point where stress is checked

V_u = factored shear

Q' = moment of section about neutral axis

I = moment of inertia

T_u = factored torque

J = torsional constant of cross-section

c = distance from neutral axis to point where stress is checked and

t = wall thickness

2.3.3 Eurocode 3

Eurocode 3 (EN 1-1, 2005, EN 1-3, 2006, EN 1-5, 2006) has design equation for plate elements. Multisided steel tubular section has been considered as a collection of individual longitudinal plate strips to find the resistance using Eurocode 3.

2.3.3.1 Multi-sided tubes under compression

The design equation of Eurocode 3 is based on the effective area concept. According to Eurocode 3, the critical compressive stress (F_{cr}) can be found from Equation 2.29 to 2.32.

$$A_{EFF} = \rho \times A_g \tag{2.29}$$

$$\rho = \begin{cases} 1, & R \leq 0.5 + \sqrt{(0.085 - 0.055\psi)} \\ \dfrac{R - 0.055(3+\psi)}{R\text{^}2} \leq 1, & R > 0.5 + \sqrt{(0.085 - 0.055\psi)} \end{cases} \tag{2.30}$$

$$F_{cr} = \rho \times F_y \tag{2.31}$$

where ψ= stress ratio and R = plate width-thickness parameter

$$R = \sqrt{\frac{Fy}{\sigma_{cr}}} \tag{2.32}$$

σ_{cr}= elastic critical plate buckling stress from Equation 2.1

2.3.3.2 Multi-sided tubes under bending

According to Eurocode 3, Class 1 and Class 2 sections can develop plastic moment. Class 3 section can reach yield stress at the extreme fiber and able to develop elastic moments. However, the class 4 section locally buckles before yielding and could reach bending capacity lower than the elastic moment.

The design resistance for bending about one principal axis of a cross-section is determined as follows-

For class 1 and class 2 $$M_n = M_p = Z \times F_y \quad (2.33)$$

For class 3 $$M_n = M_y = S \times F_y \quad (2.34)$$

For class 4 $$M_n = M_{eff} = S_{eff} \times F_y \quad (2.35)$$

where,

Z= plastic section modulus

S=elastic section modulus

S_{eff}= effective section modulus

and $\frac{Seff}{S} < 1$

The following table shows the classification of plates according to Eurocode 3. In the table, ε is $\sqrt{\frac{235}{F_y}}$

Table 2.7: Classification of plates according to Eurocode 3

$w/t \leq 33\varepsilon$	Class 1
$w/t \leq 38\varepsilon$	Class 2
$w/t \leq 42\varepsilon$	Class 3
$w/t > 42\varepsilon$	Class 4

2.3.3.3 Multi-sided tubes under combined forces

According to Eurocode 3, class 1, class 2, class 3, and class 4 sections under combined axial compression and bending should satisfy the following criteria.

For class 1 and class 2
$$\frac{P_u}{A} + \frac{M_u}{Z} \leq F_y \quad (2.36)$$

For class 3
$$\frac{P_u}{A} + \frac{M_u}{S} \leq F_y \quad (2.37)$$

For class 4
$$\frac{P_u}{A_{EFF}} + \frac{M_u + P_u \times ep}{S_{eff}} \leq F_y \quad (2.38)$$

where,

P_u= factored axial compression on member

M_u= factored bending moment on member

A_{EFF}= effective cross-sectional area

e_p= for non-symmetrical cross-sections the shift of relevant centroidal axis when the cross-section is subjected to compression only

2.3.4 EN 50341-1

The design concept of Eurocode 3 is adopted by the European design rules for overhead power lines (EN 50341-1, 2012); however, overlooking plastic reserves. All the polygonal tubular steel sections have been classified either class 3 or class 4 sections depending on the criteria provided in the following Table 2.8. This table is applicable for polygonal sections having a number of sides six to eighteen (6 to 18). In the table, b' denotes the width of mid-surface of polygonal section and ε is $\sqrt{\frac{235}{F_y}}$

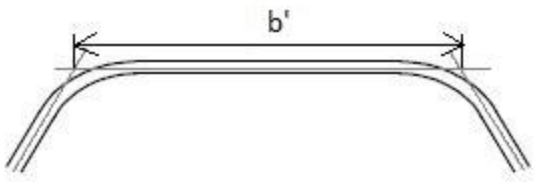

Figure 2.13: Mid-surface width of the polygonal section according to EN 50341-1

Table 2.8: Classification of tubular cross-sections in bending (EN 50341-1, 2012)

$b'/t \leq 42\varepsilon$	Class 3
$b'/t > 42\varepsilon$	Class 4

For the multi-sided tube under axial compression, the same design procedure has been followed by EN 50341-1. Moreover, for sections under bending and combined forces, the design method of class 3 and class 4 sections of Eurocode 3 has been followed.

2.4 Summary

Although there have been some research on local buckling behavior of multi-sided tubes under axial compression, research on the behavior of multi-sided tubes subjected to bending or torsion is very limited. Moreover, to the best of the author's knowledge, currently, there is no such study dealing with the local buckling behavior of multi-sided tube under combined bending and compression. Furthermore, to date, most of the research done on multi-sided tube sections are experimental in nature or based on analytical formulations based on simplified assumptions. Both experimental and analytical investigations have limitations, and a detailed FE model is required to investigate the behavior of multi-sided tube sections under different types of loading. To date, no comprehensive FE model that accurately simulates the local buckling behavior of multi-sided tube sections has been developed.

In addition, AASHTO has suggested same compact limit for all three multi-sided sections (*i.e.,* 8-, 12- and 16- sided) subjected to bending and considered same as that for flanges of rectangular

HSS sections, which is $1.12\sqrt{\frac{E}{F_y}}$. No study has been performed to evaluate the width-thickness limits in AAHSTO. This study presents a FE model based investigation of local buckling behavior of multi-sided tube sections under various loading conditions (*i.e.*, axial compression, pure bending, combined bending and compression). AASHTO provided width-thickness limits have been evaluated in the following chapters for different loadings. Moreover, other existing standards are also evaluated in this study.

Chapter 3 Development of Finite Element Model

3.1 Introduction

The aim of this chapter is to present the details of the finite element model development in order to observe the local buckling behavior of multi-sided tube sections. With the help of computers and extensive software packages, local buckling failure of members can be analyzed numerically. These software are capable of simulating the actual behavior of structures. Researchers have been using finite element analysis (FEA) to predict the capacity of different steel structural members. ABAQUS is a general-purpose FEA software, which is used to analyze the structural behavior numerically.

This chapter will describe finite element modelling techniques in detail. It also contains the assumptions made in modelling. Selection of element type, mesh configuration, material properties, boundary conditions, and application of load have been discussed in detail. Moreover, the inclusion of initial imperfection has been explained in this chapter. Finally, the finite element (FE) models are validated against experimental test results available in the literature.

3.2 FE model description

To simulate real structural behavior of multi-sided tubes, three-dimensional models have been developed in ABAQUS. Since multi-sided tube sections are fabricated with plate, shell element has been used to develop finite element (FE) model. Moreover, shell elements are more effective in applying imperfections. The effect of boundary conditions and loading were investigated to represent the real conditions. Moreover, the finite element model has been validated against experimental results available in the literature. Details of the FE models development are presented in the following subsections.

3.2.1 Elements and mesh configuration

A nonlinear finite element model is developed using ABAQUS software. Both material and geometric nonlinearities have been incorporated in the model. Thin-walled members having three different polygonal cross-sections (*i.e.,* Octagonal, Dodecagonal, and Hexadecagonal) have been modelled (Figure 3.1).

In order to analyze the local buckling failure, shell elements have been chosen as the modelling building blocks as they come up with sufficient degrees of freedom to capture the real buckling deformation and can advance the plasticity effect. Due to the simplicity of the model, the 4-node shell element has been chosen in this study. There are three different 4-node shell elements available in the default element library of ABAQUS standard version of 6.14 (*i.e.,* S4, S4R, and S4R5) (ABAQUS 2014). Among these three shell elements, S4R5 is a thin element that imposes the Kirchhoff constraint numerically. It is an isoparametric quadrilateral shell with four nodes, has five degrees of freedom per node, and uses a reduced integration method. S4 and S4R are general-purpose 4-node, finite membrane strains shell elements. In comparison to S4R5, both S4 and S4R elements have six degrees of freedom per node: three translations (u_x, u_y, u_z) and three rotations $(\theta_x, \theta_y, \theta_z)$ defined in a global coordinate system. As a result, these two elements are capable of producing more accurate results than S4R5. S4R element uses the reduced integration method with hourglass control to form element stiffness and this reduces the running time in three-dimensional FE models. Therefore, S4R element is selected for all finite element models.

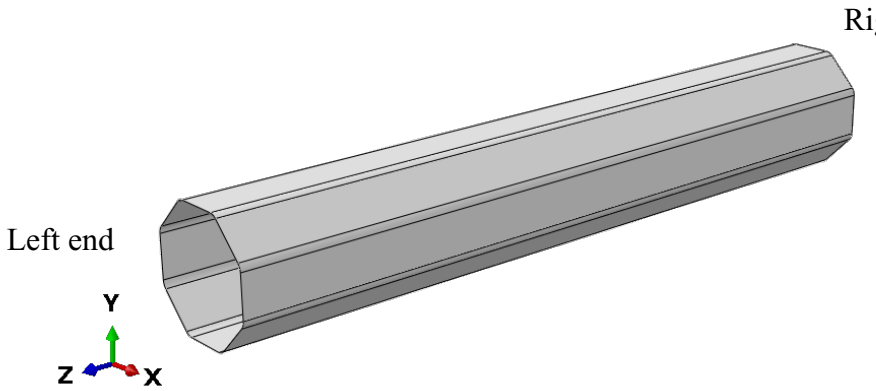

(a) Octagonal hollow section

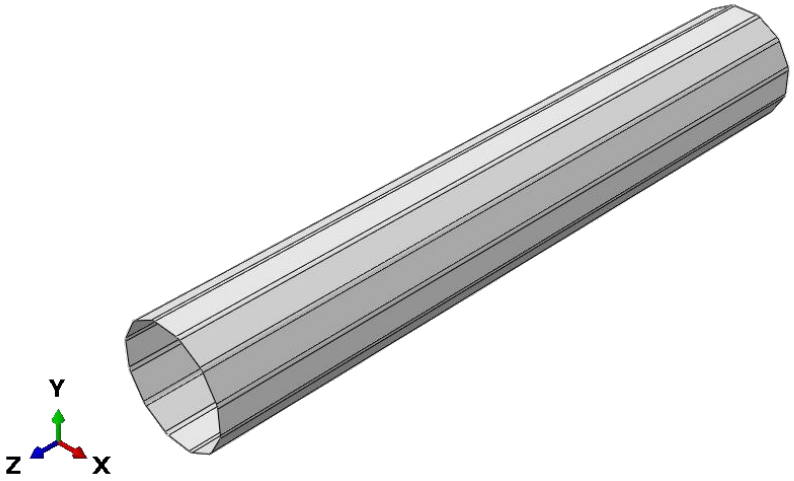

(b) Dodecagonal hollow section

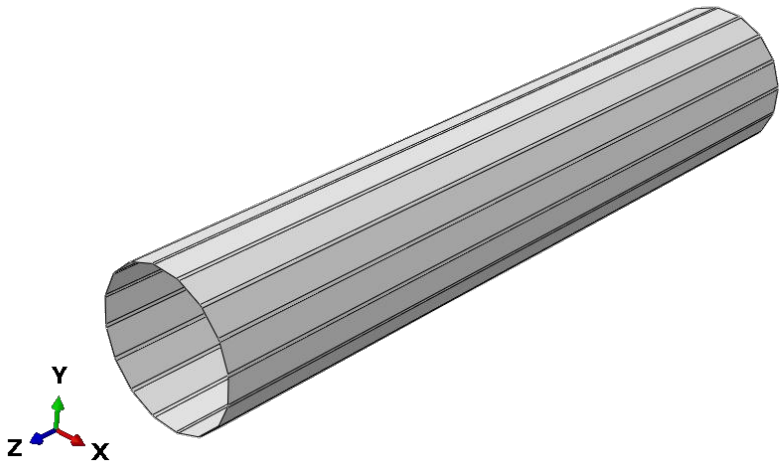

(c) Hexadecagonal hollow section

Figure 3.1: Selected multi-sided tube sections

Mesh density depends on the geometrical properties of the model. In order to achieve appropriate mesh size and to make run time manageable, mesh sensitivity analysis has been conducted. From the mesh sensitivity analysis, it was found that mesh size 30 works well for Octagonal and Dodecagonal sections. However, for Hexadecagonal shape, a mesh size of 20 has been used to get more accurate results. The following figures show the mesh configuration of Octagonal, Dodecagonal, and Hexadecagonal sections, respectively.

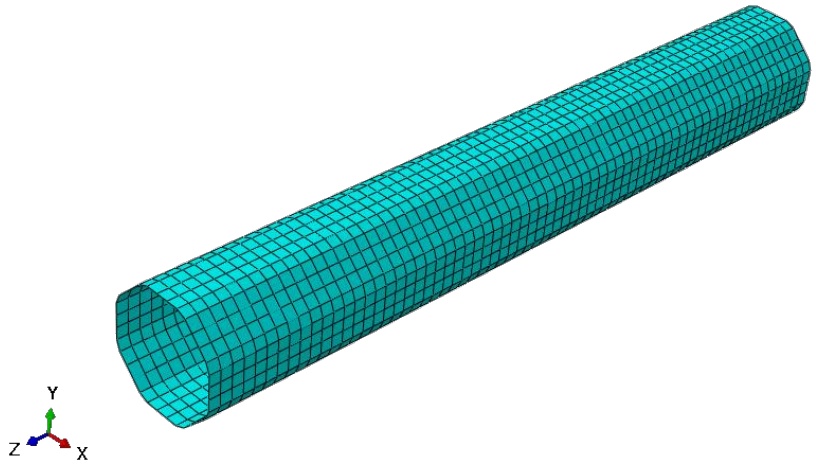

(a) Octagonal section

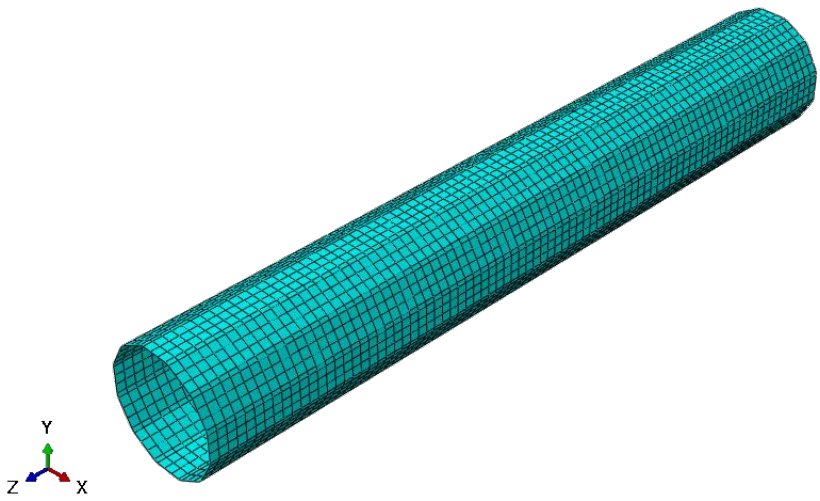

(b) Dodecagonal section

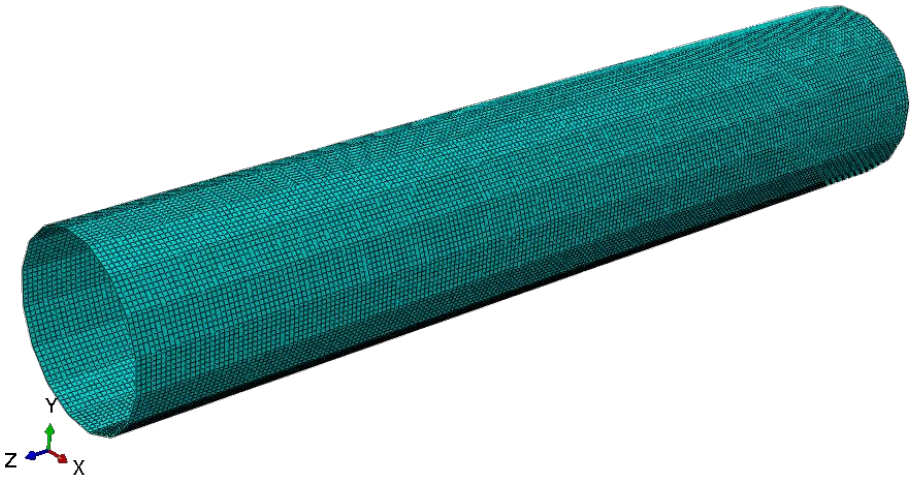

(c) Hexadecagonal section

Figure 3.2: Mesh configuration of (a) Octagonal, (b) Dodecagonal, and (c) Hexadecagonal section

3.2.2 Material properties

The ABAQUS Classical Metal Plasticity rules have been incorporated in all models. According to this rule, the Mises yield surface is used to define isotropic yielding. In ABAQUS, both Isotropic hardening and Kinematic hardening is available. In this study, Isotropic hardening has been adopted for all the models.

Since structural steel exhibit strain hardening, strain hardening properties have been incorporated into the models. As there is a scarcity of readily available strain hardening data, bilinear elastoplastic stress versus strain curve has been used. A strain-hardening of 2% of modulus of elasticity (E) of steel has been used since the post-yield slope approximately equal to 0.5% to 5% of elastic stiffness (Saatcioglu and Humar J, 2003). Modulus of elasticity (E) of 200 GPa, Yield stress (F_y) of 345 MPa, and poison's (ν) ratio of 0.3 have been considered for all the models.

3.2.3 Boundary conditions

Boundary conditions have been chosen to represent the critical condition. All the models excluding models subjected to torsion have simply supported end conditions. The models which are subjected to torsion have one end fixed and another end free.

3.2.3.1 Boundary conditions of members subjected to axial compression, pure bending, and combined bending and compression

Simply supported boundary condition that prevents in-plane and out-of-plane deflections and twists, but allows rotations about both X-axis and Y-axis and also allow warping displacements were used at the supported ends of the member. These boundary conditions were obtained using the following criteria:

i. Right end was restrained against X, Y and Z-axis deflection (U1= U2= U3= 0) and rotation about Z-axis (UR3=0). Rotation about X and Y-axis was kept unrestrained.
ii. Left end was restrained against X and Y-axis deflection (U1= U2= 0) and rotation about Z-axis (UR3=0). Rotation about X and Y-axis and deflection in Z-axis were kept unrestrained.

3.2.3.2 Boundary conditions of members subjected to torsion

For members subjected to torsion, one end has been kept free and another end in a fixed condition. At the fixed end, deflection in X, Y, and Z-axis (U1= U2= U3= 0) and rotation about X, Y, and Z-axis (UR1=UR2=UR3=0) were restrained. At the free end, deflection in X and Y-axis (U1=U2=0) was kept restrained, and all other deflection and rotation were kept unrestrained in all directions.

3.2.4 Load application

Finite element models were analyzed for four different loading conditions as follows-

i. Axial compression
ii. Pure bending
iii. Combined bending and compression
iv. Pure torsion

Constraints have been created between all the edge nodes of the multi-sided tubes and a reference point located at the center of each end. Because of the constraints, any condition applied to the reference points, simultaneously applied to the edge nodes at each end. The same procedure has been followed for all three polygonal cross-sections (*i.e.,* Octagonal, Dodecagonal, and Hexadecagonal section). The following figures show the reference point and constraints created in FE models of the Octagonal Section.

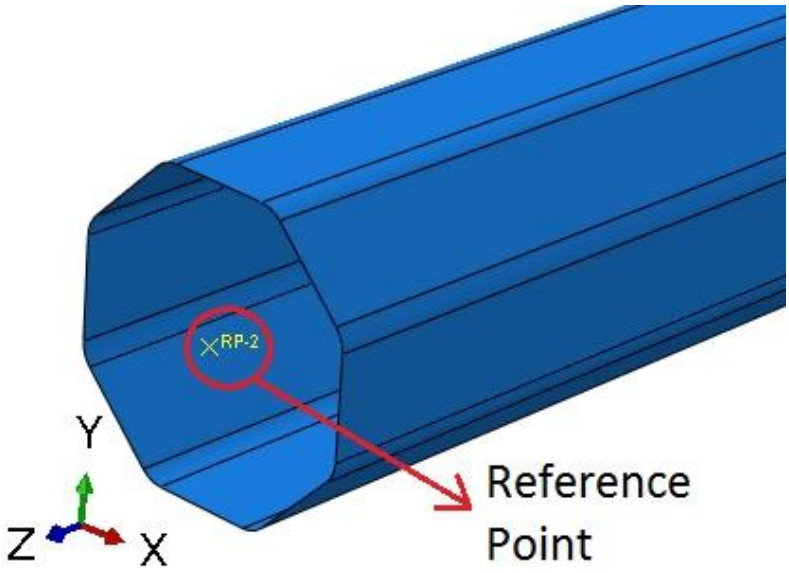

Figure 3.3: Reference point shown for Octagonal multi-sided tube section

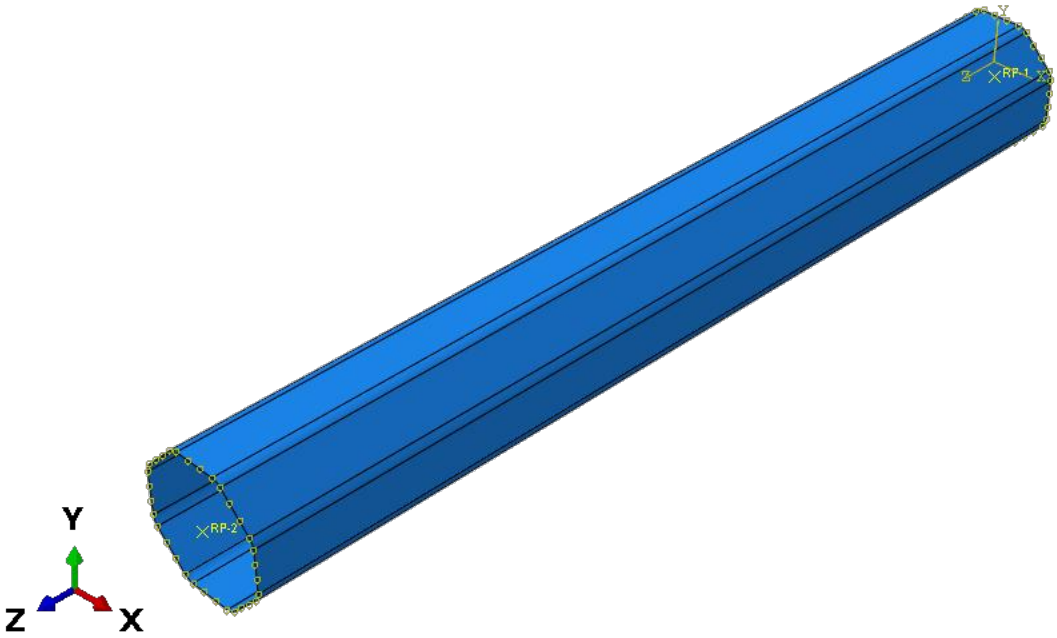

(a) Constraint created at both end

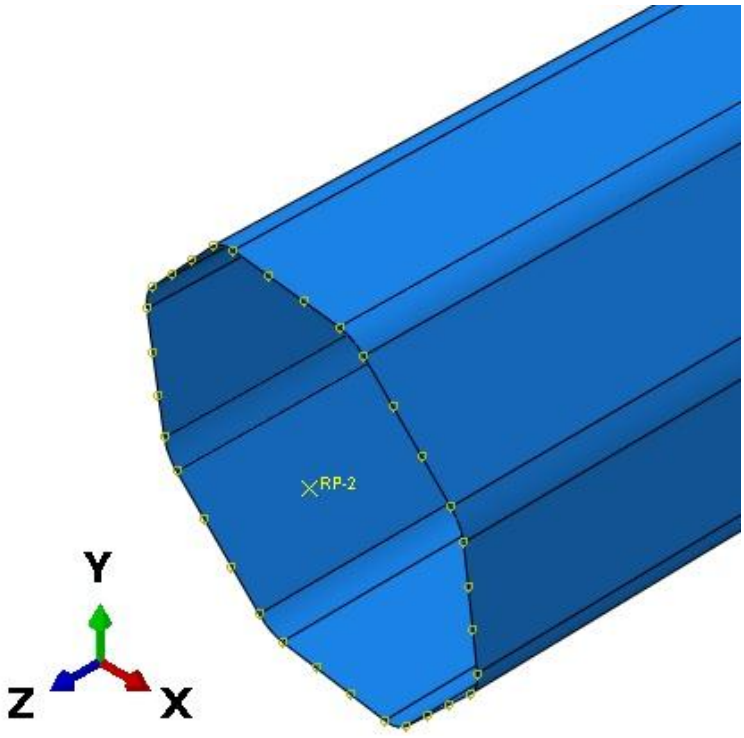

(b) Enlarged view of constraint between edge nodes and reference point

Figure 3.4: Constraints between edge nodes and reference point of Octagonal tube section

Axial load was applied at the left end of the member through a reference point, as shown in Figure 3.3. The load was applied in the negative Z-direction to create a compressive load to the hollow column.

Furthermore, for the members under pure bending, a constant bending moment along the length of the member was applied about X-axis. The bending moment was applied at the two reference points at each end of the multi-sided tube. Additionally, to see the effect of the moment gradient, some of the models were subjected to a concentrated load in the middle of the span. The concentrated load was applied at the reference point created at mid-span. The direction of the concentrated load was along Y-axis. Besides, in order to investigate the effect of support condition on local buckling capacity of multi-sided tube sections, some of the simply supported multi-sided sections previously considered for the constant bending moment are reanalyzed

when they have cantilever support conditions. The cantilever multi-sided tube sections are subjected to a constant moment along the length of the members by applying a concentrated moment (about X-axis) at the free end of the members.

Moreover, a constant bending moment about X-axis and axial force along the negative Z-axis was applied simultaneously to simulate combined loading conditions. For the members under torsion, a moment was applied at the free end about Z-axis.

3.2.5 FE model Analysis type

Both elastic buckling analysis and nonlinear static analysis have been performed to estimate the critical buckling load, flexural capacity, and torsional capacity of the multi-sided tube. First, an Eigenvalue analysis has been performed using the linear perturbation buckling analysis. From the Eigenvalue analysis, Eigenvalues of corresponding Eigenmodes have been extracted. In this study, three eigenvalues for each member are obtained.

Finally, the Static RIKS method (ABAQUS 2014) has been used to conduct the nonlinear buckling analysis. RIKS method is suitable for predicting buckling, post-buckling, or collapse of certain types of structures. RIKS method is based on the Arc-length method and a form of Newton-Raphson iteration method. It uses an additional unknown, named load proportionality factor. RIKS method provides solutions for load and displacement simultaneously. From the nonlinear buckling analysis, the maximum Load Proportionality Factor (LPF) has been extracted to estimate the critical buckling load.

3.2.6 Initial geometric imperfection

Geometric imperfections are always present in steel shapes unintentionally. These imperfections result from fabrication, transportation, or mishandling of steel shapes. These initial geometric

imperfections can be located at any location. These random imperfections initiate buckling deformations. So, it is really important to include the imperfection into the FE models.

In the FE model, geometric imperfections can be predicted by conducting Eigenvalue Analysis. Eigenvalue analysis provides the worst case of local and overall buckling modes. These modes are factored by imperfection test result magnitudes (Ellobody 2014).

It is important to note that there is a scarcity of real imperfection data to readily incorporate into FE models. In this study, an imperfection value of 10% of the thickness of the specimen was used for all the models. Geometric imperfection was applied to trigger the buckling of the models. As lowest eigenvalue refers to the load which initiates the buckling of a structure, geometric imperfection has been applied to the buckling mode obtained from the lowest eigenvalue from eigenvalue analysis (Trahair 1993).

3.3 Validation of finite element model

FE model has been validated against two different experimental test results of Godat et al. (2012) and Bräutigam et al. (2017). The following subsections present the details of validation.

3.3.1 Validation of FE model subjected to axial compression

The developed finite element model is validated against the experiment conducted by Godat et al. (2012). In the experiment, six stub columns of three different cross-sections (*i.e.,* Octagonal, Dodecagonal, and Hexadecagonal) were tested under concentric compression. For each cross-sectional profile, two different plate width-thickness ratios were considered. Columns were simply supported with 780mm length. Geometric imperfection in the plate surface was measured and reported in the study. Table 3.1 shows the geometric and mechanical properties of the specimen tested by Godat et al. (2012).

Table 3.1: Geometry and mechanical properties of the validated specimens (Godat et al. 2012)

Specimen	Number of Sides, n	Plate Thickness, t (mm)	Flat width, w (mm)	Yield Stress, F_y (Mpa)	Modulus of Elasticity, E (GPa)	Yield Strain, ε_y x 10^-3	Ultimate Strain, ε_u (%)
OCT-1-A	8	1.897	95	279	200	1.4	26
OCT-4-A	8	1.367	75	265	199	1.3	27
DODE-1-A	12	1.367	76	273	206	1.3	24
DODE-2-A	12	1.897	75	305	218	1.4	25
HEXA-1-A	16	1.519	52	277	199	1.4	26
HEXA-4-A	16	1.897	60	302	200	1.4	26

To simulate the experimental results, all the geometric and mechanical properties of specimens have been kept the same in the FE model as the experiment. End conditions have been kept simply supported as the experiment. During the test, the compressive load was applied through a top plate, which was modelled with 10-node tetrahedral element C3D10 (ABAQUS 2014). C3D10 is a general-purpose tetrahedral element. The uniformly distributed load was applied at the top surface of the top plate. To transfer the load from the top plate to the multi-sided hollow column section, tie constraints were introduced between the top surface of the plate and the top nodes of the multi-sided section. Both linear and nonlinear buckling analysis was performed to estimate the critical buckling load. Imperfections values that were measured during the test have been introduced as an amplitude of the first mode of buckling. Table 3.2 shows critical buckling loads found from FE models (P_{FEM}) from nonlinear analysis and experiment ($P_{Experiment}$) for the validated models. The table shows that the maximum difference between FE models and experiment results is around 7%. Figure 3.5 shows the deformed shape of an Octagonal section obtained from the FE analysis and experiment. Similar to the experiment, the local buckling was observed near the top end of the section.

Table 3.2: Critical buckling load obtained from FE models and experiment for the validated models

Specimen	Number of Sides, n	Critical Buckling Load from FE Models, P_{FEM} (KN)	Critical Buckling Load from Experiment, $P_{Experiment}$ (KN)	% Difference
OCT-1-A	8	313.1	327	4.24
OCT-4-A	8	186.6	198	5.75
DODE-1-A	12	301.5	325	7.22
DODE-2-A	12	482.1	515	6.38
HEXA-1-A	16	319.4	317	0.75
HEXA-4-A	16	495.6	508	2.45

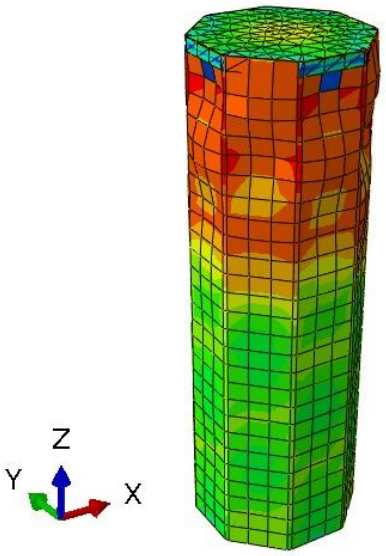

(a) Deformed shape of Octagonal section obtained from FE analysis

(b) Deformed shape of Octagonal section obtained from experiment (Godat et. al. 2012)

Figure 3.5: Deformed shape of Octagonal section from test and FE analysis

3.3.2 Validation of FE models subjected to bending

Bräutigam et al. (2017) have experimentally investigated local buckling behavior of polygonal sections having 16-sides under pure bending. Three-point bending test was conducted on two different classes of sections (*i.e.,* class 1 and class 4) of Hexadecagonal section. The classification of the section is according to Eurocode 3. Each section had a span of 8.0 m. Each specimen had yield stress (F_y) of 355 MPa. The following table shows the geometric properties used in the experiment.

Table 3.3: Geometric properties of the specimens tested by Bräutigam et al. (2017)

Specimen	Number of sides, n	Flat width, w (mm)	Plate thickness, t (mm)	w/t	Internal bend radius, r_b (mm)
Hexa-Bend-1	16	114	5	23	11
Hexa-Bend-2	16		3	38	

FE models were validated against the experiment conducted by Bräutigam et al. (2017). Geometric properties were kept the same as the test. An initial imperfection of 10% of the thickness of the specimen has been used. To apply the bending moment, a concentrated load was applied at the mid-span of the specimen. Bräutigam et al. (2017) have provided the ratio of bending resistance to yield moment ($M_{Experiment}/M_y$) for the test specimens. Yield moment (M_y) has been calculated for the specimens. To compare with the test results, FE results to yield Moment (M_{FEM}/M_y) have been found. Table 3.4 shows the result obtained from FE models and experiments of Bräutigam et al. (2017). Moreover, the following figures show the typical deformed shape obtained from the FE model and the experiment. In the FE model, local buckling was observed near the mid-span, which is similar to the experimental deformed shape.

Table 3.4: Critical bending moment capacity obtained from FE models and experiment for the validated models

Specimen	Critical Bending Moment from FE Models, M_{FEM} (KN-m)	Yield Moment, M_y (KN-m)	M_{FEM}/M_y	$M_{Experiment}/M_y$	% Difference
Hexa-Bend-1	619.09	505.86	1.22	1.21	1.14
Hexa-Bend-2	316.55	305.56	1.04	1.00	3.60

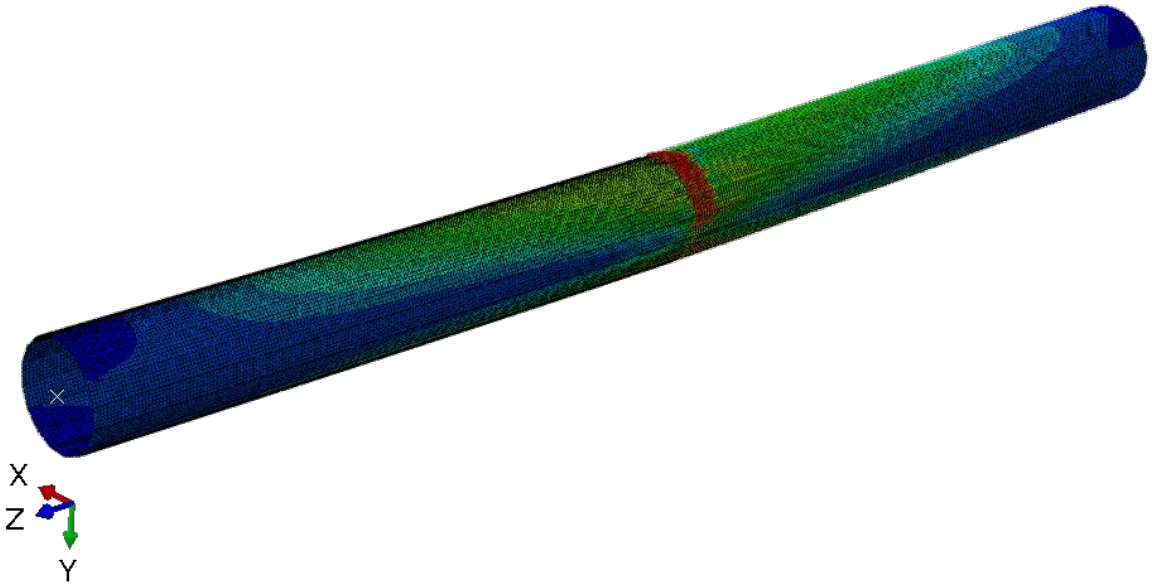

(a) Deformed shape of Hexa-Bend-1 from FE analysis

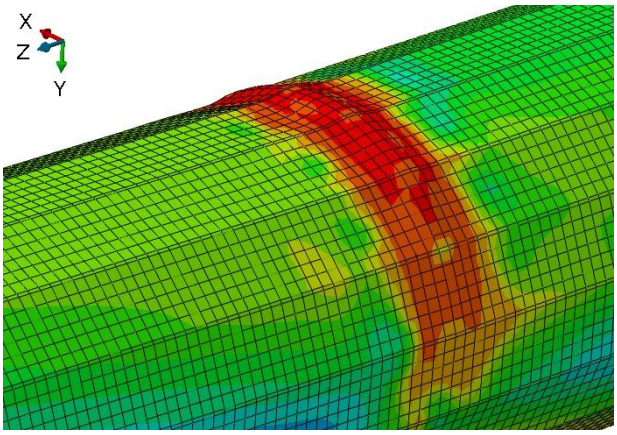

(b) Enlarged view of deformed shape of Hexa-Bend-1 from FE analysis

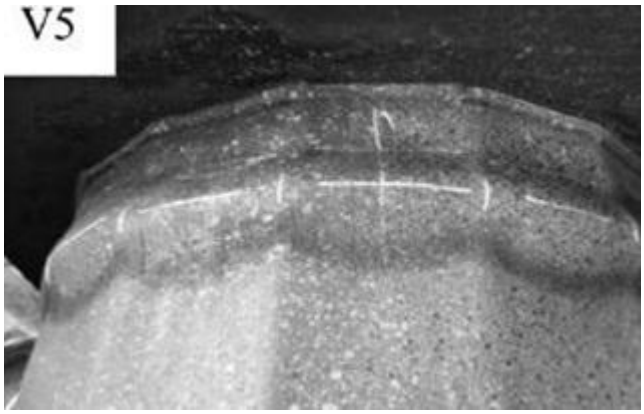

(c) Deformed shape of Hexa-Bend-1 from experiment of Bräutigam et. al. (2017)

Figure 3.6: Deformed shape of Hexa-Bend-1 from FE analysis and experiment

3.4 Summary

Details of finite element modelling have been discussed in this chapter. A nonlinear finite element model has been developed in ABAQUS. Three different geometry, namely, eight, twelve, and sixteen-sided polygonal sections have been considered. The selection of element type, mesh configuration, material properties, boundary conditions, and application of load have

been discussed in detail. This chapter also contains the details of the inclusion of initial geometric imperfection in the FE model. Both elastic buckling analysis and nonlinear static analysis have been performed to estimate the critical capacity of the multi-sided tube. The developed FE model has been validated against experimental results from stub column tests of 8, 12, and 16-sided cross-sections. The FE model is further validated against experimental test results of 16-sided cross-sections subjected to pure bending.

Chapter 4 Behavior of Multi-sided Tubes under Axial Compression and Bending

4.1 Introduction

The validated finite element (FE) model has been used to conduct more analyses to observe the local buckling behavior of multi-sided tube under different loading conditions for various width-thickness ratios (b/t). This chapter presents the local buckling behavior of the multi-sided tube under axial compression and pure bending in brief. Section 4.2 describes the geometric property selection criteria. Following sections 4.3 and 4.4 show the FE model results under axial compression and constant bending moment, respectively. Moreover, some of the models were reanalyzed under the moment gradient, which is presented in section 4.5. Furthermore, section 4.6 shows the FE analysis of models under constant moment for different end conditions. For all the models, local buckling failure was observed. Details of geometric property and FE results are provided in Appendix A.

4.2 Geometric property selection criteria

For all the FE models, element width (b), wall thickness (t), and inside bend radius (r_b) have been chosen according to AASHTO (AASHTO, 2015).

As previously discussed in Chapter 2, AASHTO provided an equation to determine the element width (b) of multi-sided tubular sections. Furthermore, according to AASHTO, multi-sided tube sections should have a minimum inside bend radius (r_b) of five times tube wall thickness (t) or 25.4 mm, whichever is larger. Element width of multi-sided tubular sections can be found using Equation 4.1:

$$b = tan\left(\frac{180}{n}\right)[D' - 2t - minimum(2r_b, 8t)] \tag{4.1}$$

where D' is the outside distance from the flat side to the flat side of multi-sided tubes, n is the number of sides of multi-sided tubes and ($\frac{180}{n}$) is in degrees.

Figure 4.1 shows the cross-section of the Octagonal section and the geometric property definition used in this study. In Figure 4.1, w indicates the flat width and D indicates the mid-surface distance from flat side to flat side of multi-sided tubes.

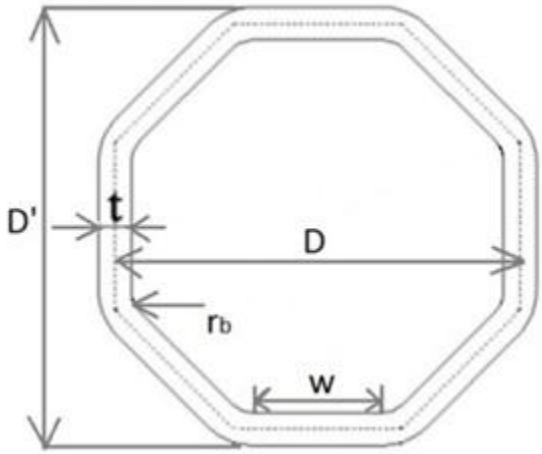

Figure 4.1: Typical cross-section of an Octagonal tube section

Moreover, AASHTO has provided compact limit (λ_p), non-compact limit (λ_r), and maximum width-thickness ratio limit (λ_{max}) for the multi-sided tubes having eight (08), twelve (12) and Sixteen (16) sides as shown in Table 2.1. For detailed FE analysis, b/t ratios were chosen in such a way that compact, non-compact, and slender sections meet the slenderness limits provided by AASHTO for a steel yield strength of 345 MPa. For each polygonal section, element width (b) was kept constant for all FE models, and the wall thickness (t) was varied.

4.2.1 Element width and inside bend radius of FE models

For each polygonal cross-section, one specific element width (b) has been used for all the models under all the loading conditions. The following table shows the element width (b) and internal bend radius (r_b) used for all the FE models.

Table 4.1: Element width and inside bend radius of the FE models

Specimen	Number of Sides, n	Element Width, b (mm)	Inside Bend Radius, r_b (mm)
Octagonal	8	100	Five times tube wall thickness or 25.4 mm, whichever is larger
Dodecagonal	12	95	
Hexadecagonal	16	140	

4.2.2 Length of FE models

Length sensitivity analysis was conducted to get suitable lengths for each polygonal cross-section under axial compression and pure bending. From the length sensitivity analysis, the following lengths were chosen for the FE models. Table 4.2 shows the length (L) for each polygonal section under axial compression and pure bending.

Table 4.2: Length of FE models for different loading conditions

Loading Conditions	Length, L (mm)		
	Octagonal	Dodecagonal	Hexadecagonal
Axial Compression	1000	1200	2000
Pure Bending	2000	2500	4000

4.3 Multi-sided tubes subjected to axial compression

Sixteen (16) models of each cross-section, a total of forty-eight (48) models have been analyzed under axial compression. The critical compressive resistance of FE models subjected to axial compression has been compared with yield stress (F_y) to verify the width-thickness limit (λ_r) provided by AASHTO. It is also compared with existing codes and studies. Following subsections 4.3.1, 4.3.2 and 4.3.3 present FE results of models under axial compression,

comparison of FE results with codes and previous studies, and comparison of FE results with the yield stress, respectively.

4.3.1 FE Results of models under axial compression

The following Figure 4.2 shows the typical deformed shape of Octagonal, Dodecagonal, and Hexadecagonal tube sections under axial compression. For all the models, local buckling failure was obtained. Furthermore, Figure 4.3 shows the critical buckling load obtained from FE models (P_{FEM}) along with the width-thickness ratio (b/t) for each polygonal section. As expected, with an increase in slenderness ratio, local buckling capacities of multi-sided tube sections decrease.

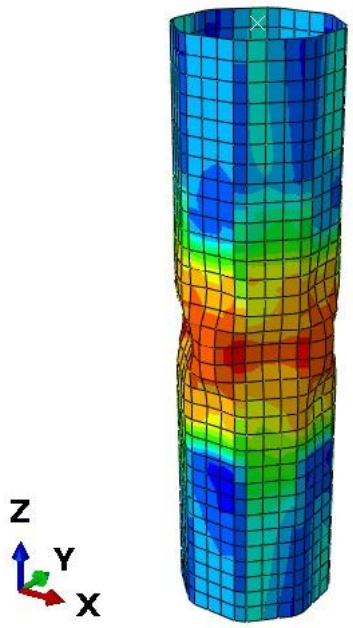

(a) Deformed shape of Octagonal section

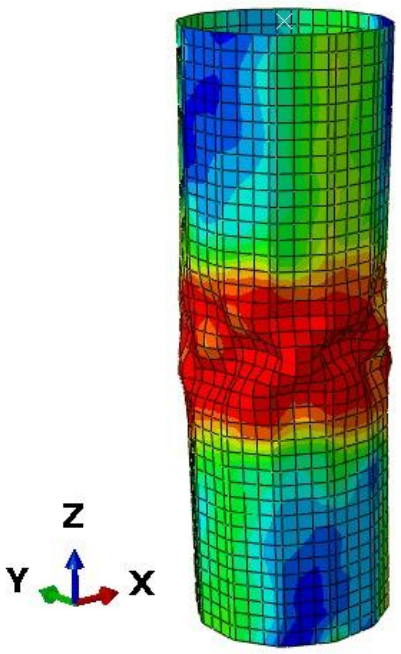

(b) Deformed shape of Dodecagonal section

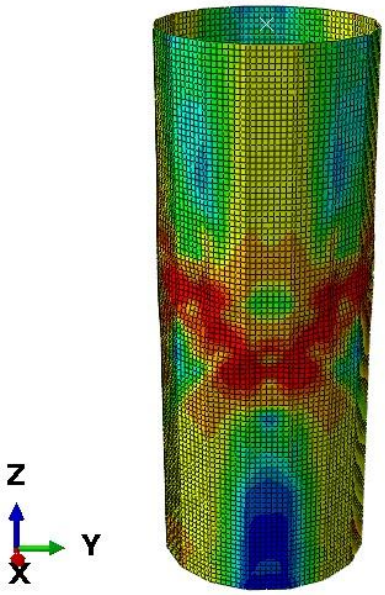

(c) Deformed shape of Hexadecagonal section

Figure 4.2: Deformed shape of (a) Octagonal, (b) Dodecagonal, and (c) Hexadecagonal section under axial compression

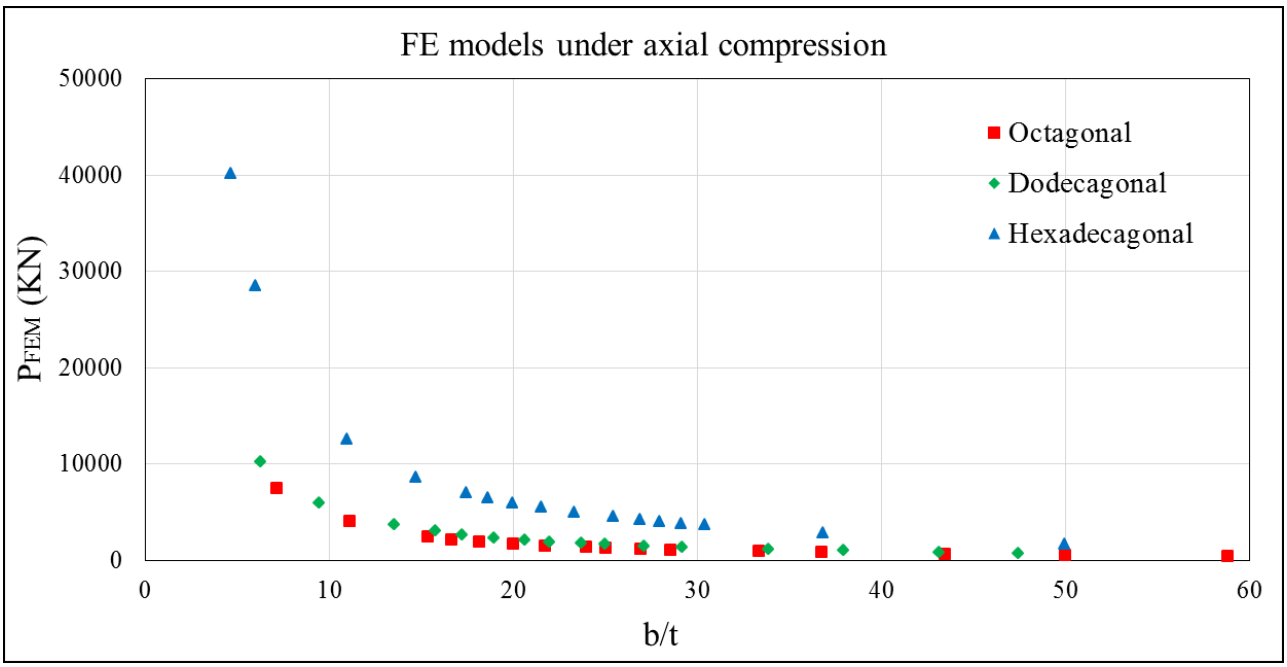

Figure 4.3: Critical buckling load of multi-sided tube sections under axial compression

4.3.2 Comparison of FE results with codes and previous studies

FE results obtained from models under axial compression have been compared with AASHTO, ASCE/SEI 48-11, Eurocode 3, and studies from the literature.

As discussed in Chapter 2, AASHTO has provided equations to calculate critical compressive stress (F_{cr}) of the multi-sided tubular column (AASHTO 2015). Equations 2.11 to 2.15 have been used to calculate critical compressive stress (F_{cr}) for each FE model. ASCE/SEI 48-11 has provided design equations for local buckling capacity of multi-sided steel tubular columns. In this study, equations provided in Table 2.5 have been used to find local buckling capacity of multi-sided tubes under axial compression according to ASCE/SEI 48-11. Moreover, Eurocode 3 (EN 1-1, 2005, EN 1-3, 2006, EN 1-5, 2006) has design equations for plate elements. A multi-sided steel tubular section has been considered as a collection of individual longitudinal plate strips to find the resistance using Eurocode 3. In this study, Equations 2.29 to 2.32 have been used to calculated compressive strength according to Eurocode 3.

Based on the analytical and experimental results, Migita and Fukumoto (1997) have proposed formulas to find the local buckling strength of polygonal sections, as shown in Equation 4.2. Moreover, Godat et al. (2012) have also proposed a design equation for the multi-sided tube subjected to axial compression (Equation 4.3). In Equation 4.3, N-value was proposed to be taken as 2.0.

$$\frac{F_{cr}}{F_y} = \begin{cases} 1 & (\mathrm{R} \leq 0.67) \\ \dfrac{0.74}{\mathrm{R}^{0.75}} & (0.67 < \mathrm{R} \leq 1.3) \end{cases} \tag{4.2}$$

$$F_{cr} = F_y \left(1 + R^{2N}\right)^{\left(-\frac{1}{N}\right)} \tag{4.3}$$

The following Figure 4.4 shows the graphical comparison between FE results of models subjected to axial compression with existing codes and studies. In this figure, critical compressive stress (F_{cr}) has been normalized by yield stress (F_y). Here, F_{cr}/F_y has been plotted against Plate width-thickness parameter (R), which was calculated using Equation 2.6.

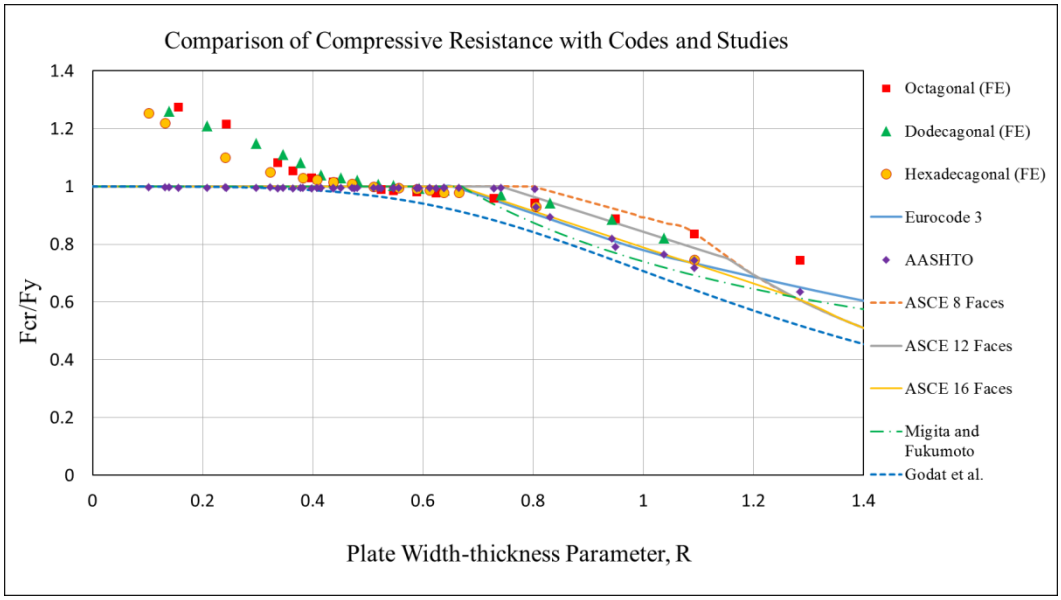

Figure 4.4: Comparison of compressive resistance from FE analysis with different codes and studies

Following observations can be made from comparison of compressive resistance of FE models with different codes and studies (Figure 4.4):

i. FE analyses provide capacities either close to the three codes or higher than the codes for plate width-thickness parameter (R) value up to 0.66, indicating that codes' equations for compressive resistance are conservative in this range.
ii. Beyond the R-value of 0.66, ASCE/SEI 48-11 provides three different curves for 8-, 12-, and 16-sided sections. Both 12- and 16-sided curves are predicting pretty close results to FE results up to R-value of around 1.1. However, for octagonal sections, ASCE/SEI 48-11 predictions are higher than that obtained from FE analyses in this range.
iii. Both AASHTO and Eurocode 3 provide good predictions for the compressive resistance for multi-sided tube sections. Moreover, equation of Migita and Fukumoto (1997) is predicting pretty close results to AASHTO and Eurocode 3.
iv. Design equation of Godat et. al. (2012) is conservative as compared to all other resistances.

4.3.3 Comparison of FE results with yield stress

FE results obtained from models under axial compression have been compared with yield stress (F_y). The ratio of compressive stress obtained from the FE model (F_{FEM}) and yield stress (F_y) is plotted in the same graph along with the non-compact limit (λ_r) provided by AASHTO for different multi-sided tubes (Figure 4.5). Non-compact limit (λ_r) has been shown to verify if the non-compact sections are able to reach yield stress or not before buckling locally. This figure includes all the FE models of each polygonal cross-section (i.e. Octagonal, Decagonal and Hexadecagonal) under axial compression.

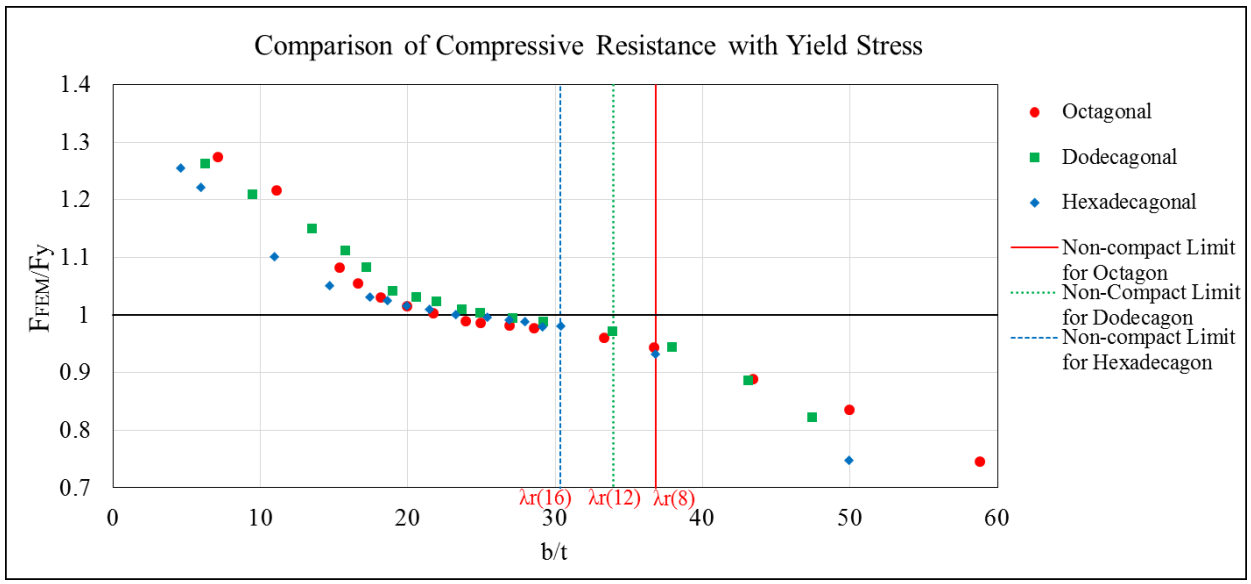

Figure 4.5: Comparison of compressive resistance from FE analysis with yield stress

From Figure 4.5 it is observed that, some of the Octagonal and Dodecagonal sections having a width-thickness ratio (b/t) within the non-compact limit (λ_r) could not reach yield stress (F_y). Though AASHTO has provided three different non-compact limits (λ_r) for different cross-sections, all sections having a width-thickness ratio (b/t) within the non-compact limit (λ_r) of Hexadecagonal section could reach capacities close to yield stress (F_y). This means using the non-compact limit (λ_r) of the Hexadecagonal section for all three sections under axial compression is safer.

4.4 Multi-sided tubes subjected to constant moment

Twenty-six (26) models of each cross-sectional profile, a total of seventy-eight (78) models, were subjected to constant moment along the lengths. These models include compact, non-compact, and slender sections according to AASHTO. Moreover, ten (10) models of each cross-section, a total of thirty (30) models were developed with a different width (b), 120mm, 115mm and 160mm for Octagonal, Dodecagonal and Hexadecagonal, respectively.

Following subsections 4.4.1, 4.4.2 and 4.4.3 presents FE results of models under constant moment, comparison of bending capacity with codes, and comparison of bending capacity with plastic moment and yield moment, respectively.

4.4.1 FE Results of models under constant moment

Deformed shape of each cross-section has been extracted from FE models. Figure 4.6 shows deformed shapes of Octagonal, Dodecagonal, and Hexadecagonal sections subjected to constant moment along the length. Furthermore, Figures 4.7 and 4.8 show the bending capacities (M_{FEM}) obtained from nonlinear FE analyses. Here two separate diagrams have been used for two distinguished widths (b) of each polygonal cross-section. As shown in Figure 4.7 and 4.8, for all three multi-sided tube shapes, bending moment capacity decreases with an increase in width-thickness ratio (b/t).

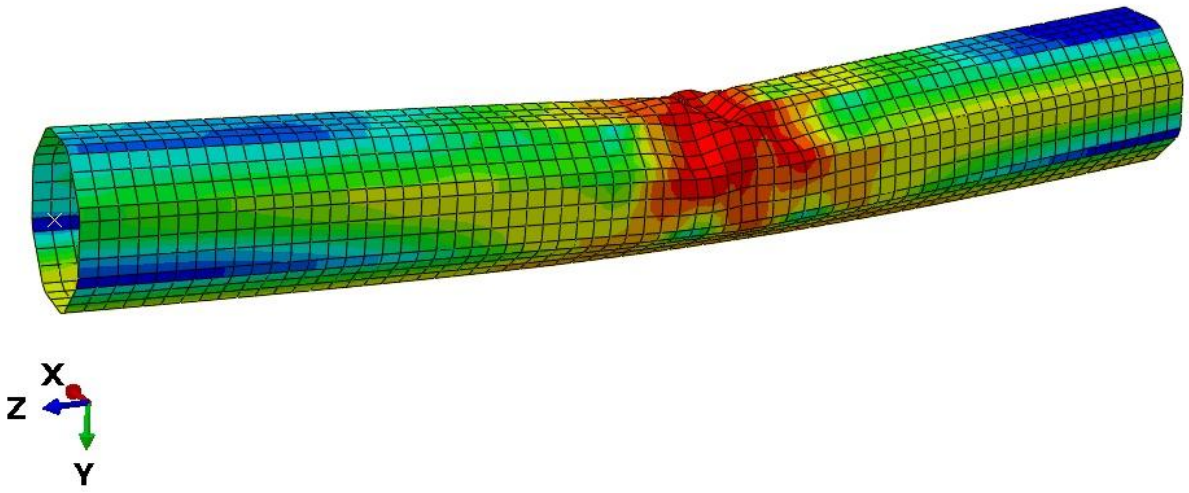

(a) Deformed shape of Octagonal section

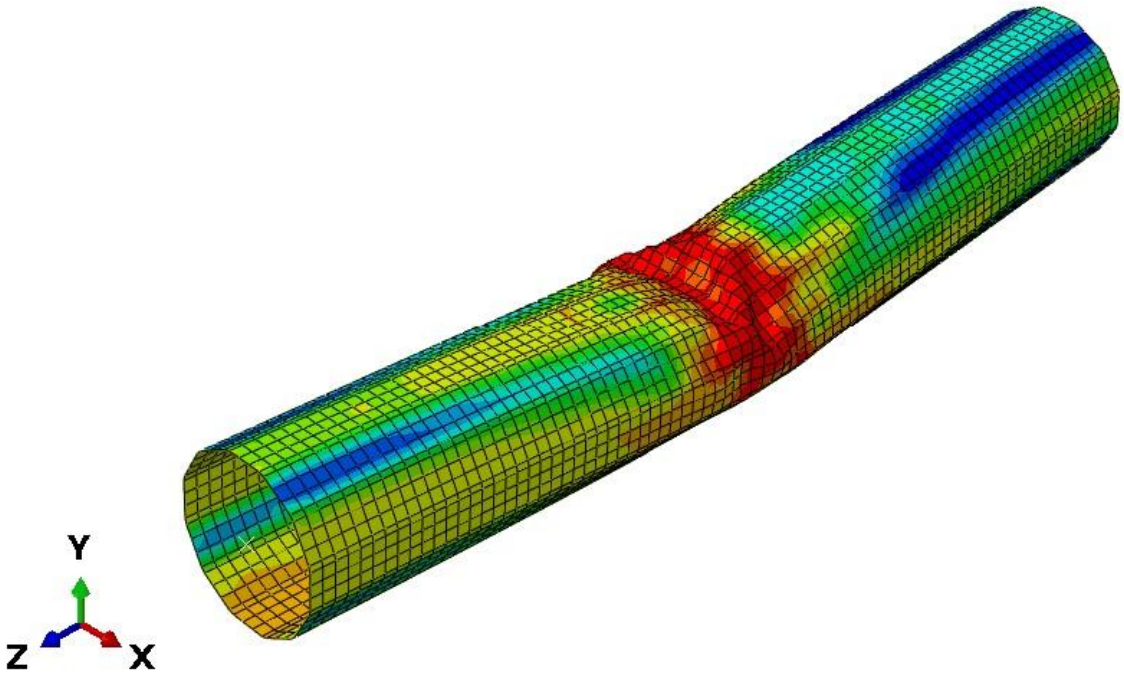

(b) Deformed shape of Dodecagonal Section

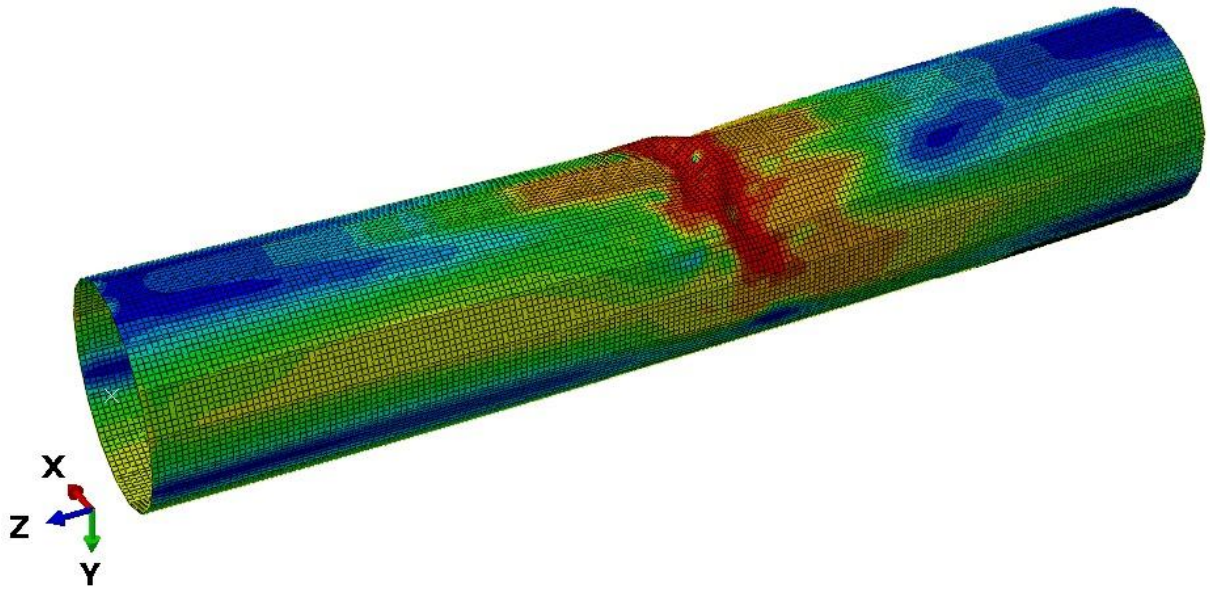

(c) Deformed shape of Hexadecagonal section

Figure 4.6: Deformed shape of (a) Octagonal, (b) Dodecagonal, and (c) Hexadecagonal section under constant moment

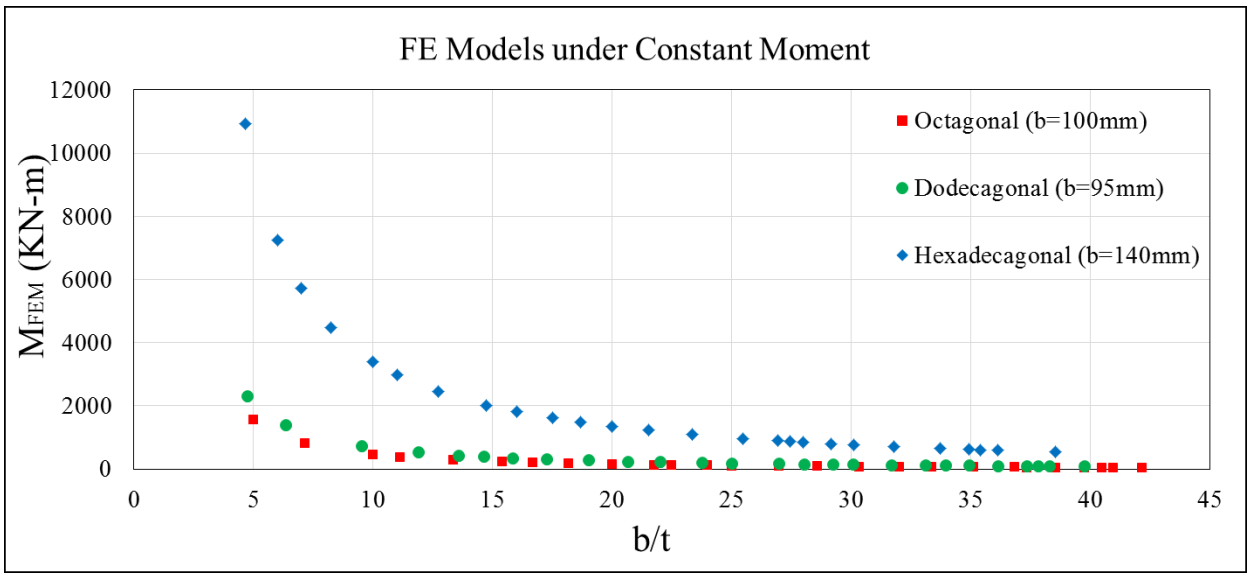

Figure 4.7: Critical bending capacity of multi-sided tube sections under constant moment

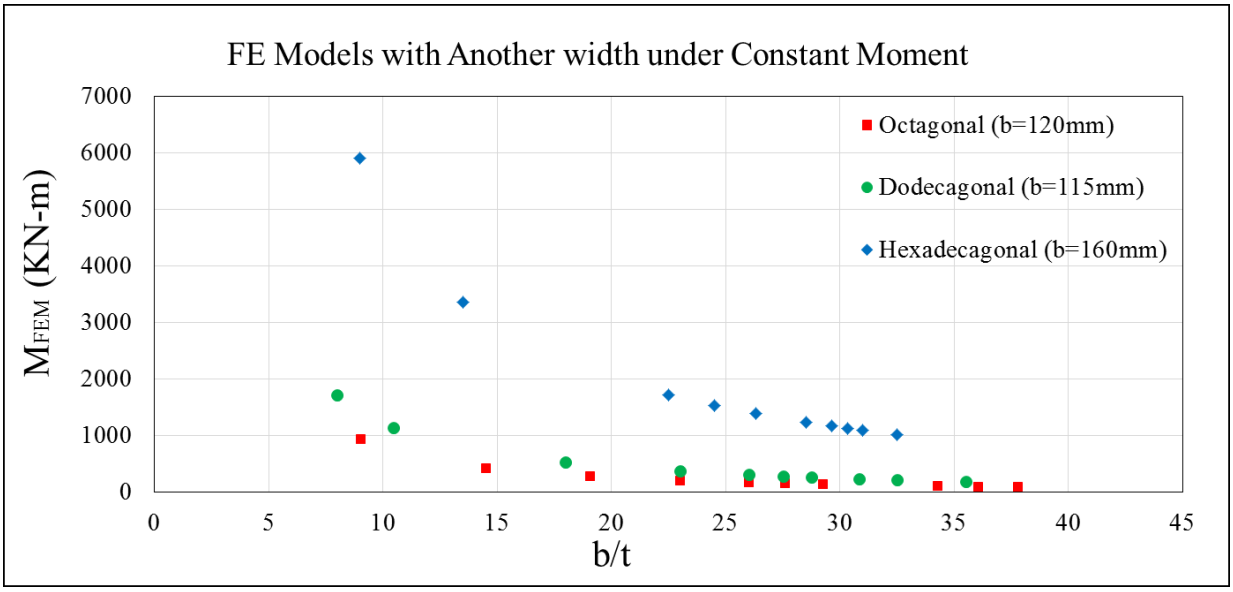

Figure 4.8: Critical bending capacity of multi-sided tube sections under constant moment with different width

4.4.2 Comparison of bending capacity with codes

Finite element analysis results obtained from models subjected to pure bending have been compared with the flexural strength predicted in AASHTO, ASCE/SEI 48-11, Eurocode 3, and EN 50341-1. As discussed in Chapter 2, AASHTO has provided nominal bending capacity equations for compact, non-compact and slender sections (Table 2.3). It is also mentioned in

AASHTO that the nominal bending capacity of the multi-sided tube section should not exceed the bending capacity of the round tube section with equivalent diameter. AASHTO has suggested plastic moment capacity for the compact sections under bending. ASCE/SEI 48-11 has suggested yield moment capacity for all the multi-sided tube sections. On the other hand, Eurocode 3 has suggested bending moment capacity based on the class of the section (*i.e.,* class 1, class 2, class 3, and class 4). For class 1 and class 2 multi-sided tube section, Eurocode 3 suggests plastic moment capacity. For the class 3 section, the yield moment capacity should be considered. For class 4 multi-sided tube sections, effective widths may be used to make the necessary allowances for reductions in resistance to include the effects of local buckling. On the other hand, EN 50341-1 has considered all the multi-sided tube sections either class 3 or class 4. For the class 3 section, yield moment capacity should be considered, and for class 4 cross-sections, effective widths may be used due to the effects of local buckling. For all the multi-sided tube sections subjected to constant moment, bending capacity has been calculated according to AASHTO, ASCE/SEI 48-11, Eurocode 3, and EN 50341-1.

Figures 4.9 to 4.11 show the graphical comparison of bending moment capacities obtained from FE analyses with that obtained from four different codes for Octagonal, Dodecagonal, and Hexadecagonal sections, respectively. Moreover, in these figures, compact (λ_p) and non-compact limit (λ_r) of AASHTO are shown.

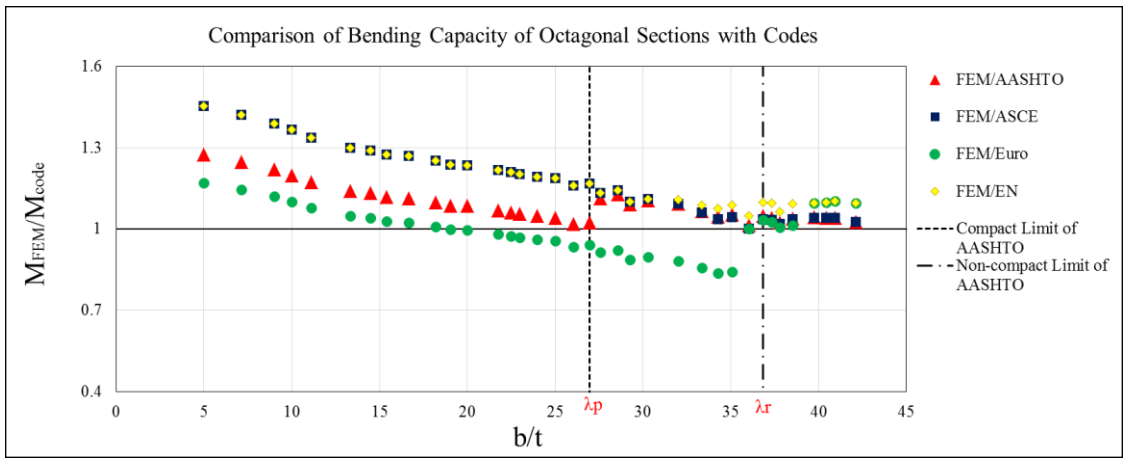

Figure 4.9: Comparison of critical bending capacity of Octagonal sections with codes

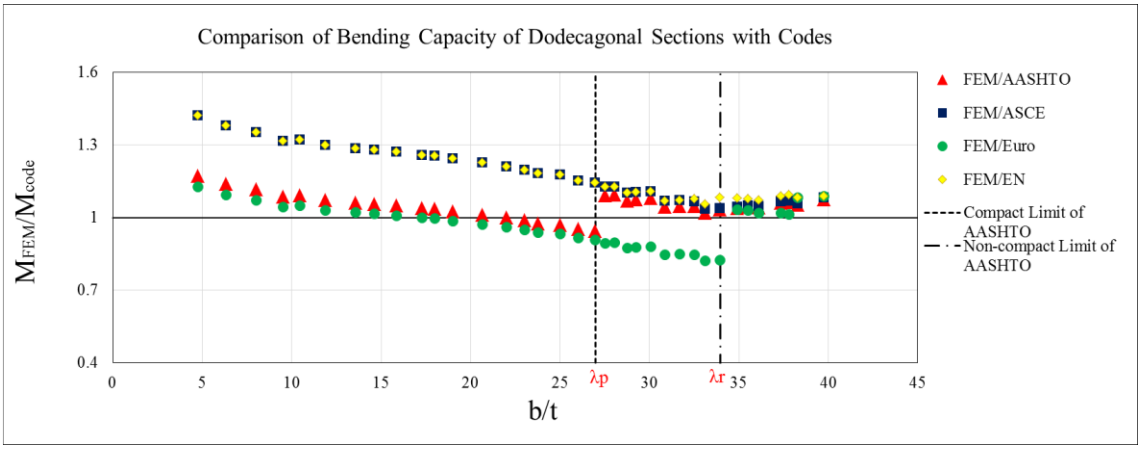

Figure 4.10: Comparison of critical bending capacity of Dodecagonal sections with codes

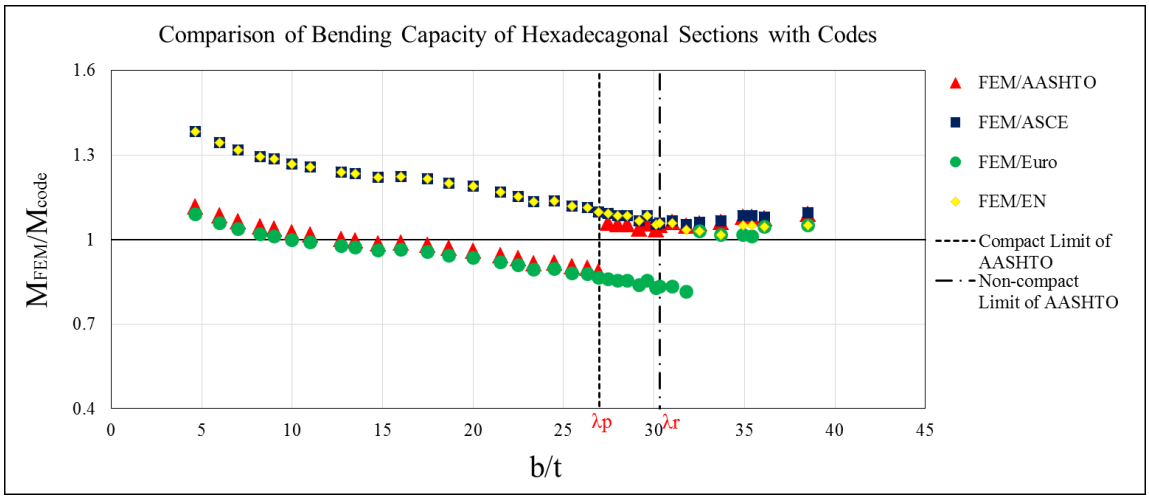

Figure 4.11: Comparison of critical bending capacity of Hexadecagonal sections with codes

Following observations can be made from the comparison between bending resistance of FE models, and code suggested capacities (Figures 4.9 to 4.11):

i. M_{FEM}/M_{AASHTO} ratios are more than 1.0 for the entire Octagonal sections. However, the ratio is less than 1.0 for a few Dodecagonal and a large number of Hexadecagonal compact sections, indicating that AASHTO overestimates the flexural strength for the compact Dodecagonal and Hexadecagonal section.

ii. M_{FEM}/M_{ASCE} ratio is more than 1.0 for all FE models. Since ASCE/SEI 48-11 suggests the use of elastic bending capacity for the design of all multi-sided tube sections, the ratio is pretty higher than 1.0 for the compact sections.

iii. Since EN 50341-1 also suggests the elastic capacity for the design of compact and non-compact multi-sided tube sections subjected to flexure, M_{FEM}/M_{EN} ratios are exactly the same as M_{FEM}/M_{ASCE} ratios for the majority of the sections. However, for the rest of the sections, EN 50341-1 is suggesting class 4 section capacities.

iv. M_{FEM}/M_{Euro} ratio is less than 1.0 for most of the sections as Eurocode 3 suggests full plastic moment capacity for class 1 and class 2 sections, which includes the entire compact and most of the non-compact sections (Compact and non-compact defined as AASHTO). However, near the non-compact limit (λ_r), there is a sudden increase in the ratio as Eurocode 3 suggests the elastic capacity for class 3 sections.

4.4.3 Comparison of bending capacity with the plastic moment and yield moment

For each model subjected to constant moment along the length, plastic moment (M_p) and yield moment (M_y) have been calculated. Details calculation of plastic moment (M_p) and yield moment (M_y) have been shown in Appendix B.

The following Figures 4.12 to 4.14 show the comparison of the bending capacity of the FE model (M_{FEM}) with the plastic moment (M_p) for Octagonal, Dodecagonal, and Hexadecagonal, respectively. The compact limit (λ_p) of AASHTO has been shown in Figures 4.12 to 4.14. In these figures, two different widths (b) for each section were considered.

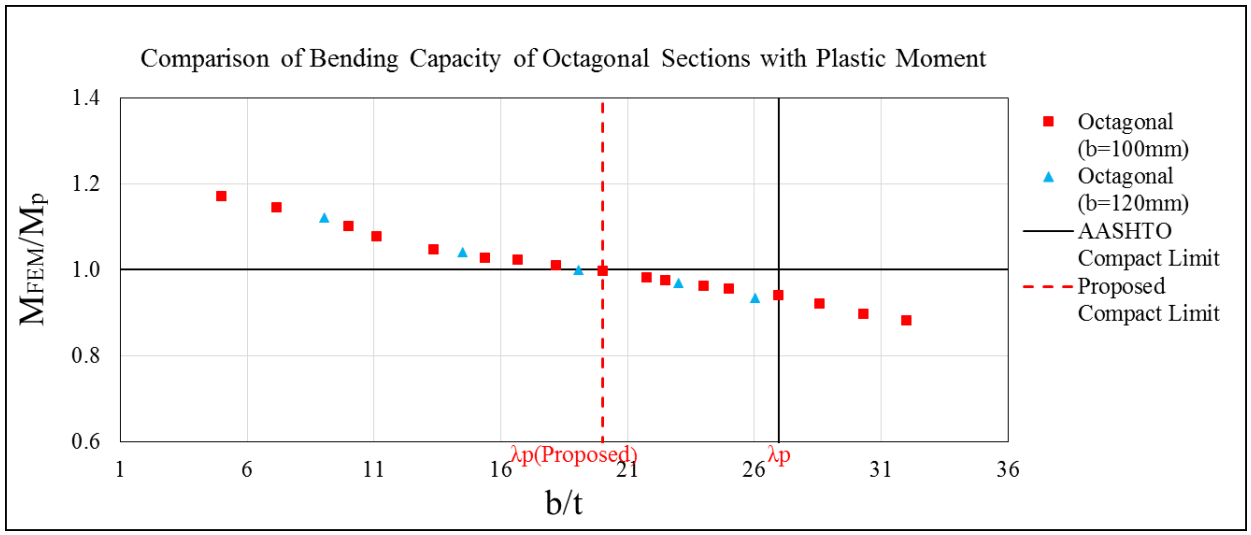

Figure 4.12: Evaluation of compact slenderness limit of Octagonal section

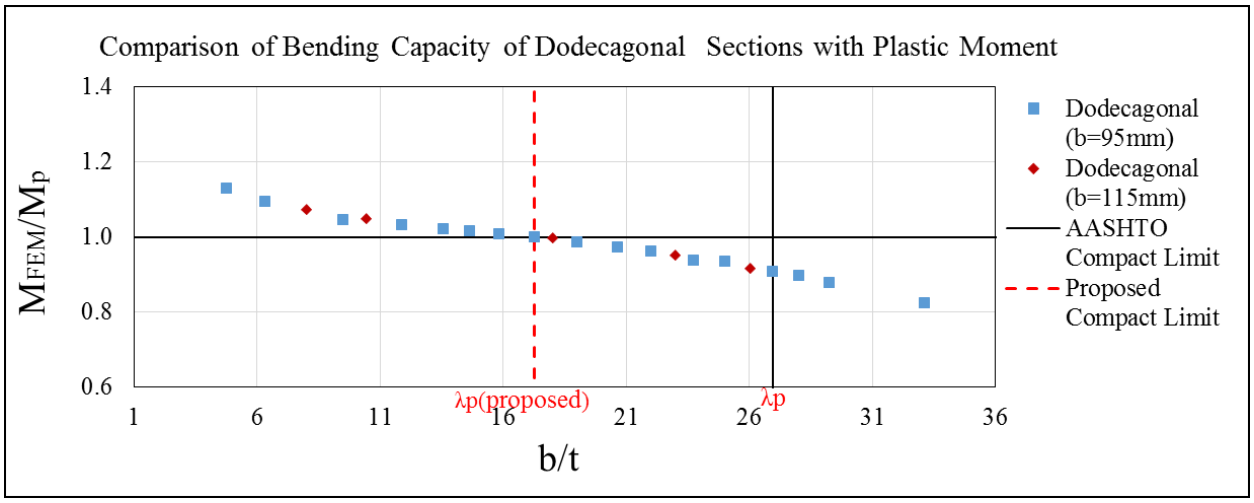

Figure 4.13: Evaluation of compact slenderness limit of Dodecagonal section

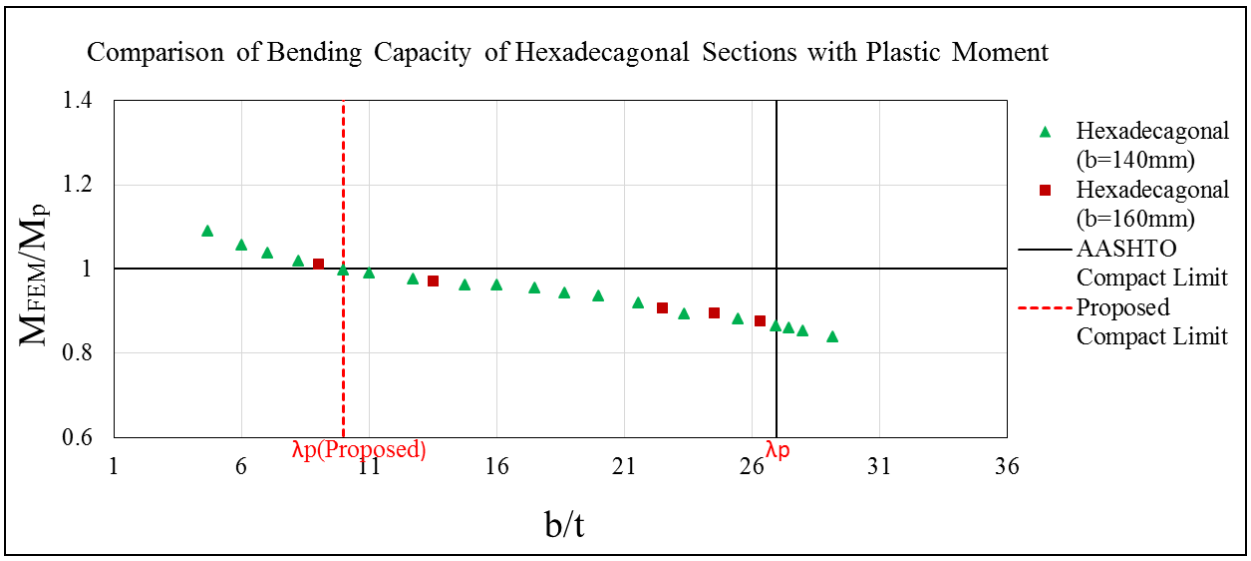

Figure 4.14: Evaluation of compact slenderness limit of Hexadecagonal section

Following observations can be made from the comparison of bending resistance of FE models with plastic moment capacity (M_p) (Figures 4.12 to 4.14):

i. AASHTO has the same compact limit (λ_p) of $1.12\sqrt{E/Fy}$ for Octagonal, Dodecagonal, and Hexadecagonal multi-sided tube sections. However, several compact sections (according to AASHTO) are not able to reach plastic moment capacity. The number of compact sections not reaching plastic moment is increasing with the increasing number of sides.

ii. Thus, a revision may be required for the compact limit (λ_p) suggested by AASHTO for sections subjected to pure bending.

iii. Figures also indicate the proposed width-thickness ratios (b/t) below which all the sections were able to reach their plastic moment capacities (M_p). The proposed compact limits ($\lambda_{p(Proposed)}$) are found as $0.83\sqrt{E/Fy}$, $0.72\sqrt{E/Fy}$ and $0.42\sqrt{E/Fy}$ for Octagonal, Dodecagonal, and Hexadecagonal sections, respectively.

Moreover, Figures 4.15, 4.16, and 4.17 present the comparisons of the bending capacities of the non-compact sections with the yield moments (M_y) for Octagonal, Dodecagonal, and Hexadecagonal sections, respectively. The compact (λ_p) and non-compact (λ_r) limits of AASHTO are also indicated in these figures. Similar to compact sections, two different widths (b) were considered for all three multi-sided tube sections.

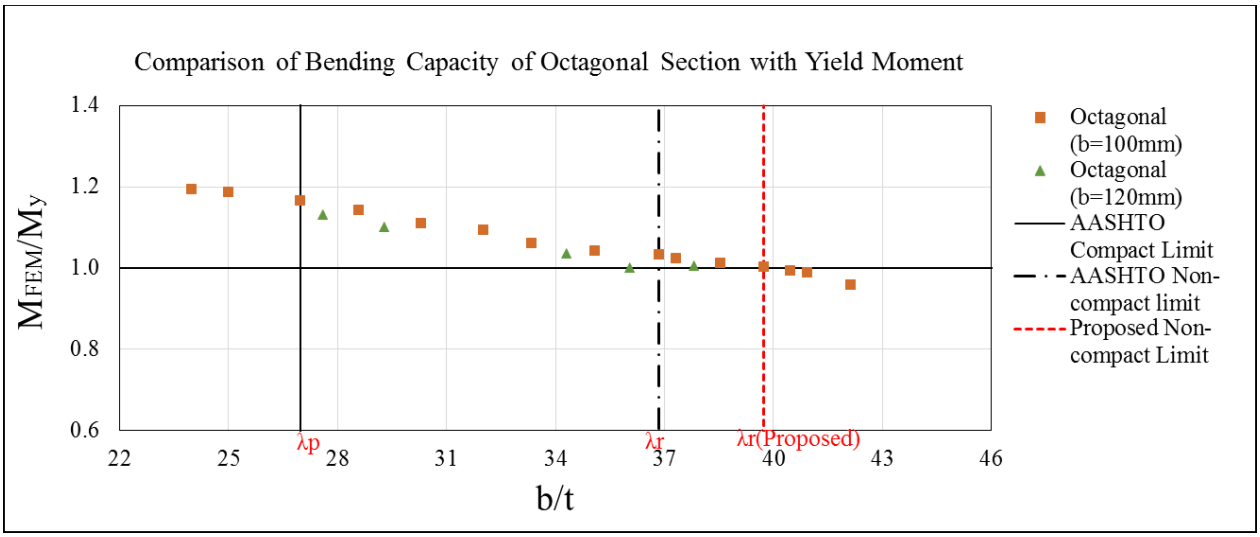

Figure 4.15: Evaluation of non-compact slenderness limit of Octagonal section

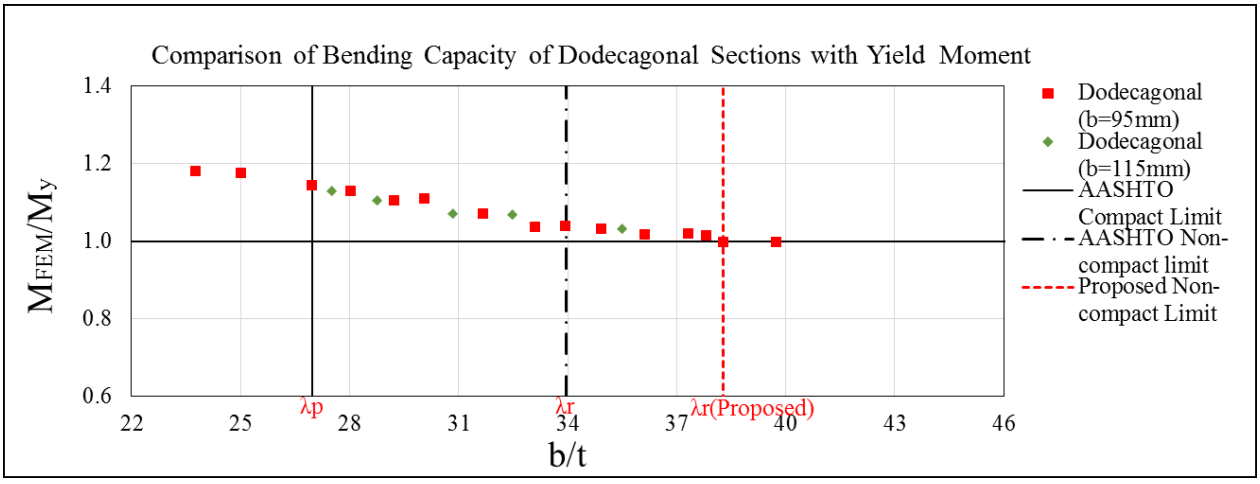

Figure 4.16: Evaluation of non-compact slenderness limit of Dodecagonal section

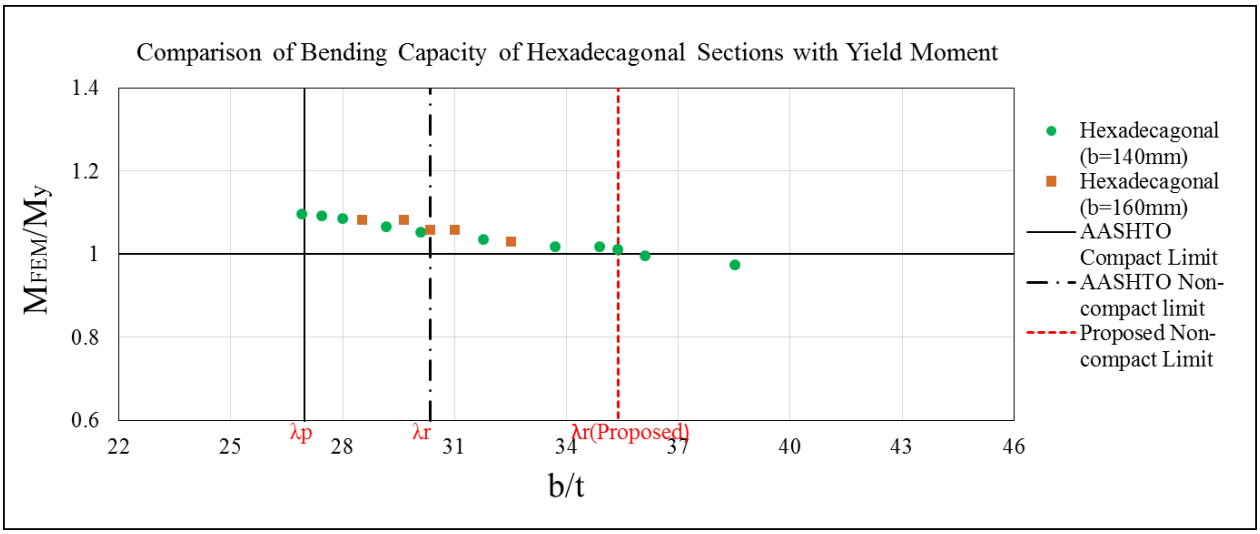

Figure 4.17: Evaluation of non-compact slenderness limit of Hexadecagonal section

The following observations can be drawn from the comparison of bending resistance of FE models with yield moment (M_y) (Figures 4.15 to 4.17):

i. Unlike the compact limit, AASHTO has provided three different non-compact limits (λ_r) for the Octagonal, Dodecagonal, and Hexadecagonal sections.

ii. All the non-compact sections, along with some of the slender sections, could reach yield moment capacities.

iii. Moreover, the width-thickness ratios (b/t) for which the M_{FEM}/M_y ratio is approximately1.0 are also identified. These width-thickness ratios are indicated as the revised non-compact limit ($\lambda_{r(Proposed)}$) in the figure.

iv. It is observed that current AASHTO non-compact limits of $1.53\sqrt{E/Fy}$, $1.41\sqrt{E/Fy}$ and $1.26\sqrt{E/Fy}$ can be increased to $1.65\sqrt{E/Fy}$, $1.59\sqrt{E/Fy}$ and $1.47\sqrt{E/Fy}$ for Octagonal, Dodecagonal, and Hexadecagonal sections, respectively.

4.5 Multi-sided tubes subjected to moment gradient

Local buckling behavior of compact and non-compact multi-sided tube sections was further investigated by subjecting fifteen (15) selected sections to a moment gradient. The sections were subjected to a concentrated load at the middle of the spans. Details of the selected sections are presented in Table A.10 (Appendix A). Following Figures 4.18, 4.19 and 4.20 compare the moment capacities obtained from the concentrated load case with those obtained from the cases when the same sections were subjected to a constant bending moment for Octagonal, Dodecagonal, and Hexadecagonal, respectively. It is observed from the figures that the local buckling capacities obtained from all selected multi-sided tube sections subjected to a concentrated load at their mid-spans are higher than those obtained when the selected sections were subjected to constant moment. In addition, Figure 4.21 shows that except for one Hexadecagonal compact section, all the selected multi-sided tube sections were able to reach their capacities before any local buckling.

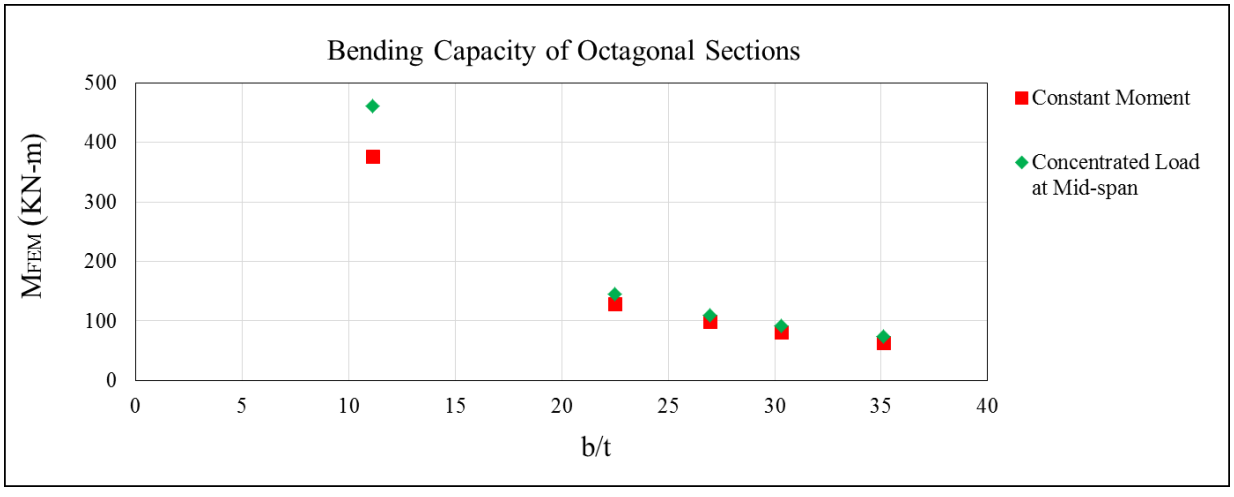

Figure 4.18: Bending capacities obtained from Octagonal section subjected to constant moment and concentrated load at mid-span

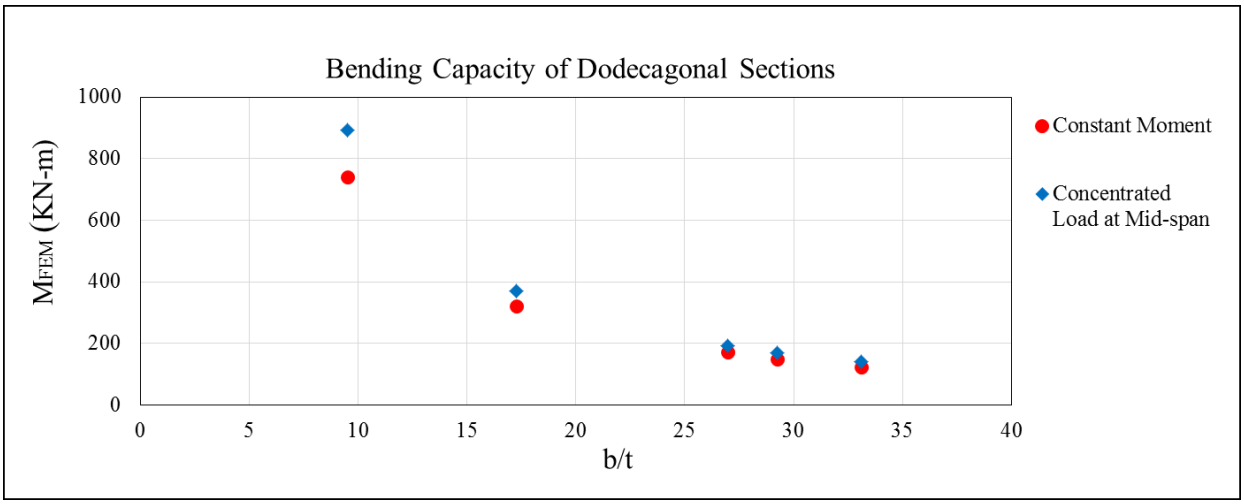

Figure 4.19: Bending capacities obtained from Dodecagonal section subjected to constant moment and concentrated load at mid-span

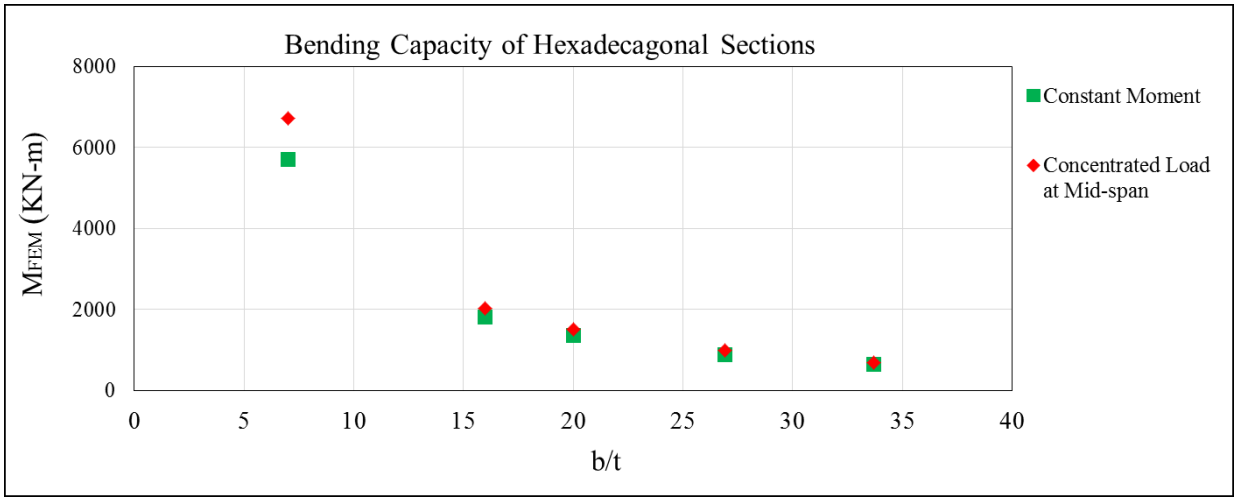

Figure 4.20: Bending capacities obtained from Hexadecagonal section subjected to constant moment and concentrated load at mid-span

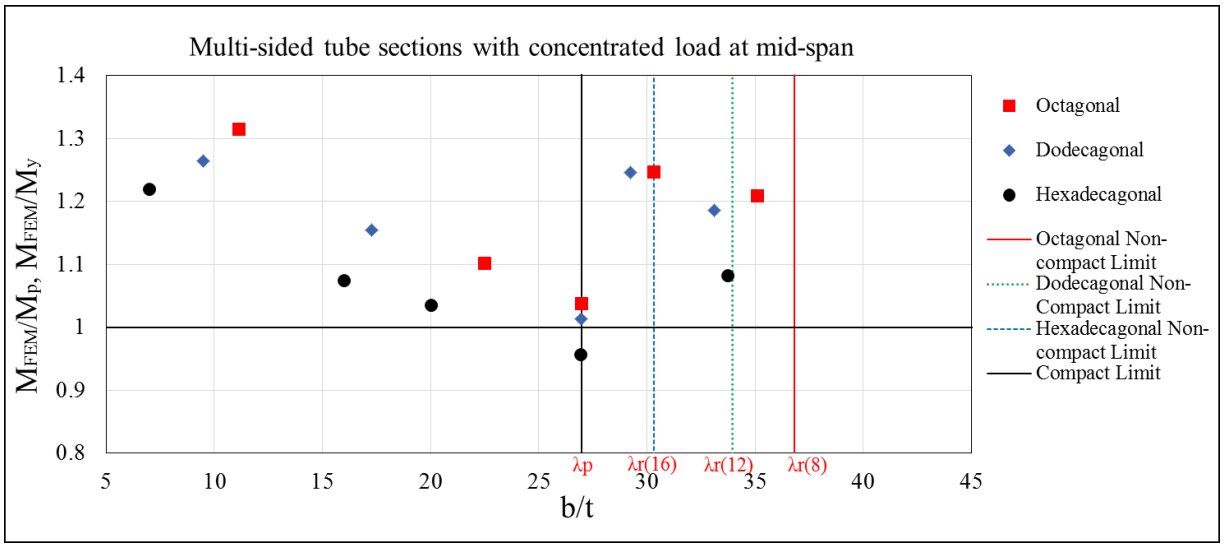

Figure 4.21: Multi-sided tube sections subjected to concentrated load at mid-span

4.6 Local buckling of multi-sided tube sections with different end conditions

In order to investigate the effect of support condition on local buckling capacity of multi-sided tube sections, eight (08) simply supported multi-sided sections previously considered for the constant bending moment are reanalyzed when they have cantilever support conditions. The cantilever multi-sided tube sections are subjected to a constant moment along the length of the members by applying a concentrated moment at the free end of the members. Table 4.3 compares the bending resistances of multi-sided tube sections with different support conditions. It is observed that there is no significant difference in local buckling capacities of the multi-sided sections when they have different end conditions. Thus, the same local buckling limit can be used for both simply supported and cantilever end conditions.

Table 4.3: Comparison of bending resistance from FE Models with different end conditions

Specimen	M_{FEM} (KN-m)	
	Simply supported beam	Cantilever beam
OCTAGONAL-B-11	280.60	281.63
OCTAGONAL-B-12	98.74	98.35
OCTAGONAL-B-13	128.63	127.47
DODECAGONAL-B-8	1407.32	1412.47
DODECAGONAL-B-12	204.73	204.45
DODECAGONAL-B-13	170.94	172.26
HEXADECAGON-B-1	1623.52	1624.95
HEXADECAGON-B-12	892.52	894.24

4.7 Summary

This chapter presents the local buckling behavior of the multi-sided tube under axial compression and pure bending. Geometric property selection criteria have been discussed in detail. Finite element results of models under axial compression and constant bending moment have been presented. FE analyses indicate that AASHTO suggested non-compact limit of the Hexadecagonal section can also be used for the other two sections (i.e., Octagonal and Dodecagonal) under axial compression. FE analyses showed that AASHTO provided compact limit for members under flexure might need to be revised. However, AASHTO provided non-compact limits are quite relaxed for the sections subjected to pure bending. Based on FE results, revised compact and non-compact limits have been proposed for Octagonal, Dodecagonal, and Hexadecagonal sections subjected to flexure. Additionally, FE results have also been compared with capacities suggested by different codes. Furthermore, some of the models which were previously subjected to constant moment were reanalyzed under moment gradient, and local buckling capacity was found to be higher for the models subjected to moment gradient. To observe the effect of support condition on local buckling capacity of multi-sided tube sections,

some of the simply supported multi-sided sections previously considered for constant bending moment are reanalyzed when they have cantilever support conditions and no significant difference in local buckling capacities have been found.

Chapter 5 Behavior of Multi-sided Tubes under Combined Bending and Compression and Pure Torsion

5.1 Introduction

The validated finite element (FE) model is used to conduct more analyses to observe the behavior of multi-sided tube under combined bending and compression and pure torsion for various width-thickness ratios (b/t). The selected width and lengths of FE models subjected to combined bending and compression and pure torsion are shown in section 5.2. Sections 5.3 and 5.4 show the FE model results under combined bending and compression and pure torsion, respectively. Details of geometric property and FE results are provided in Appendix A.

5.2 Geometric property selection criteria

For all the FE models, element width (b), wall thickness (t), and inside bend radius (r_b) have been chosen according to AASHTO (AASHTO, 2015). The geometric selection criteria are the same as discussed in Chapter 4. The following table shows the element width (b) and internal bend radius (r_b) used for all the FE models subjected to combined bending and compression and pure torsion. The selected lengths for the three multi-sided sections are the same as that considered for the pure bending conditions.

Table 5.1: Selected width and lengths of FE models subjected to combined bending and compression and pure torsion

Specimen	Number of Sides, n	Element Width, b (mm)	Inside Bend Radius, r_b (mm)	Length, L (mm)
Octagonal	8	100	Five times tube wall thickness or 25.4 mm, whichever is larger	2000
Dodecagonal	12	95		2500
Hexadecagonal	16	140		4000

5.3 Multi-sided tube sections subjected to combined bending and compression

Twenty-two (22) models of each cross-sectional profile, a total of sixty-six (66) models, were subjected to combined bending and axial compression. These models include both compact and non-compact sections. For each model, three different compressive loads of 20%, 30%, and 45% of axial capacity ($P_y = AF_y$) of the corresponding section were applied. Bending capacity for the combined loading ($M_{FEM(COMB)}$) was obtained for each compressive load case from FE analysis. FE results are compared with existing codes. Following subsection 5.3.1 present FE results of models under combined bending and compression. A detailed comparison of FE results with different codes is made in section 5.3.2.

5.3.1 FE results of models under combined bending and compression

Following figures show the typical deformed shapes of the Octagonal, Dodecagonal, and Hexadecagonal sections under combined bending and compression. For all the models, local buckling failure was observed.

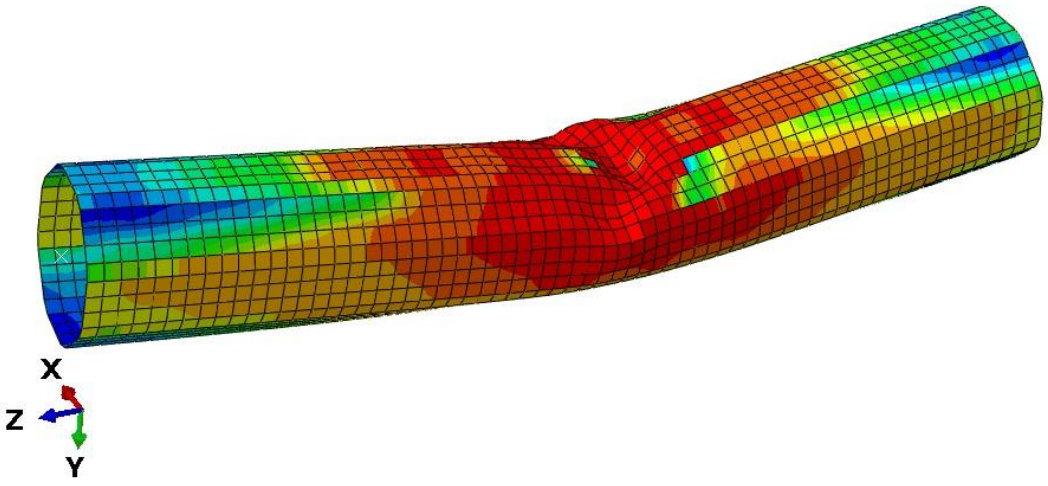

(a) Deformed shape of Octagonal section

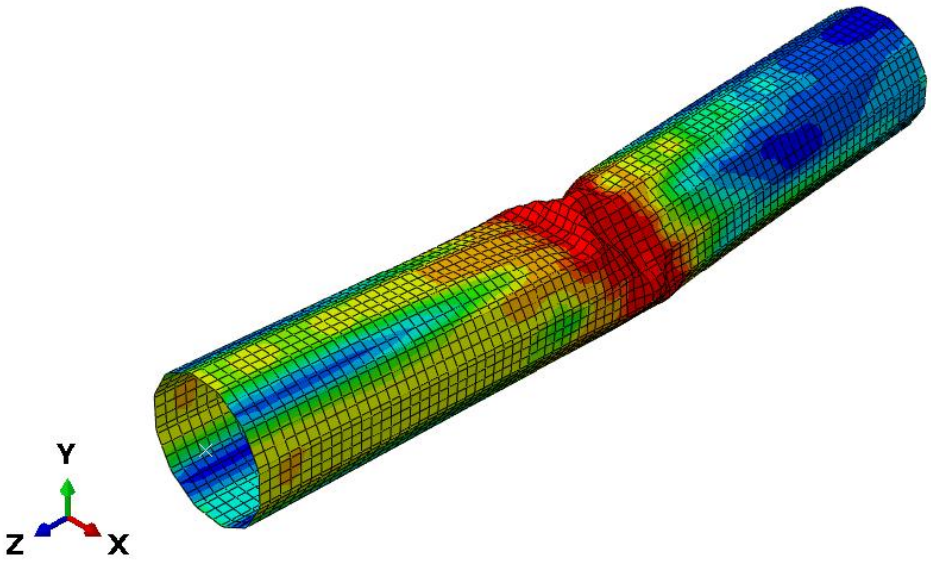

(b) Deformed shape of Dodecagonal section

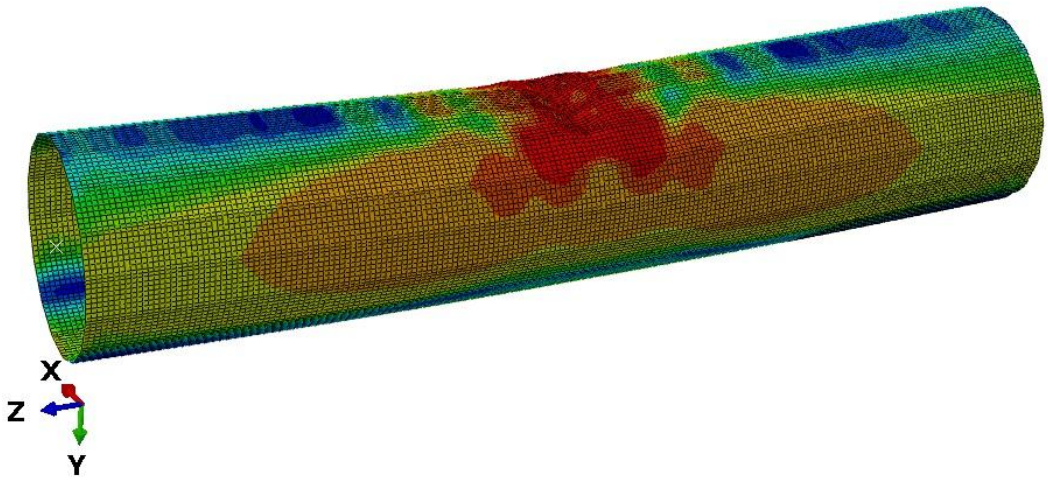

(c) Deformed shape of Hexadecagonal section

Figure 5.1: Deformed shape of (a) Octagonal, (b) Dodecagonal, and (c) Hexadecagonal section under combined bending and compression

Furthermore, Figure 5.2, 5.3, and 5.4 show the bending moments ($M_{FEM(COMB)}$) obtained from nonlinear FE analyses for Octagonal, Dodecagonal, and Hexadecagonal sections, respectively. Each figure shows the bending moment ($M_{FEM(COMB)}$) obtained for the applied compressive load of 20%, 30%, and 45% of P_y for different width-thickness ratios (b/t). For all multi-sided tube

sections, it is observed from the figures that bending capacities decrease with an increase in the axial compressive load.

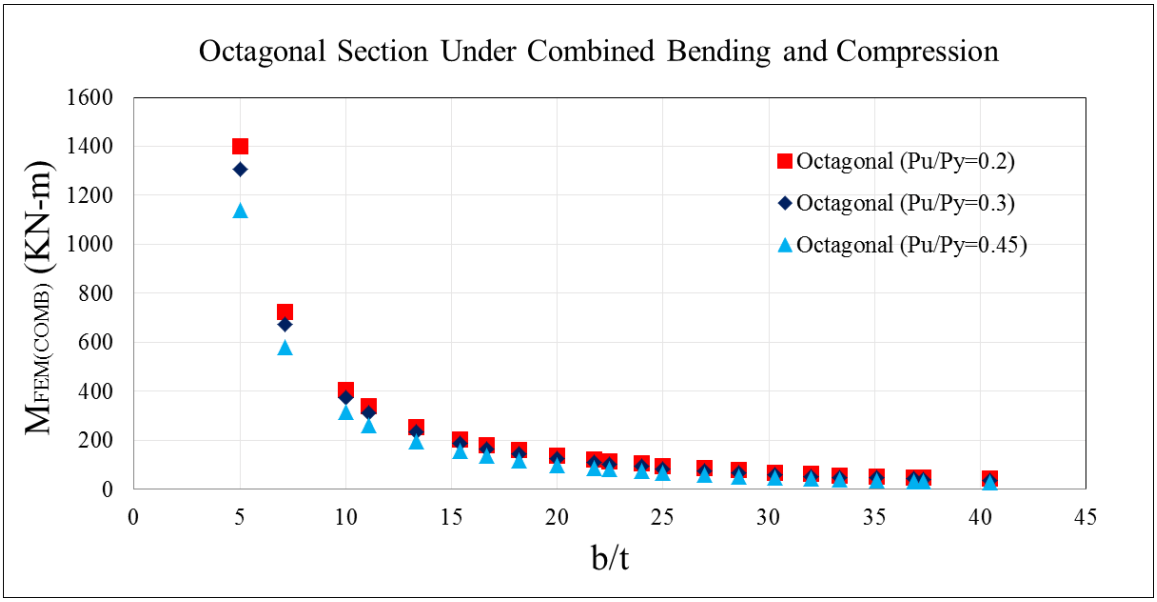

Figure 5.2: Critical bending moment ($M_{FEM(COMB)}$) capacity of Octagonal section under combined bending and compression

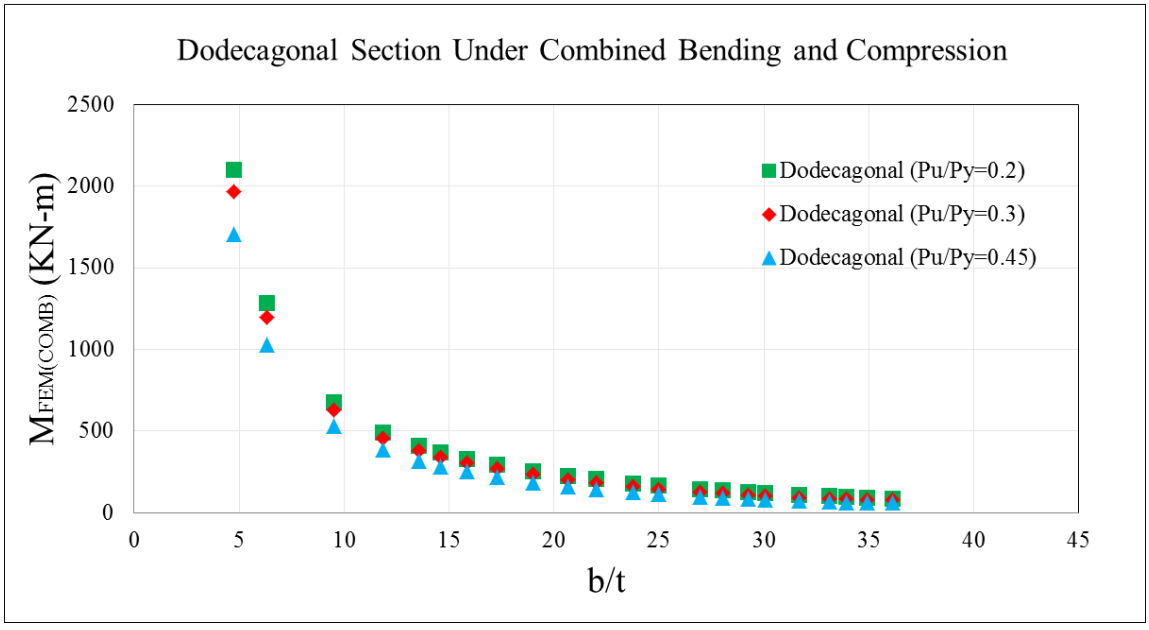

Figure 5.3: Critical bending moment ($M_{FEM(COMB)}$) capacity of Dodecagonal section under combined bending and compression

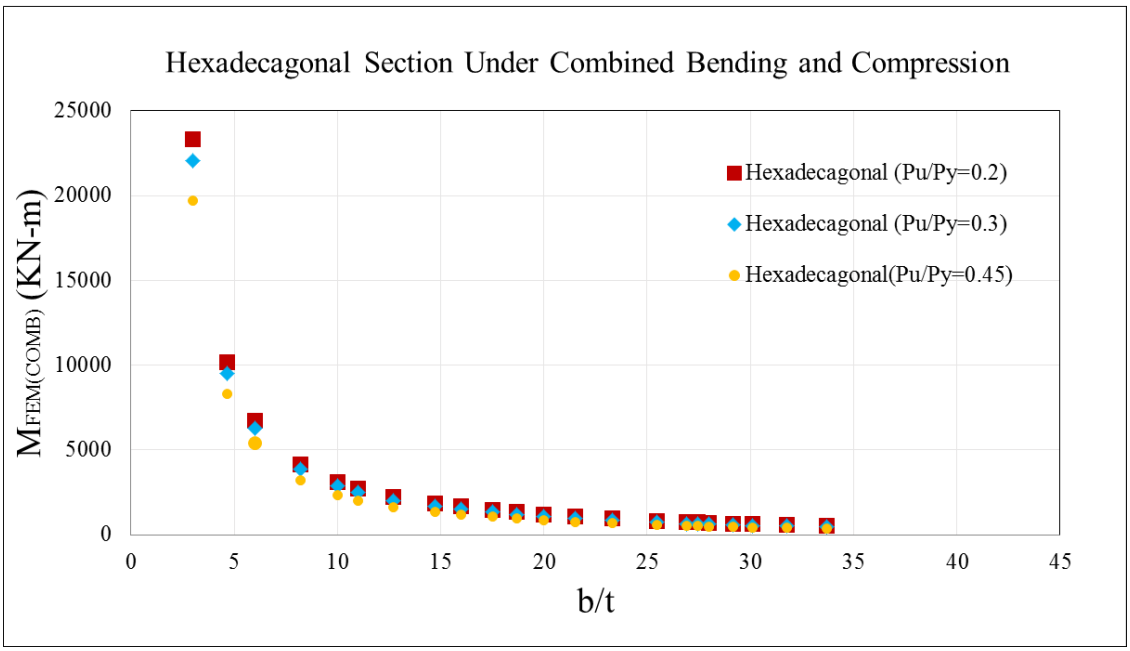

Figure 5.4: Critical bending moment ($M_{FEM(COMB)}$) capacity of Hexadecagonal section under combined bending and compression

5.3.2 Comparison of FE results with existing codes

Critical bending resistance from FE analyses ($M_{FEM(COMB)}$) subjected to combined bending and compression is compared with the existing codes (*i.e.,* AASHTO, ASCE/SEI 48-11, Eurocode 3 and EN 50341-1). AASHTO, ASCE/SEI 48-11, Eurocode 3 and EN 50341-1 have provided equations to check the capacity of the sections subjected to combined loadings.

As discussed in Chapter 2, AASHTO provides Equation 5.1 for combined bending and axial compression. In this equation, M_u is considered as the bending resistance of sections subjected to combined bending and compression ($M_{AASHTO(COMB)}$), according to AASHTO.

When $\frac{P_u}{P_r} \geq 0.2$

$$\frac{P_u}{P_r} + \frac{8}{9}\frac{BM_u}{M_r} \leq 1.0 \qquad (5.1)$$

$$M_u = (1 - \frac{P_u}{P_r}) \times \frac{9}{8}\frac{M_r}{B} \quad (5.2)$$

Similarly, Equation 5.3 provided by ASCE/SEI 48-11 for combined bending and axial compression loading (Chapter 2) has been simplified, and from that equation, M_u is calculated, which is taken as the bending resistance of sections subjected to combined bending and axial compression ($M_{ASCE(COMB)}$) according to ASCE/SEI 48-11.

$$\frac{P_u}{A} + \frac{M_u c}{I} \leq F_t \; or \; F_{cr} \quad (5.3)$$

$$M_u = \left\{(F_t \; or \; F_{cr}) - \frac{P_u}{A}\right\} \times \frac{I}{c} \quad (5.4)$$

The maximum value for allowable stress, F_t or F_{cr} by ASCE/SEI 48-11 is F_y and the limits at which the compressive stress is equal to yield strength are as follows:

$\frac{b}{t} \leq \frac{260\Omega}{\sqrt{F_y}}$ for Octagonal section

$\frac{b}{t} \leq \frac{240\Omega}{\sqrt{F_y}}$ for Dodecagonal section

$\frac{b}{t} \leq \frac{215\Omega}{\sqrt{F_y}}$ for Hexadecagonal section

These limits are also reported in Chapter 2 in Table 2.5. It should be noted that the width-thickness limits for combined bending and axial compression suggested by ASCE/SEI 48-11 are almost the same as that suggested by AASHTO for non-compact (Class 3) multi-sided tube sections. ASCE/SEI 48-11 does not provide any width-thickness limits for compact (Class 2) multi-sided tube sections subjected to combined bending and compression.

Currently, no strength equations have been provided in Eurocode 3 for multi-sided tube sections for combined bending and axial compression. However, as an alternative, a linear interaction of

moment and axial force proposed in Eurocode 3, as shown in the following equation, has been adopted in this research.

$$\frac{P_{uz}}{P_r} + \frac{M_{ux}}{M_{rx}} + \frac{M_{uy}}{M_{ry}} \leq 1 \tag{5.5}$$

where P_r, M_{rx}, and M_{ry} are design cross-sectional resistances. In this research, only uniaxial bending (bending about X-axis) is considered. For Class 1 and Class 2 sections, the bending resistance is based on plastic sections. For the Class 3 section, the maximum longitudinal stress due to combined compression and bending loading must be less than the yield stress. For Class 4 sections, the same condition as Class 3 sections is applied; however, the stress is calculated based on effective cross-section properties.

The strength equations for combined bending and axial compression loading provided by Eurocode 3 have been simplified, and M_u has been calculated, which is considered as the bending moment of sections subjected to combined bending and compression ($M_{Euro(COMB)}$), according to Eurocode 3.

For class 1 and class 2

$$\frac{P_u}{A} + \frac{M_u}{Z} \leq F_y \tag{5.6}$$

$$M_u = (F_y - \frac{P_u}{A}) \times Z \tag{5.7}$$

For class 3

$$\frac{P_u}{A} + \frac{M_u}{S} \leq F_y \tag{5.8}$$

$$M_u = (F_y - \frac{P_u}{A}) \times S \tag{5.9}$$

For class 4

$$\frac{P_u}{A_{EFF}} + \frac{M_u}{S_{eff}} \leq F_y \tag{5.10}$$

$$M_u = (F_y - \frac{P_u}{A_{EFF}}) \times S_{eff} \tag{5.11}$$

Furthermore, EN 50341-1 has adopted the same equation as Eurocode 3 but only considering class 3 and class 4 sections. For EN 50341-1, bending resistances of multi-sided tube sections subjected to combined bending and axial compression ($M_{EN(COMB)}$) have been calculated by considering sections that are either class 3 or class 4.

The following figures show the ratio of bending resistance obtained from FE models under combined bending and compression and the resistances from different codes for different width-thickness ratios (b/t). For each multi-sided tube, three different compressive loads (*i.e.,* 20%, 30%, and 45% of P_y) have been applied, and corresponding bending resistance has been obtained. Currently, design codes do not provide any separate width-thickness limits for multi-sided tube sections subjected to axial compression and bending. In this research, the applicability of using the same width-thickness limits (compact and non-compact limits) as suggested for multi-sided tube sections when subjected to bending for combined axial compression and bending. Thus, the current AASHTO compact limit (λ_p) and non-compact limit (λ_r) are included in the figures which compare the FE analysis results with existing combined strength equations of different codes.

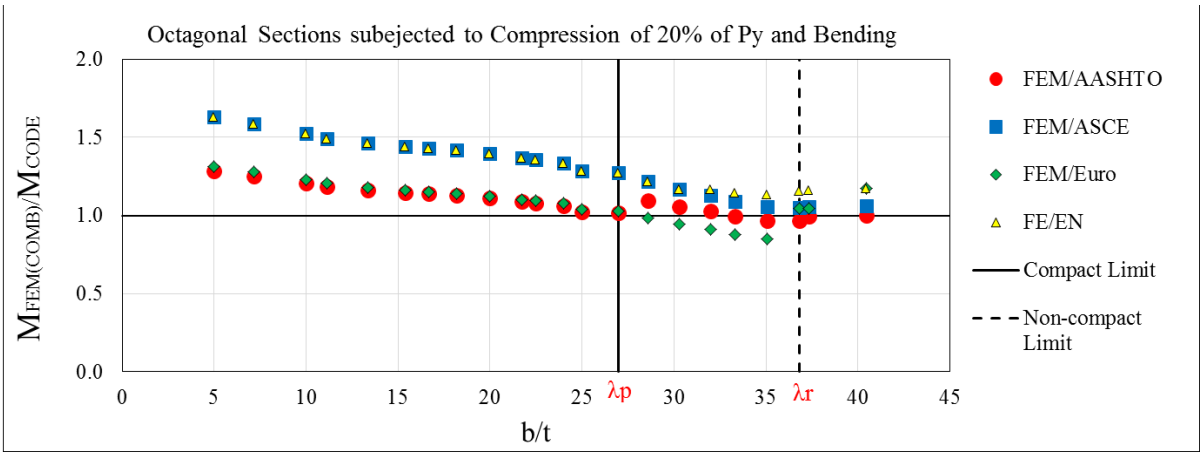

Figure 5.5: Comparison of bending resistances of Octagonal sections subjected to compression of 20% of P_y and bending with codes

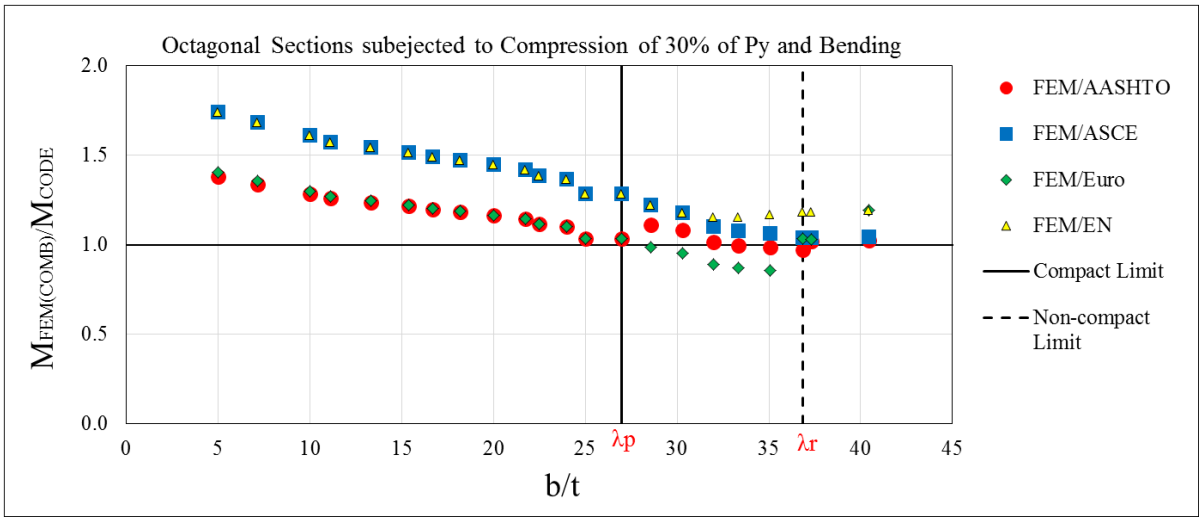

Figure 5.6: Comparison of bending resistances of Octagonal sections subjected to compression of 30% of P_y and bending with codes

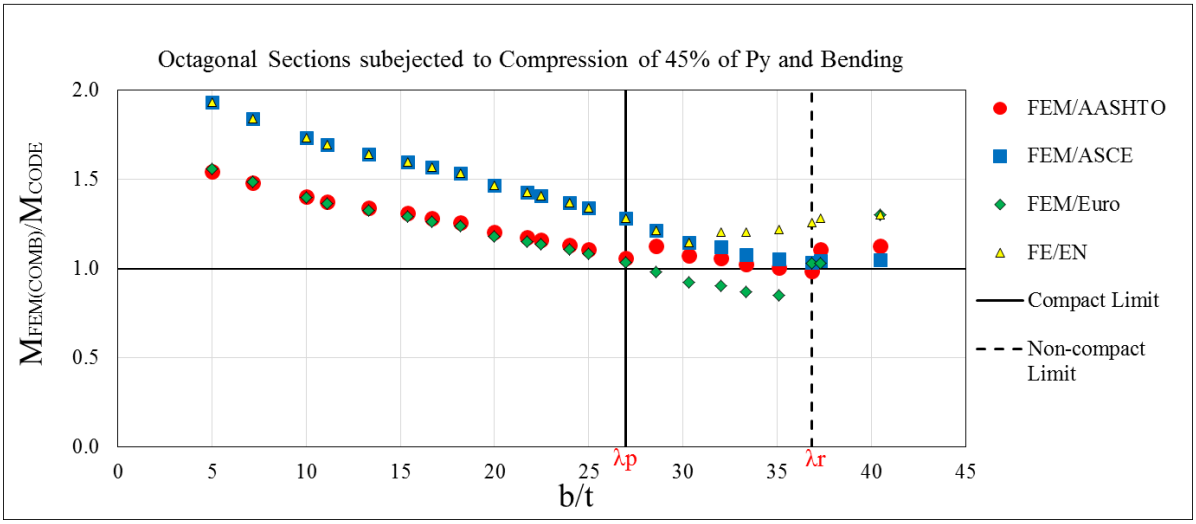

Figure 5.7: Comparison of bending resistances of Octagonal sections subjected to compression of 45% of P_y and bending with codes

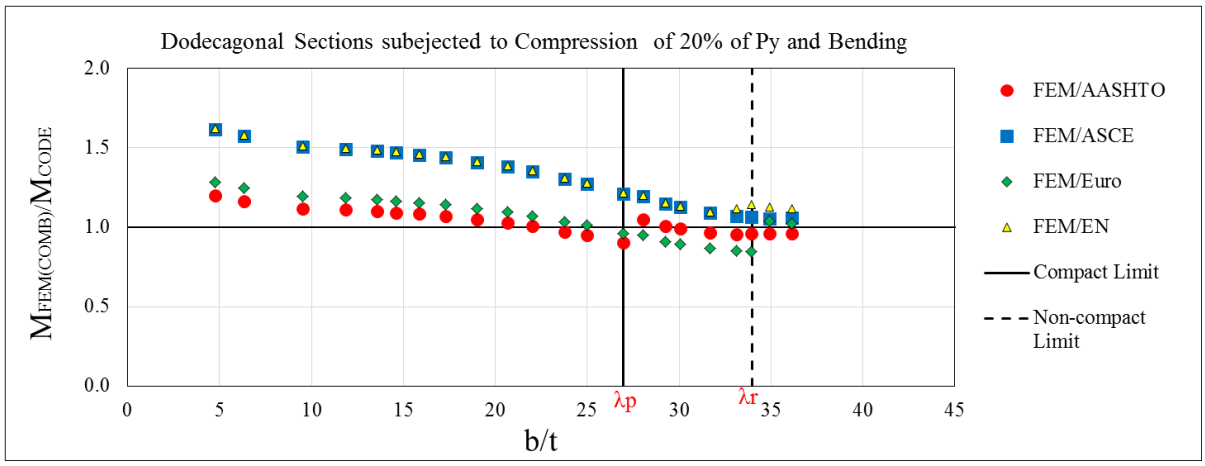

Figure 5.8: Comparison of bending resistances of Dodecagonal sections subjected to compression of 20% of P_y and bending with codes

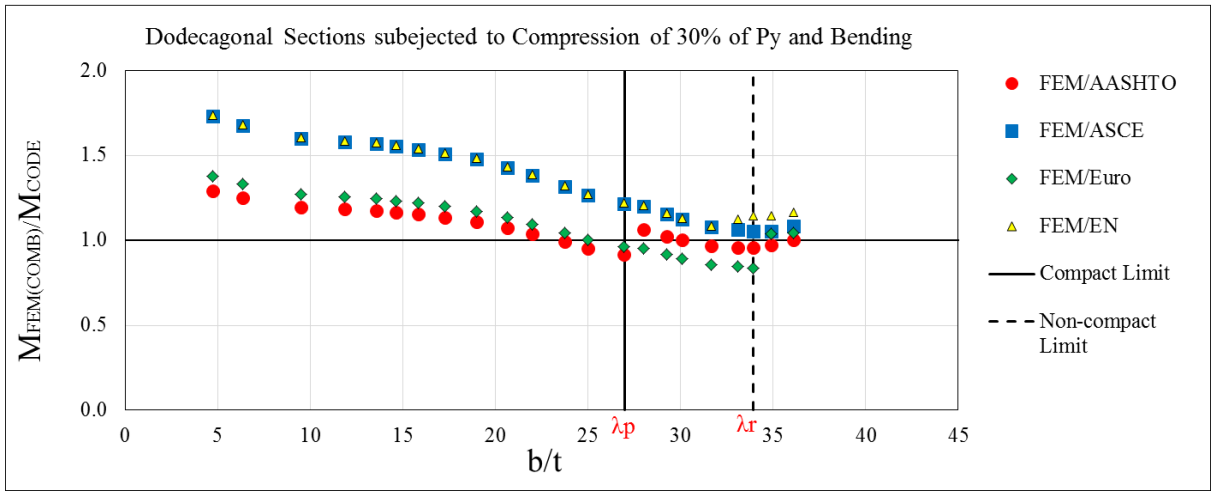

Figure 5.9: Comparison of bending resistances of Dodecagonal sections subjected to compression of 30% of P_y and bending with codes

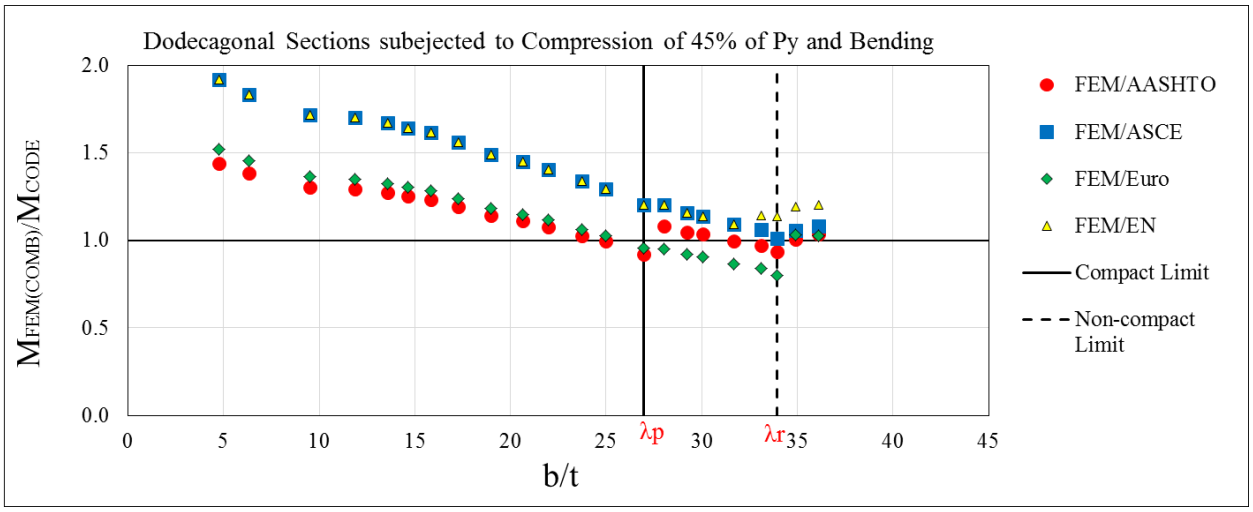

Figure 5.10: Comparison of bending resistances of Dodecagonal sections subjected to compression of 45% of P_y and bending with codes

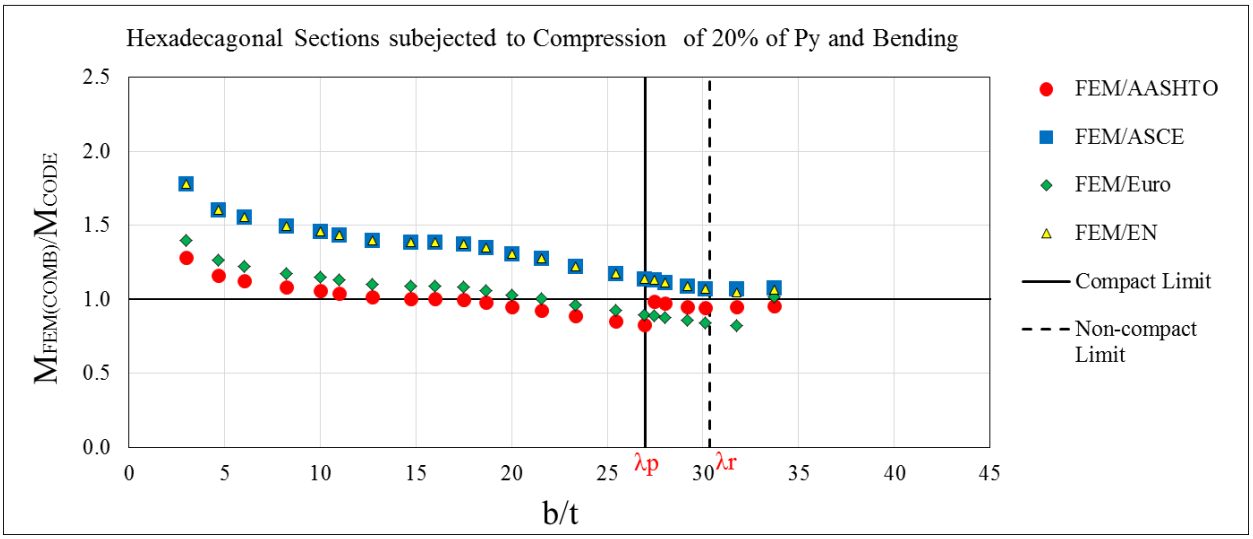

Figure 5.11: Comparison of bending resistances of Hexadecagonal sections subjected to compression of 20% of P_y and bending with codes

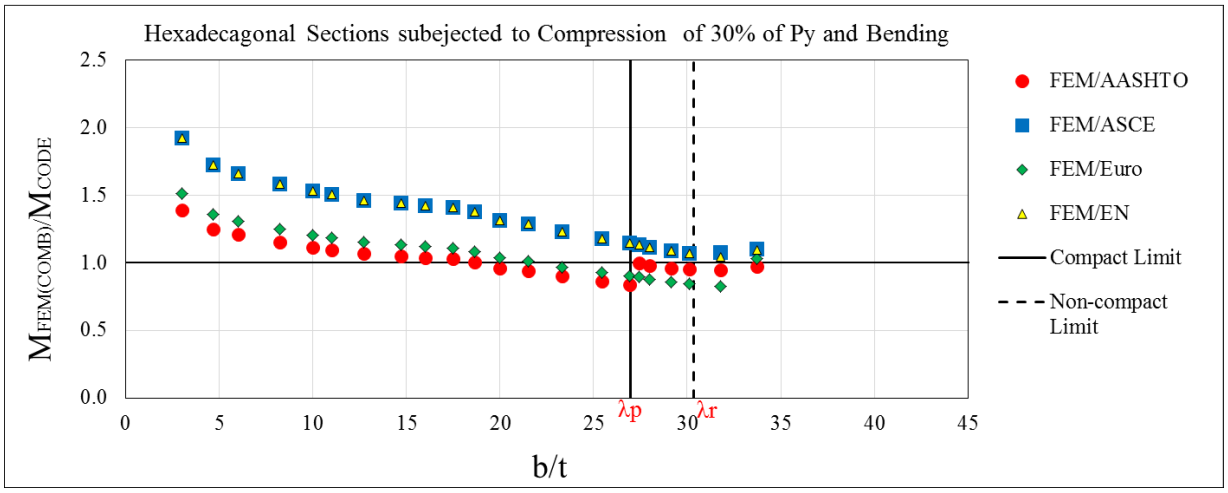

Figure 5.12: Comparison of bending resistances of Hexadecagonal sections subjected to compression of 30% of P_y and bending with codes

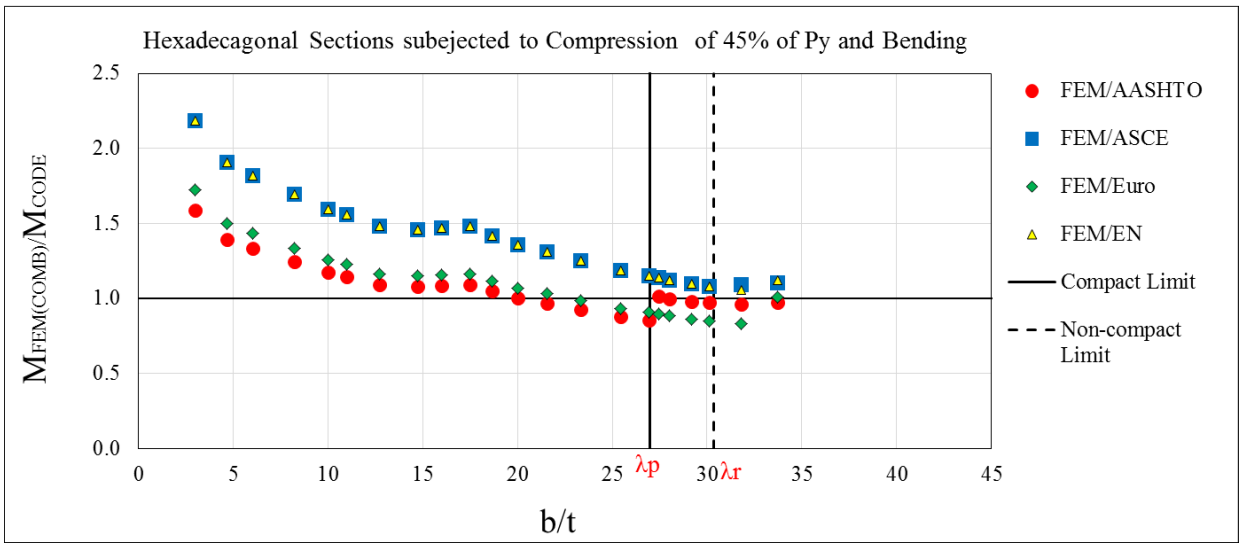

Figure 5.13: Comparison of bending resistances of Hexadecagonal sections subjected to compression of 45% of P_y and bending with codes

Following observations can be made from the comparison between bending resistance obtained from FE analysis with code suggested capacities for Octagonal sections under combined bending and compression (Figure 5.5 to 5.7):

- For the Octagonal sections subjected to axial compression of 20%, 30%, and 45% of axial capacity P_y (=AF_y) and bending, the ratio of resistance from the FE model to code suggested resistance ($M_{FEM(COMB)}/M_{CODE}$) has a pretty similar pattern.
- Graphs show that for the Octagonal compact sections, AASHTO and Eurocode 3 provide very close results. However, Eurocode 3 results are less than 1.0 for the non-compact Octagonal sections, indicating that Eurocode 3 overestimates bending capacity for the selected non-compact Octagonal sections. Also, based on FE analysis results, it can be observed that all the Octagonal multi-sided tube sections can reach their reduced plastic and elastic moment capacities when subjected up to 45% of axial load capacity in addition to bending. Thus, current AASHTO compact and non-compact limits for Octagonal multi-sided tube sections can be considered adequate for combined axial compression and bending. To be consistent with bending only case, it is suggested $0.83\sqrt{E/Fy}$ be used for compact Octagonal multi-sided beam-column section.
- In all cases, the ratio between FE models and ASCE/SEI 48-11 is much higher than 1.0, indicating ASCE/SEI 48-11 is being conservative.
- For all compact and some of the non-compact sections, EN 50341-1 and ASCE/SEI 48-11 provide the same bending strength. For few non-compact octagonal sections, EN 50341-1 provides higher $M_{FEM(COMB)}/M_{CODE}$ ratios.

Following observations can be made from the comparison between bending resistance obtained from FE analyses with code suggested capacities for Dodecagonal sections when subjected to combined bending and compression (Figure 5.8 to 5.10):

- The ratios of bending resistance obtained from FE models and different codes ($M_{FEM(COMB)}/M_{CODE}$) of Dodecagonal sections subjected to axial compression of 20%, 30%, and 45% of axial capacity, P_y (=AF_y) and bending have a very similar pattern.
- For most of the Dodecagonal compact sections, $M_{FEM(COMB)}/M_{CODE}$ ratio is higher than 1.0, indicating codes are conservative, and the ratio is highest for ASCE/SEI 48-11. It is also observed that only for few Dodecagonal multi-sided tube sections current AASHTO compact limit is unconservative when subjected to axial compression and bending. To be consistent with bending only case, it is suggested $0.72\sqrt{E/Fy}$ be used for compact Dodecagonal multi-sided beam-column section.
- Unlike other codes, AASHTO provides different bending strength equation than elastic capacity (SF_y, where S is elastic section modulus) for Class 3 multi-sided tube sections. Some of selected Dodecagonal and Hexadecagonal non-compact sections couldn't reach AASHTO suggested capacities. Thus, AASHTO bending strengths for all Class 3 multi-sided tube sections should be revisited.
- For the non-compact sections, Eurocode 3 provides ratios less than 1.0, indicating Eurocode 3 can be unconservative.
- For all compact and majority of the non-compact sections, EN 50341-1 and ASCE/SEI 48-11 provide the same ratio. However, for few non-compact sections, EN 50341-1 provides a higher $M_{FEM(COMB)}/M_{CODE}$ ratio.

Finally, the following observations can be made from the comparison between bending resistance from FE analyses and code suggested capacities for Hexadecagonal sections subjected to combined bending and compression (Figure 5.11 to 5.13):

- For the Hexadecagonal sections subjected to axial compression of 20%, 30%, and 45% of axial capacity, P_y (=AF_y) and bending, the ratio of resistance from the FE model and code suggested resistance ($M_{FEM(COMB)}/M_{CODE}$) has a similar trend.
- The ratio of FE models and AASHTO is less than 1.0 for a number of Hexadecagonal multi-sided compact sections and some of the non-compact sections. Thus, current AASHTO compact limit is not conservative for Hexadecagonal multi-sided tube sections when subjected to axial compression and bending. To be consistent with bending only case, a compact limit of $0.42\sqrt{E/Fy}$ can be used for Hexadecagonal multi-sided beam-column section.
- Eurocode 3 provide $M_{FEM(COMB)}/M_{CODE}$ ratios less than 1.0 for some of the compact and for all non-compact sections, indicating that Eurocode 3 predicts higher capacities for a wide range of width-thickness ratios.
- ASCE/SEI 48-11 provides much higher $M_{FEM(COMB)}/M_{CODE}$ ratios than 1.0, and thus ASCE/SEI 48-11 provides a conservative estimation of bending strength for Hexadecagonal multi-sided tube sections when subjected to axial compression and bending.
- For all compact and non-compact sections, EN 50341-1 and ASCE/SEI 48-11 provide the same strength predictions for Hexadecagonal multi-sided tube sections when subjected to axial compression and bending.

5.4 Multi-sided tube sections subjected to pure torsion

Eleven (11) models of each cross-sectional profile, a total of thirty-three (33) models, were subjected to uniform Torsion. These models include both compact and non-compact sections.

The critical torsional moment of FE models (T_{FEM}) subjected to pure torsion has been compared with existing codes (*i.e.,* AASHTO, and ASCE/SEI 48-11). Following subsections 5.4.1 and 5.4.2 present FE results of models under pure torsion and comparison of FE results with different codes.

5.4.1 FE results of models under pure torsion

The following figures show the deformed shapes of the Octagonal, Dodecagonal, and Hexadecagonal multi-sided tube sections subjected to pure torsion. Furthermore, Figure 5.15 shows the torsional moments (T_{FEM}) obtained from nonlinear FE analyses. It is observed from Figure 5.15 that with the increase in the width-thickness ratio, the torsional capacities of all three multi-sided tube sections decrease.

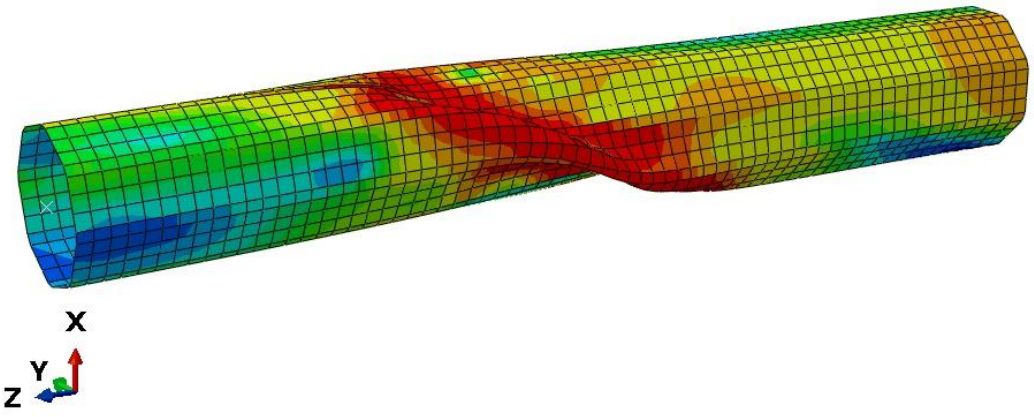

(a) Deformed shapes of Octagonal sections

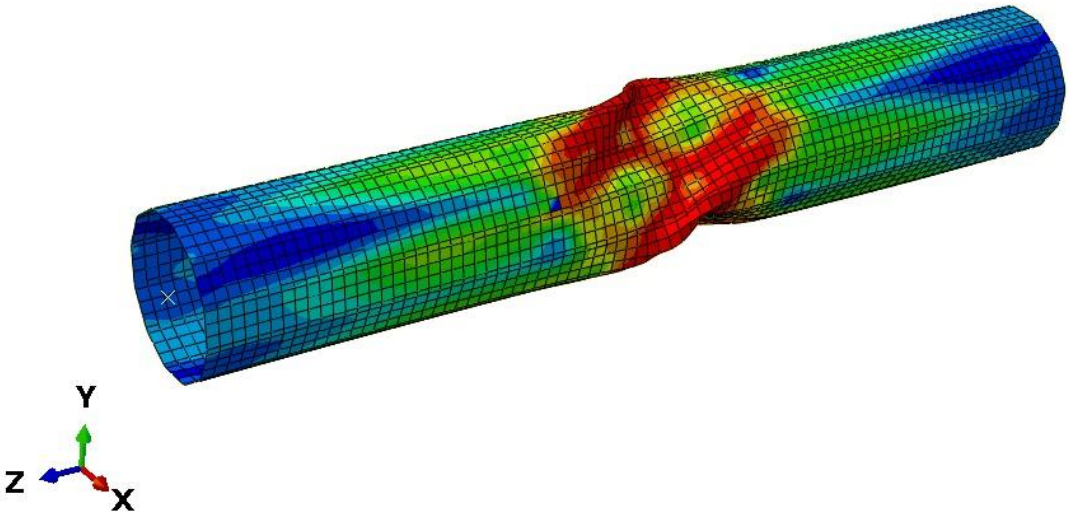

(b) Deformed shapes of Dodecagonal sections

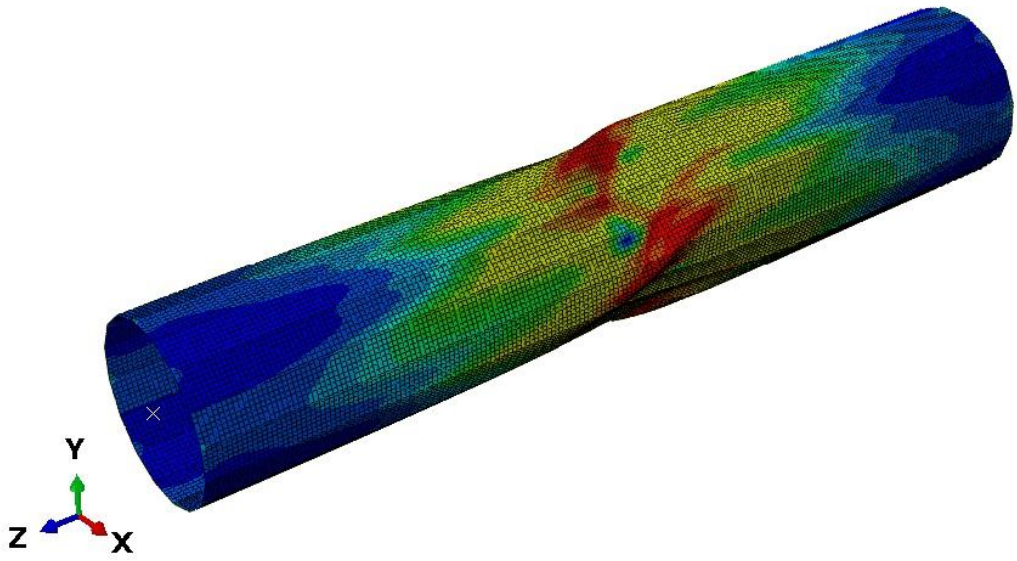

(c) Deformed shapes of Hexadecagonal sections

Figure 5.14: Deformed shapes of (a) Octagonal, (b) Dodecagonal, and (c) Hexadecagonal sections under uniform torsion

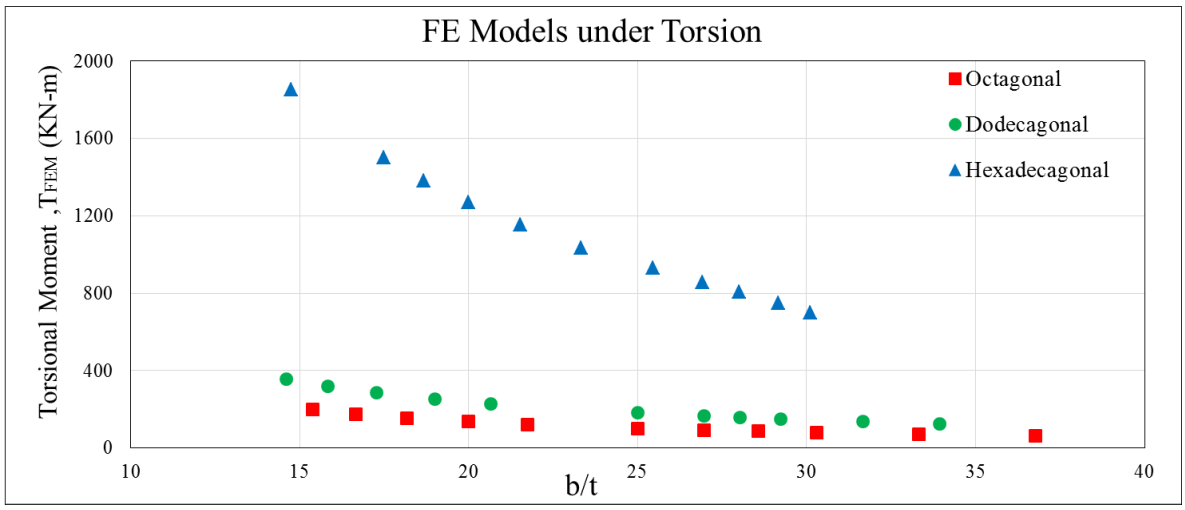

Figure 5.15: Critical torsional capacity (T_{FEM}) of multi-sided tube sections under constant moment

5.4.2 Comparison of FE results with existing codes

For all the sections, torsional capacities have been calculated according to AASHTO and ASCE/SEI 48-11. Chapter 2 contains the equations provided by AASHTO and ASCE/SEI 48-11 to calculate the torsional moments. Figures 5.16 to 5.18 show the ratio of torsional moments obtained from FE models and two codes (*i.e.,* AASHTO and ASCE/SEI 48-11) along with width-thickness ratios for compact Octagonal, Dodecagonal and Hexadecagonal sections.

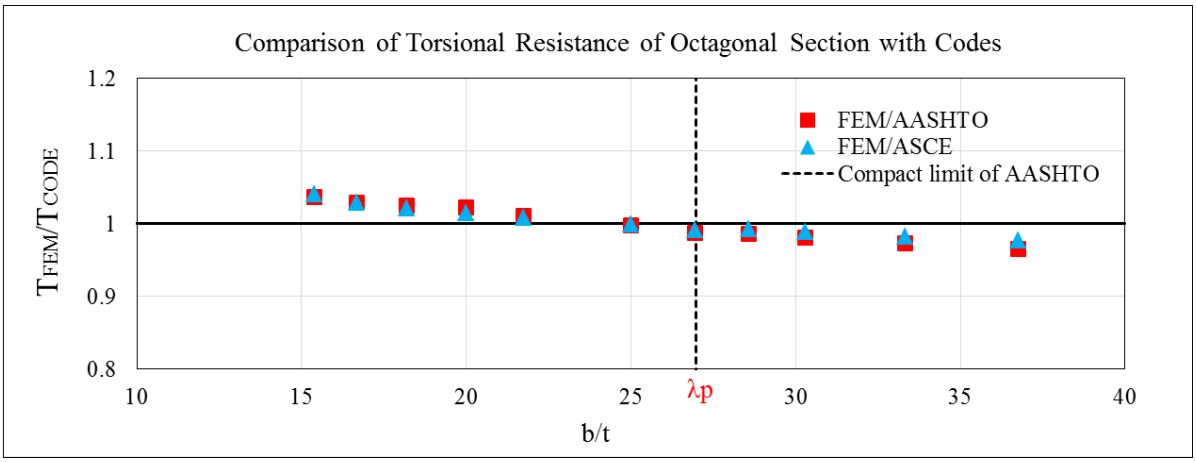

Figure 5.16: Comparison of torsional resistance of Octagonal sections with codes

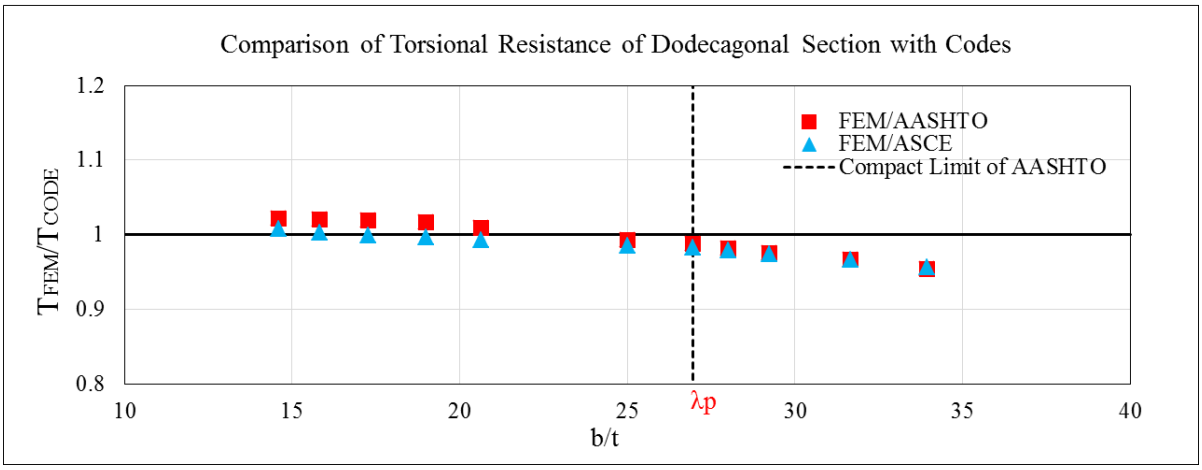

Figure 5.17: Comparison of torsional resistance of Dodecagonal sections with codes

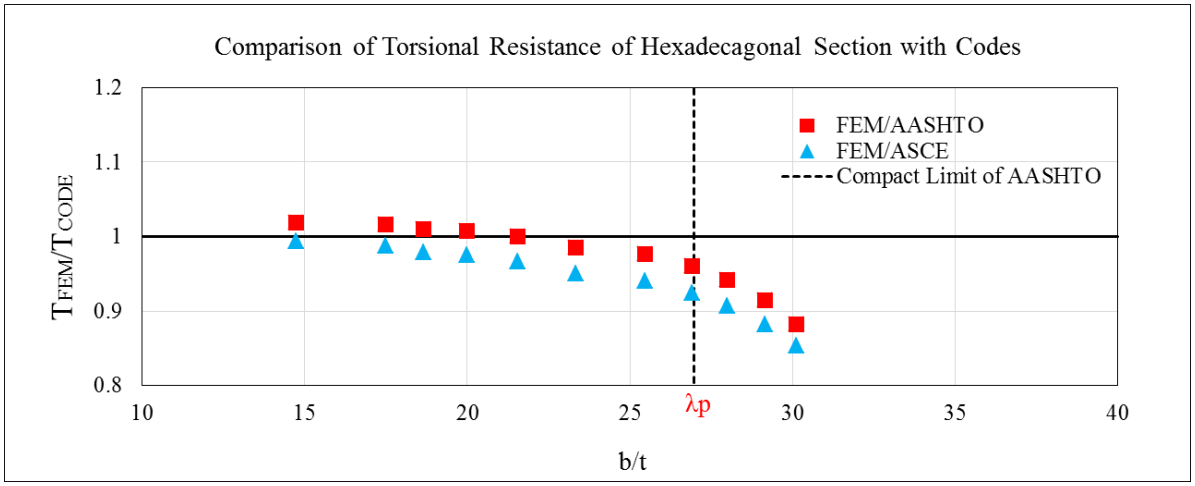

Figure 5.18: Comparison of torsional resistance of Hexdecagonal sections with codes

From the comparison of FE analysis results with the codes, it is observed that Octagonal compact sections mostly have higher torsional capacities than the AASHTO, and ASCE/SEI 48-11 suggested torsional capacities. On the other hand, Octagonal non-compact sections are not capable of reaching the torsional capacities indicated by the two codes. For Dodecagonal compact sections, most of the sections could reach torsional capacities higher than AASHTO provided capacities. The ratios of capacities from FE analyses and ASCE/SEI 48-11 are close to 1.0 for most of the compact Dodecagonal sections. However, the Dodecagonal compact sections

near the non-compact limit and all the non-compact sections have lower torsional capacities than AASTO and ASCE/SEI 48-11, indicating that the two codes are overestimating the torsional capacities of Dodecagonal non-compact sections to some extent. It is also observed from Figure 5.18 that ASCE/SEI 48-11 provides higher torsional capacities for Hexadecagonal sections. Except for few Hexadecagonal compact sections, AASHTO also provides higher torsional capacities than that predicted by FE analysis.

5.5 Summary

This chapter contains the behavior of the multi-sided tube subjected to combined bending and compression and pure torsion. Finite element results of models under combined bending and compression and pure torsion are presented. The selected width and lengths of FE models subjected to combined bending and compression and pure torsion are also presented. FE results are compared with existing codes to check the capacity equations provided in different codes. FE analyses for the sections under combined bending and compression show that ASCE/SEI 48-11 and EN 50341-1 suggested capacities are pretty conservative, whereas Eurocode 3 is suggesting the higher capacity for the non-compact sections. FE analyses show that while AASHTO provides a pretty good prediction for the Octagonal and Dodecagonal sections under combined bending and compression, it overestimates the capacities of several selected Hexadecagonal sections. It is also observed that torsional capacities for the Octagonal and Dodecagonal sections are predicted well for the compact sections in AASHTO and ASCE/SEI 48-11 and for a large number of selected Hexadecagonal compact sections, both codes are predicting higher torsional resistance.

Chapter 6 Summary, Conclusions and Recommendations

6.1 Summary

A detailed numerical study using the finite element program ABAQUS was performed to investigate local buckling behavior of multi-sided steel tube sections under different loading conditions. Past Canadian steel standards did not have any width-thickness limits for multi-sided tube sections to prevent premature local buckling. It is just in the recent Canadian steel standard CAN/CSA S16-19, width-thickness limits are suggested for multi-sided tube sections. These slenderness limits, which are similar to the limits suggested in AASHTO, have never been evaluated in detail. Thus, one of the main objectives of this research is to investigate width-thickness limits for different multi-sided tube sections. This research is based on a parametric study conducted by a FE model which is able to simulate the realistic behavior of multi-sided steel tube sections under different loading conditions. Summary of all the studies carried out in this research are as follows:

1. A nonlinear finite element model was developed to study the behavior of multi-sided tube sections. The FE model considered both material and geometric nonlinearities. The developed FE model was validated against experiments conducted by Godat et al. (2012) and Bräutigam et al. (2017).
2. The validated FE model was used to analyze a series of multi-sided steel tubular sections under axial compression, constant bending moment, combined bending and compression, and pure torsion. In addition to constant bending moment, moment gradient with a concentrated load at the mid-span of multi-sided tube sections was considered. Three different polygonal cross-sections, namely, Octagonal (8-sided), Dodecagonal (12-sided), and Hexadecagonal (16-sided) sections were considered.

3. Sixteen (16) models of each cross-section, a total of forty-eight (48) models were analyzed under axial compression to observe the local buckling behavior of multi-sided tubes for various width-thickness ratios (b/t). Also, one hundred and thirty-one (131) models were subjected to pure bending to investigate compact and non-compact limits of multi-sided tube sections. Moreover, twenty-two (22) models of each cross-sectional profile, a total of sixty-six (66) models were subjected to combined bending and compression. For each model under combined loading, three different compressive loads were applied with 20%, 30%, and 45% of axial yield capacity (P_y). Finally, a total of thirty-three (33) multi-sided tube sections were subjected to uniform torsion to investigate the behavior of these sections when subjected to torsion.
4. FE analysis results were used to evaluate the width-thickness limits of AASHTO and capacity equations of different codes (*i.e.,* AASHTO, ASCE/SEI 48-11, Eurocode 3, and EN 50341-1).

Section 6.2 contains a summary of the key findings and conclusions drawn from this study. Furthermore, section 6.3 presents the recommendations for future work, which includes other contributing factors that were not considered in this research.

6.2 Conclusions

The principal findings of this research can be divided into several parts as follows.

The following observations can be made from the validation of FE models:

- The results of the FE model showed a good correlation with the test results of Godat et al. (2012). In the experiment, six stub columns of three different cross-sections (*i.e.,* Octagonal, Dodecagonal, and Hexadecagonal) were tested under concentric compression.

Six FE models were developed similar to the test program, and the Critical Buckling Load of each member was captured. A maximum of 7% difference was found between test and FE results.

- The results of the FE model showed an excellent correlation with the test results of Bräutigam et al. (2017). In the experiment, local buckling behavior of polygonal sections having 16-sides was investigated under pure bending. Two FE models were developed similar to the test program and the maximum bending moment capacity of each member was captured. A maximum of 3.6% difference was found between test and FE results.

The following conclusions can be made for the FE models under axial compression:

- AASHTO and Eurocode 3 provide good predictions for the compressive resistance for multi-sided tube sections. While AASHTO provides three different non-compact limits (λ_r) for different multi-sided tube sections, all sections having at least the width-thickness ratio (b/t) of the Hexadecagonal section could reach capacities close to yield stress (F_y). Thus, it is recommended to use the same width-thickness limit, the non-compact limit of the Hexadecagonal section, for all three sections subjected to axial compression.
- ASCE/SEI 48-11 predictions for compressive strength for multi-sided tube sections subjected to compressive axial force are higher than that obtained from FE analyses for the Octagonal section.
- The compressive strength equation by Migita and Fukumoto (1997) predicts very close results to AASHTO and Eurocode 3. However, the proposed compressive strength equation of Godat et al. (2012) is conservative when compared to the codes.

The following conclusions can be drawn from the comparison between bending resistances from FE analysis and code (*i.e.,* AASHTO, ASCE/SEI 48-11, Eurocode 3, and EN 50341-1) suggested capacities:

- M_{FEM}/M_{AASHTO} ratios are more than 1.0 for the entire Octagonal multi-sided tube sections. However, the ratio is less than 1.0 for a few Dodecagonal and a large number of Hexadecagonal compact sections, indicating that AASHTO overestimates the flexural strength for the compact Dodecagonal and Hexadecagonal multi-sided tube sections.
- M_{FEM}/M_{ASCE} ratios are pretty higher than 1.0 for all the Octagonal, Dodecagonal, and Hexadecagonal sections. This is because ASCE/SEI 48-11 suggests elastic strength as the design flexural strength for all multi-sided tube sections whether they are compact or non-compact. For the majority of the selected multi-sided tube sections, EN 50341-1 is also suggesting the same resistance as ASCE/SEI 48-11 and for the remaining sections, EN 50341-1 recommends class 4 section capacities.
- M_{FEM}/M_{Euro} ratio is less than 1.0 for most of the Octagonal, Dodecagonal, and Hexadecagonal sections, as Eurocode 3 is suggesting full plastic moment capacity for class 1 and class 2 sections, which includes all compact and most of the non-compact sections (Compact and non-compact defined as AASHTO). However, near the non-compact limit (λ_r), there is a sudden increase in the ratio as Eurocode 3 suggests the elastic capacity for class 3 sections.

The following conclusions can be drawn from the comparison of bending resistance of FE models under pure bending with plastic moment (M_p) and yield moment (M_y):

- The study showed that, several compact sections (according to AASHTO) subjected to constant moment were not able to reach their plastic moment capacities. This was observed more for the Hexadecagonal multi-sided tube sections. Thus, it is recommended to revise the current AASHTO compact limits for the multi-sided tube sections. The proposed compact limits ($\lambda_{p(Proposed)}$) are $0.83\sqrt{E/Fy}$, $0.72\sqrt{E/Fy}$ and $0.42\sqrt{E/Fy}$ for Octagonal, Dodecagonal, and Hexadecagonal sections, respectively. Consistent with the current ASSHTO, the same compact limit of $0.42\sqrt{E/Fy}$ can be used for all three multi-sided tube sections.
- AASHTO provided non-compact limits for multi-sided tube sections are conservative when subjected to constant bending moment and can be relaxed more. Thus, the current AASHTO non-compact limits of $1.53\sqrt{E/Fy}$, $1.41\sqrt{E/Fy}$ and $1.26\sqrt{E/Fy}$ can be increased to $1.65\sqrt{E/Fy}$, $1.59\sqrt{E/Fy}$ and $1.47\sqrt{E/Fy}$ for Octagonal, Dodecagonal, and Hexadecagonal multi-sided tube sections, respectively. In addition, it will be convenient to practicing engineers to have a single non-compact width-thickness limit, similar to the one for the Hexadecagonal section, for all three multi-sided tube sections.
- Bending moment capacities obtained when the multi-sided tube sections were subjected to concentrated load at their mid-spans were all higher than those obtained from the constant bending moment cases. Thus, the width-thickness limits obtained in this study are applicable for any moment gradient.
- The local buckling capacities of multi-sided tube sections obtained from this study for both simply supported end condition and cantilever support conditions were almost the

same. Thus, the width-thickness limits obtained from the analyses of simply supported multi-sided tube sections are applicable for other support conditions.

The following observations can be made from the comparison between bending resistance of FE models under combined bending and compression and code (*i.e.,* AASHTO, ASCE/SEI 48-11, Eurocode 3, and EN 50341-1) suggested capacities:

- For each cross-section (*i.e.,* Octagonal, Dodecagonal and Hexadecagonal) subjected to compression of 20%, 30% and 45% of axial capacity, P_y ($=AF_y$) and bending, the ratio of resistance from FE model and code suggested resistance ($M_{FEM(COMB)}/M_{CODE}$) has a pretty similar pattern.
- All the models could reach capacities much higher than ASCE/SEI 48-11 and EN 50341-1 provided capacities, indicating both codes are pretty conservative. Moreover, for the majority of the sections, both ASCE/SEI 48-11 and EN 50341-1 are suggesting exactly the same capacity.
- Octagonal compact sections could reach Eurocode 3 suggested capacity, and it is very close to AASHTO suggested capacity. However, the non-compact Octagonal sections could not reach Eurocode 3 suggested resistance. The majority of the Dodecagonal compact and some of the Hexadecagonal compact sections could reach Eurocode 3 suggested capacity. However, Eurocode 3 is suggesting higher capacity than FE results for the non-compact sections.
- All the Octagonal sections could reach capacities suggested by AASHTO. Based on FE results, current AASHTO compact and non-compact limits for Octagonal multi-sided tube sections can be considered adequate for combined axial compression and bending.

To be consistent with bending only case, it is suggested $0.83\sqrt{E/Fy}$ be used for compact Octagonal multi-sided beam-column section.

- Most of the Dodecagonal compact section could reach AASHTO suggested capacity. Only for few Dodecagonal multi-sided tube sections, current AASHTO compact limit is unconservative when subjected to axial compression and bending. To be consistent with bending only case, it is suggested $0.72\sqrt{E/Fy}$ be used for compact Dodecagonal multi-sided beam-column section.
- Unlike other codes, AASHTO provides different bending strength equation than elastic capacity (SF_y, where S is elastic section modulus) for Class 3 multi-sided tube sections. Some of selected Dodecagonal and Hexadecagonal non-compact sections couldn't reach AASHTO suggested capacities. Thus, AASHTO bending strengths for all Class 3 multi-sided tube sections should be revisited.
- The ratio of FE models and AASHTO is less than 1.0 for a number of Hexadecagonal multi-sided compact sections. Thus, current AASHTO compact limit is not conservative for Hexadecagonal multi-sided tube sections when subjected to axial compression and bending. To be consistent with bending only case, a compact limit of $0.42\sqrt{E/Fy}$ can be used for Hexadecagonal multi-sided beam-column section.

From the comparison of torsional capacities of FE models subjected to pure torsion with codes (*i.e.,* AASHTO and ASCE/SEI 48-11), the following conclusions can be listed:

- Both AASHTO and ASCE/SEI 48-11 suggest very close torsional capacities for Octagonal sections. Octagonal compact sections mostly have higher capacities than the

AASHTO and ASCE/SEI 48-11 suggested torsional capacities. However, the selected Octagonal non-compact FE models were not capable of reaching the capacities indicated by the two codes.

- Most of the Dodecagonal compact sections could reach capacities higher than AASHTO. Also the majority of the Dodecagonal compact FE models are providing very close results to ASCE/SEI 48-11. Both codes are suggesting similar torsional resistances for Dodecagonal non-compact sections. However, all the FE non-compact sections have lower capacities than AASTO and ASCE/SEI 48-11; indicating codes are overestimating to some extent.
- ASCE/SEI 48-11 provides higher capacities for Hexadecagonal sections when they are subjected to pure torsion. Moreover, except for a few Hexadecagonal compact sections, AASHTO also suggests higher torsional capacities than FE analysis results.

It is recognized that the proposed width-thickness limits are obtained based on the analysis of a limited number of multi-sided tube sections. It is suggested that the proposed limits be re-evaluated with experimental tests and more analysis with different geometry and loading conditions.

6.3 Recommendations for future work

Based on the findings and results obtained during this investigation the following recommendations can be made for future work on local buckling behavior of multi-sided steel tube sections-

- Currently, there is no test available for multi-sided tube sections subjected to bending and axial compression. Thus, multi-sided tube sections should be investigated for combined bending and compression.
- Both experimental and analytical studies should be conducted for multi-sided tube sections subjected to combined axial compression, bending, shear and torsion.
- The effect of initial imperfection on the local buckling behavior of multi-sided steel tube sections should be considered in future investigations.
- The influence of residual stress on the strength of multi-sided tube sections subjected to different loading should be investigated in detail.
- The effect of inside bend radius (r_b) on the strength and behavior of multi-sided steel tube sections need to be investigated in future studies.
- Different end conditions and effect of bracings should be evaluated in future studies.
- The effect of strain hardening of steel material on the local buckling behavior and strength of multi-sided tube sections need to be investigated in future studies.

REFERENCES

ABAQUS. (2014). ABAQUS standard user's manual, 6.14. Dassault Systèmes.

American Association of State Highway and Transportation Officials (AASHTO). (2015). "LRFD Specifications for Structural Supports for Highway Signs, Luminaires, and Traffic Signals." Washington, DC.

American Society of Civil Engineers (ASCE). (2011). "Design of Steel Transmission Pole Structures." ASCE/SEI 48-11, Reston, Virginia.

Aoki, T., Migita, Y., and Fukumoto, Y. (1991). "Local buckling strength of closed polygon folded section columns." Journal of Constructional Steel Research, 20 (4) 259–270.

Avent, R. R., and Robinson J.H. (1976). "Elastic stability of polygonal folded plates columns." Journal of Structural Division (ASCE); 102, 1015–1029.

Bräutigam, K., Knoedel, P., and Ummenhofer, T. (2017). "Plastic behaviour of polygonal hollow sections in bending." Steel Construction, 10 (3) 222-226.

Bryan, G. H. (1891), "On the Stability of a Plane Plate under Thrusts in Its Own Plane, with Applications to the 'Buckling' of the Sides of a Ship." Proc. London Math. Soc., Vol. 22.

Bulson, PS. (1969). "The strength of thin walled tubes formed from flat elements." International Journal of Mechanical Science, 11, 613–620.

Canadian Standards Association, (CSA). (2019). "Limit States Design of Steel Structures." CAN/CSA-S16-19, Toronto, Ontario, Canada.

ECVV. (n.d.). Light Post. Retrieved from https://www.ecvv.com/product/1000088796.html

Ellobody, E. (2014). "Finite Element Analysis and Design of Steel and Steel-Concrete Composite Bridges." Elsevier Inc.

EN 50341-1. (2012). "Overhead electrical lines exceeding AC 1 kV - Part 1: General requirements -Common specifications." European Committee for Electrotechnical Standardization, Brussels, Belgium.

EN 40-3-3. (2013). "Lighting columns – Part 3-3: Design and verification – Verification by calculation."

Eurocode 3. (2005). EN 1993-1-1 Eurocode 3: "Design of steel structures - Part 1–1: general rules and rules for buildings." European Committee for Standardization (CEN), Brussels, Belgium.

Eurocode 3. (2006). EN 1993-1-3 Eurocode 3: "Design of steel structures - Part 1–3: General rules- Supplementary rules for cold-formed members and sheeting." European Committee for Standardization (CEN), Brussels, Belgium.

Eurocode 3. (2006). EN 1993-1-5 Eurocode 3: "Design of steel structures - Part 1–5: General rules - Plated structural elements." European Committee for Standardization (CEN), Brussels, Belgium.

Godat, A., Legeron, F., and Bazonga, D. (2012). "Stability investigation of local buckling behavior of tubular polygon columns under concentric compression." Thin-Walled Structures, 53, 131-140.

Gonçalves, R., and Camotim, D. (2013). "Buckling behaviour of thin-walled regular polygonal tubes subjected to bending or torsion." Thin-Walled Structures, 73, 185–197.

Gonçalves, R., and Camotim, D. (2013). "Elastic buckling of uniformly compressed thin-walled regular polygonal tubes." Thin-Walled Structures, 71, 35-45.

Loov, R. (1996). "A simple equation for axially loaded steel column design curves." Canadian Journal of Civil Engineering, 23 (1) 272–276.

Martins, A. D., Gonçalves, R., and Camotim, D. (2018). "Post-buckling behaviour of regular convex polygonal columns buckling in local and distortional modes." Eighth International Conference on THIN-WALLED STRUCTURES, Lisbon, Portugal.

Migita, Y. and Fukumoto, Y. (1997). "Local buckling behaviour of polygonal sections." Journal of Constructional Steel Research, 41 (2/3) 221–233.

Nishimura, N., Yosida, N. S. and Takeuchi, S. (1990). "Strength formula for steel beam columns with box section considering local buckling." Journal of JSCE Engineers, 416 (I-13), 385-393.

Nova Pole. (n.d.). Signpost. Retrieved from https://www.novapole.com/product-details-82-ferry-toll-booth-double-arm-sign-bridge

Nova Pole. (n.d.). Transmission Pole. Retrieved from https://www.novapole.com/product-details-86-dead-end-transmission-pole

Reinke, T., Knoedel, P. and Ummenhofer, T. (2014). "Steel poles with polygonal sections in bending." European Conference on Steel and Composite Structures, Naples, Italy.

Saatcioglu M., and Humar J. (2003). “Dynamic analysis of buildings for earthquake resistant design.” Can J Civ Eng, 30, 338–359.

Teng, J.G., Smith, S.T., and Ngok, L.Y. (1999). “Local buckling of thin-walled tubular polygon columns subjected to axial compression or bending.” Proceedings of the Second International Conference on Advances in Steel Structures, Elsevier Steel Structures Division, Hong Kong, China, 1, 109–115.

Timoshenko, S.P., and Gere J. M. (1961). “Theory of elastic stability.” 2nd ed., McGraw Hill, New York, NY, USA.

Trahair, N. S. (1993). “Flexural-Torsional buckling of structures.” CRC Press, Boca Raton, FL.

Wittrick, W. H., and Curzon, P. L. V. (1968). “Local buckling of long polygonal tubes in combined bending and torsion.” International Journal of Mechanical Sciences, 10, 849-857.

Appendix A

Appendix A contains the geometric property tables for all the models subjected to axial compression, pure bending, combined bending and compression, and pure torsion.

Table A.1: Geometric Properties of Octagonal (8-sided) Sections Subjected to Axial Compression

Specimen	Element Width, b (mm)	Thickness, t (mm)	Compact Limit, λ_p (AASHTO)	Non-compact Limit, λ_r (AASHTO)	b/t	Inside Bend Radius, r_b (mm)	Mid-Surface Distance from Flat Side to Flat Side, D (mm)
OCTAGONAL-C-1	100	6	26.97	36.84	16.67	30	295.42
OCTAGONAL-C-2		5			20	25.4	286.42
OCTAGONAL-C-3		4.6			21.74	25.4	282.82
OCTAGONAL-C-4		3.5			28.57	25.4	272.92
OCTAGONAL-C-5		3			33.33	25.4	268.42
OCTAGONAL-C-6		2.3			43.48	25.4	262.12
OCTAGONAL-C-7		2			50	25.4	259.42
OCTAGONAL-C-8		1.7			58.82	25.4	256.72
OCTAGONAL-C-9		6.5			15.38	32.5	299.92
OCTAGONAL-C-10		5.5			18.18	27.5	290.92
OCTAGONAL-C-11		2.72			36.76	25.4	265.90
OCTAGONAL-C-12		4			25	25.4	277.42
OCTAGONAL-C-13		14			7.14	70	367.42
OCTAGONAL-C-14		9			11.11	45	322.42
OCTAGONAL-C-15		3.71			26.95	25.4	274.81
OCTAGONAL-C-16		4.17			23.98	25.4	278.95

Table A.2: Geometric Properties of Dodecagonal (12-sided) Sections Subjected to Axial Compression

Specimen	Element Width, b (mm)	Thickness, t (mm)	Compact Limit, λ_p (AASHTO)	Non-compact Limit, λ_r (AASHTO)	b/t	Inside Bend Radius, r_b (mm)	Mid-Surface Distance from Flat Side to Flat Side, D (mm)
DODECAGONAL-C-1	95	6	26.97	33.95	15.83	30	408.54
DODECAGONAL-C-2		5.5			17.27	27.5	404.04
DODECAGONAL-C-3		5			19	25.4	399.54

Table A.2: (Cont.) Geometric Properties of Dodecagonal (12-sided) Sections Subjected to Axial Compression

Specimen	Element Width, b (mm)	Thickness, t (mm)	Compact Limit, λ_p (AASHTO)	Non-compact Limit, λ_r (AASHTO)	b/t	Inside Bend Radius, r_b (mm)	Mid-Surface Distance from Flat Side to Flat Side, D (mm)
DODECAGONAL-C-4	95	3.8	26.97	33.95	25	25.4	388.74
DODECAGONAL-C-5		2.5			38	25.4	377.04
DODECAGONAL-C-6		2.2			43.18	25.4	374.34
DODECAGONAL-C-7		2			47.5	25.4	372.54
DODECAGONAL-C-8		3.5			27.14	25.4	386.04
DODECAGONAL-C-9		3.25			29.23	25.4	383.79
DODECAGONAL-C-10		2.8			33.93	25.4	379.74
DODECAGONAL-C-11		4.6			20.65	25.4	395.94
DODECAGONAL-C-12		15			6.33	75	489.54
DODECAGONAL-C-13		10			9.5	50	444.54
DODECAGONAL-C-14		7			13.57	35	417.54
DODECAGONAL-C-15		4			23.75	25.4	390.54
DODECAGONAL-C-16		4.318			22	25.4	393.41

Table A.3: Geometric Properties of Hexadecagonal (16-sided) Sections Subjected to Axial Compression

Specimen	Element Width, b (mm)	Thickness, t (mm)	Compact Limit, λ_p (AASHTO)	Non-compact Limit, λ_r (AASHTO)	b/t	Inside Bend Radius, r_b (mm)	Mid-Surface Distance from Flat Side to Flat Side, D (mm)
HEXADECAGONAL-C-1	140	7	26.97	30.34	20	35	766.83
HEXADECAGONAL-C-2		6.5			21.54	32.5	762.33
HEXADECAGONAL-C-3		5.5			25.45	27.5	753.33
HEXADECAGONAL-C-4		5			28	25.4	748.83
HEXADECAGONAL-C-5		4.6			30.43	25.4	745.23
HEXADECAGONAL-C-6		3.8			36.84	25.4	738.03
HEXADECAGONAL-C-7		2.8			50	25.4	729.03
HEXADECAGONAL-C-8		8			17.5	40	775.83
HEXADECAGONAL-C-9		7.5			18.67	37.5	771.33
HEXADECAGONAL-C-10		4.8			29.17	25.4	747.03
HEXADECAGONAL-C-11		5.2			26.92	26	750.63
HEXADECAGONAL-C-12		6			23.33	30	757.83
HEXADECAGONAL-C-13		30			4.67	150	973.83

Table A.3: (Cont.) Geometric Properties of Hexadecagonal (16-sided) Sections Subjected to Axial Compression

Specimen	Element Width, b (mm)	Thickness, t (mm)	Compact Limit, λ_p (AASHTO)	Non-compact Limit, λ_r (AASHTO)	b/t	Inside Bend Radius, r_b (mm)	Mid-Surface Distance from Flat Side to Flat Side, D (mm)
HEXADECAGONAL-C-14	140	23.3	26.97	30.34	6.01	116.5	913.53
HEXADECAGONAL-C-15		9.5			14.74	47.5	789.33
HEXADECAGONAL-C-16		12.73			11	63.65	818.4

Table A.4: Geometric Properties of Octagonal (8-sided) Compact Sections Subjected to Pure Bending

Specimen	Element Width, b (mm)	Thickness, t (mm)	Compact Limit, λ_p (AASHTO)	b/t	Inside Bend Radius, r_b (mm)	Mid-Surface Distance from Flat Side to Flat Side, D (mm)
OCTAGONAL-B-1	100	6.5	26.97	15.38	32.5	299.92
OCTAGONAL-B-2		6		16.67	30	295.42
OCTAGONAL-B-3		5.5		18.18	27.5	290.92
OCTAGONAL-B-4		5		20	25.4	286.42
OCTAGONAL-B-5		4.6		21.74	25.4	282.82
OCTAGONAL-B-6		4		25	25.4	277.42
OCTAGONAL-B-7		20		5	100	421.42
OCTAGONAL-B-8		14		7.14	70	367.42
OCTAGONAL-B-9		10		10	50	331.42
OCTAGONAL-B-10		9		11.11	45	322.42
OCTAGONAL-B-11		7.5		13.33	37.5	308.92
OCTAGONAL-B-12		3.71		26.95	25.4	274.81
OCTAGONAL-B-13		4.45		22.47	25.4	281.47
OCTAGONAL-B-14		4.17		23.98	25.4	278.95
OCTAGONAL-B-15	120	4.61		26.03	25.4	331.19
OCTAGONAL-B-16		5.22		22.99	26.1	336.68
OCTAGONAL-B-17		6.3		19.05	31.5	346.4
OCTAGONAL-B-18		8.28		14.49	41.4	364.22
OCTAGONAL-B-19		13.3		9.02	66.5	409.4

Table A.5: Geometric Properties of Octagonal (8-sided) Non-compact Sections Subjected to Pure Bending

Specimen	Element Width, b (mm)	Thickness, t (mm)	Compact Limit, λ_p (AASHTO)	Non-compact Limit, λ_r (AASHTO)	b/t	Inside Bend Radius, r_b (mm)	Mid-Surface Distance from Flat Side to Flat Side, D (mm)
OCTAGONAL-B-N-1	100	3.5	26.97	36.84	28.57	25.4	272.92
OCTAGONAL-B-N-2		3.3			30.3	25.4	271.12
OCTAGONAL-B-N-3		3			33.33	25.4	268.42
OCTAGONAL-B-N-4		3.125			32	25.4	269.55
OCTAGONAL-B-N-5		2.85			35.09	25.4	267.07
OCTAGONAL-B-N-6		2.715			36.83	25.4	265.86
OCTAGONAL-B-N-7		2.6796			37.32	25.4	265.54
OCTAGONAL-B-N-8		2.59582			38.52	25.4	264.78
OCTAGONAL-B-N-9		2.44312			40.93	25.4	263.41
OCTAGONAL-B-N-10		2.51716			39.73	25.4	264.08
OCTAGONAL-B-N-11		2.47221			40.45	25.4	263.67
OCTAGONAL-B-N-12		2.37332			42.14	25.4	262.78
OCTAGONAL-B-N-13	120	3.175			37.8	25.4	318.28
OCTAGONAL-B-N-14		3.33			36.04	25.4	319.67
OCTAGONAL-B-N-15		3.5			34.29	25.4	321.2
OCTAGONAL-B-N-16		4.1			29.27	25.4	326.6
OCTAGONAL-B-N-17		4.35			27.59	25.4	328.85

Table A.6: Geometric Properties of Dodecagonal (12-sided) Compact Sections Subjected to Pure Bending

Specimen	Element Width, b (mm)	Thickness, t (mm)	Compact Limit, λ_p (AASHTO)	b/t	Inside Bend Radius, r_b (mm)	Mid-Surface Distance from Flat Side to Flat Side, D (mm)
DODECAGONAL-B-1	95	6.5	26.97	14.62	32.5	413.04
DODECAGONAL-B-2		6		15.83	30	408.54
DODECAGONAL-B-3		5.5		17.27	27.5	404.04
DODECAGONAL-B-4		5		19	25.4	399.54
DODECAGONAL-B-5		4.6		20.65	25.4	395.94
DODECAGONAL-B-6		3.8		25	25.4	388.74
DODECAGONAL-B-7		20		4.75	100	534.54
DODECAGONAL-B-8		15		6.33	75	489.54
DODECAGONAL-B-9		10		9.5	50	444.54
DODECAGONAL-B-10		8		11.88	40	426.54
DODECAGONAL-B-11		7		13.57	35	417.54

Table A.6: (Cont.) Geometric Properties of Dodecagonal (12-sided) Compact Sections Subjected to Pure Bending

Specimen	Element Width, b (mm)	Thickness, t (mm)	Compact Limit, λ_p (AASHTO)	b/t	Inside Bend Radius, r_b (mm)	Mid-Surface Distance from Flat Side to Flat Side, D (mm)
DODECAGONAL-B-12	95	4	26.97	23.75	25.4	390.54
DODECAGONAL-B-13		3.524		26.96	25.4	386.26
DODECAGONAL-B-14		4.318		22	25.4	393.41
DODECAGONAL-B-15	115	4.42		26.02	25.4	468.96
DODECAGONAL-B-16		5		23	25.4	474.18
DODECAGONAL-B-17		6.39		18	31.95	486.69
DODECAGONAL-B-18		11		10.45	55	528.18
DODECAGONAL-B-19		14.375		8	71.875	558.56

Table A.7: Geometric Properties of Dodecagonal (12-sided) Non-compact Sections Subjected to Pure Bending

Specimen	Element Width, b (mm)	Thickness, t (mm)	Compact Limit, λ_p (AASHTO)	Non-compact Limit, λ_r (AASHTO)	b/t	Inside Bend Radius, r_b (mm)	Mid-Surface Distance from Flat Side to Flat Side, D (mm)
DODECAGONAL-B-N-1	95	3.25	26.97	33.95	29.23	25.4	383.79
DODECAGONAL-B-N-2		3			31.67	25.4	381.54
DODECAGONAL-B-N-3		2.8			33.93	25.4	379.74
DODECAGONAL-B-N-4		3.39			28.02	25.4	385.05
DODECAGONAL-B-N-5		3.16			30.06	25.4	382.98
DODECAGONAL-B-N-6		2.87			33.1	25.4	380.37
DODECAGONAL-B-N-7		2.72114			34.91	25.4	379.03
DODECAGONAL-B-N-8		2.3913			39.73	25.4	376.07
DODECAGONAL-B-N-9		2.54558			37.32	25.4	377.45
DODECAGONAL-B-N-10		2.51315			37.8	25.4	377.16
DODECAGONAL-B-N-11		2.48154			38.28	25.4	376.88
DODECAGONAL-B-N-12		2.63043			36.12	25.4	378.22
DODECAGONAL-B-N-13	115	4.18			27.51	25.4	466.8
DODECAGONAL-B-N-14		4			28.75	25.4	465.18
DODECAGONAL-B-N-15		3.73			30.83	25.4	462.75
DODECAGONAL-B-N-16		3.54			32.49	25.4	461.04
DODECAGONAL-B-N-17		3.24			35.49	25.4	458.34

Table A.8: Geometric Properties of Hexadecagonal (16-sided) Compact Sections Subjected to Pure Bending

Specimen	Element Width, b (mm)	Thickness, t (mm)	Compact Limit, λ_p (AASHTO)	b/t	Inside Bend Radius, r_b (mm)	Mid-Surface Distance from Flat Side to Flat Side, D (mm)
HEXADECAGONAL-B-1	140	8	26.97	17.5	40	775.83
HEXADECAGONAL-B-2		7.5		18.67	37.5	771.33
HEXADECAGONAL-B-3		7		20	35	766.83
HEXADECAGONAL-B-4		6.5		21.54	32.5	762.33
HEXADECAGONAL-B-5		5.5		25.45	27.5	753.33
HEXADECAGONAL-B-6		6		23.33	30	757.83
HEXADECAGONAL-B-7		30		4.67	150	973.83
HEXADECAGONAL-B-8		23.3		6.01	116.5	913.53
HEXADECAGONAL-B-9		14		10	70	829.83
HEXADECAGONAL-B-10		17		8.24	85	856.83
HEXADECAGONAL-B-11		11		12.73	55	802.83
HEXADECAGONAL-B-12		5.2		26.92	26	750.63
HEXADECAGONAL-B-13		9.5		14.74	47.5	789.33
HEXADECAGONAL-B-14		12.73		11	63.65	818.4
HEXADECAGONAL-B-15		8.75		16	43.75	782.58
HEXADECAGONAL-B-16		20		7	100	883.83
HEXADECAGONAL-B-17	160	17.78		9	88.9	964.39
HEXADECAGONAL-B-18		11.85		13.5	59.25	911.02
HEXADECAGONAL-B-19		6.53		24.5	32.65	863.14
HEXADECAGONAL-B-20		7.11		22.5	35.55	868.36
HEXADECAGONAL-B-21		6.08		26.32	30.4	859.09

Table A.9: Geometric Properties of Hexadecagonal (16-sided) Non-compact Sections Subjected to Pure Bending

Specimen	Element Width, b (mm)	Thickness, t (mm)	Compact Limit, λ_p (AASHTO)	Non-compact Limit, λ_r (AASHTO)	b/t	Inside Bend Radius, r_b (mm)	Mid-Surface Distance from Flat Side to Flat Side, D (mm)
HEXADECAGONAL-B-N-1	140	5.1	26.97	30.34	27.45	25.5	749.73
HEXADECAGONAL-B-N-2		5			28	25.4	748.83
HEXADECAGONAL-B-N-3		4.8			29.17	25.4	747.03
HEXADECAGONAL-B-N-4		4.65			30.11	25.4	745.68
HEXADECAGONAL-B-N-5		3.87642			36.12	25.4	738.71
HEXADECAGONAL-B-N-6		3.63415			38.52	25.4	736.53
HEXADECAGONAL-B-N-7		3.95554			35.39	25.4	739.43

Table A.9**:** (Cont.) Geometric Properties of Hexadecagonal (16-sided) Non-compact Sections Subjected to Pure Bending

Specimen	Element Width, b (mm)	Thickness, t (mm)	Compact Limit, λ_p (AASHTO)	Non-compact Limit, λ_r (AASHTO)	b/t	Inside Bend Radius, r_b (mm)	Mid-Surface Distance from Flat Side to Flat Side, D (mm)
HEXADECAGONAL-B-N-8	140	4.01009	26.97	30.34	34.91	25.4	739.92
HEXADECAGONAL-B-N-9		4.40503			31.78	25.4	743.47
HEXADECAGONAL-B-N-10		4.15331			33.71	25.4	741.21
HEXADECAGONAL-B-N-11	160	5.61			28.52	28.05	854.86
HEXADECAGONAL-B-N-12		5.4			29.63	27	852.97
HEXADECAGONAL-B-N-13		5.274			30.34	26.37	851.84
HEXADECAGONAL-B-N-14		5.16			31.01	25.8	850.81
HEXADECAGONAL-B-N-15		4.92			32.52	25.4	848.65

Table A.10: Multi-sided tube sections with concentrated load at mid-spans

Specimen	Number of Sides, n	Element Width, b (mm)	Thickness, t (mm)	b/t	M_{FE} (Concentrated Load)	M_{FE} (Constant moment)
OCTAGONAL-B-10	8	100	9	11.11	460.55	377.13
OCTAGONAL-B-12			3.71	26.95	108.94	98.74
OCTAGONAL-B-13			4.45	22.47	145.53	128.63
OCTAGONAL-B-N-2			3.3	30.3	91.37	81.38
OCTAGONAL-B-N-6			2.85	35.09	74.2	64.05
DODECAGONAL-B-3	12	95	5.5	17.27	370.73	320.76
DODECAGONAL-B-9			10	9.5	893.41	739.09
DODECAGONAL-B-13			3.524	26.96	190.55	170.94
DODECAGONAL-B-N-2			3.25	29.23	169.3	150.18
DODECAGONAL-B-N-7			2.87	33.1	139.74	122.26
HEXADECAGONAL-B-3	16	140	7	20	1502.94	1357.77
HEXADECAGONAL-B-12			5.2	26.92	988.9	892.52
HEXADECAGONAL-B-15			8.75	16	2031.74	1819.43
HEXADECAGONAL-B-16			20	7	6717.56	5715.58
HEXADECAGONAL-B-N-10			4.15331	33.71	685.77	644.6

Table A.11: Geometric Properties of Octagonal (8-sided) Compact Sections Subjected to Combined Bending and Compression

Specimen	Element Width, b (mm)	Thickness, t (mm)	Compact Limit, λ_p (AASHTO)	b/t	Inside Bend Radius, r_b (mm)	Mid-Surface Distance from Flat Side to Flat Side, D (mm)
OCTAGONAL-COMB-1	100	6.5	26.97	15.38	32.5	299.92
OCTAGONAL-COMB-2		6		16.67	30	295.42
OCTAGONAL-COMB-3		5.5		18.18	27.5	290.92
OCTAGONAL-COMB-4		5		20	25.4	286.42
OCTAGONAL-COMB-5		4.6		21.74	25.4	282.82
OCTAGONAL-COMB-6		4		25	25.4	277.42
OCTAGONAL-COMB-7		20		5	100	421.42
OCTAGONAL-COMB-8		14		7.14	70	367.42
OCTAGONAL-COMB-9		10		10	50	331.42
OCTAGONAL-COMB-10		9		11.11	45	322.42
OCTAGONAL-COMB-11		7.5		13.33	37.5	308.92
OCTAGONAL-COMB-12		3.71		26.95	25.4	274.81
OCTAGONAL-COMB-13		4.45		22.47	25.4	281.47
OCTAGONAL-COMB-14		4.17		23.98	25.4	278.95

Table A.12: Geometric Properties of Octagonal (8-sided) Non-compact Sections Subjected to Combined Bending and Compression

Specimen	Element Width, b (mm)	Thickness, t (mm)	Compact Limit, λ_p (AASHTO)	Non-compact Limit, λ_r (AASHTO)	b/t	Inside Bend Radius, r_b (mm)	Mid-Surface Distance from Flat Side to Flat Side, D (mm)
OCTAGONAL-COMB-N-1	100	3.5	26.97	36.84	28.57	25.4	272.92
OCTAGONAL-COMB-N-2		3.3			30.3	25.4	271.12
OCTAGONAL-COMB-N-3		3			33.33	25.4	268.42
OCTAGONAL-COMB-N-4		3.125			32	25.4	269.55
OCTAGONAL-COMB-N-5		2.85			35.09	25.4	267.07
OCTAGONAL-COMB-N-6		2.715			36.83	25.4	265.86
OCTAGONAL-COMB-N-7		2.6796			37.32	25.4	265.54
OCTAGONAL-COMB-N-8		2.47221			40.45	25.4	263.67

Table A.13: Geometric Properties of Dodecagonal (12-sided) Compact Sections Subjected to Combined Bending and Compression

Specimen	Element Width, b (mm)	Thickness, t (mm)	Compact Limit, λ_p (AASHTO)	b/t	Inside Bend Radius, r_b (mm)	Mid-Surface Distance from Flat Side to Flat Side, D (mm)
DODECAGONAL-COMB-1	95	6.5	26.97	14.62	32.5	413.04
DODECAGONAL-COMB-2		6		15.83	30	408.54
DODECAGONAL-COMB-3		5.5		17.27	27.5	404.04
DODECAGONAL-COMB-4		5		19	25.4	399.54
DODECAGONAL-COMB-5		4.6		20.65	25.4	395.94
DODECAGONAL-COMB-6		3.8		25	25.4	388.74
DODECAGONAL-COMB-7		20		4.75	100	534.54
DODECAGONAL-COMB-8		15		6.33	75	489.54
DODECAGONAL-COMB-9		10		9.5	50	444.54
DODECAGONAL-COMB-10		8		11.88	40	426.54
DODECAGONAL-COMB-11		7		13.57	35	417.54
DODECAGONAL-COMB-12		4		23.75	25.4	390.54
DODECAGONAL-COMB-13		3.524		26.96	25.4	386.26
DODECAGONAL-COMB-14		4.318		22	25.4	393.41

Table A.14: Geometric Properties of Dodecagonal (12-sided) Non-compact Sections Subjected to Combined Bending and Compression

Specimen	Element Width, b (mm)	Thickness, t (mm)	Compact Limit, λ_p (AASHTO)	Non-compact Limit, λ_r (AASHTO)	b/t	Inside Bend Radius, r_b (mm)	Mid-Surface Distance from Flat Side to Flat Side, D (mm)
DODECAGONAL-COMB-N-1	95	3.25	26.97	33.95	29.23	25.4	383.79
DODECAGONAL-COMB-N-2		3			31.67	25.4	381.54
DODECAGONAL-COMB-N-3		2.8			33.93	25.4	379.74
DODECAGONAL-COMB-N-4		3.39			28.02	25.4	385.05
DODECAGONAL-COMB-N-5		3.16			30.06	25.4	382.98
DODECAGONAL-COMB-N-6		2.87			33.10	25.4	380.37
DODECAGONAL-COMB-N-7		2.72114			34.91	25.4	379.03
DODECAGONAL-COMB-N-8		2.63043			36.12	25.4	378.22

Table A.15: Geometric Properties of Hexadecagonal (16-sided) Compact Sections Subjected to Combined Bending and Compression

Specimen	Element Width, b (mm)	Thickness, t (mm)	Compact Limit, λ_p (AASHTO)	b/t	Inside Bend Radius, r_b (mm)	Mid-Surface Distance from Flat Side to Flat Side, D (mm)
HEXADECAGONAL-COMB-1	140	8	26.97	17.5	40	775.83
HEXADECAGONAL-COMB-2		7.5		18.67	37.5	771.33
HEXADECAGONAL-COMB-3		7		20	35	766.83
HEXADECAGONAL-COMB-4		6.5		21.54	32.5	762.33
HEXADECAGONAL-COMB-5		5.5		25.45	27.5	753.33
HEXADECAGONAL-COMB-6		6		23.33	30	757.83
HEXADECAGONAL-COMB-7		30		4.67	150	973.83
HEXADECAGONAL-COMB-8		23.3		6.01	116.5	913.53
HEXADECAGONAL-COMB-9		14		10	70	829.83
HEXADECAGONAL-COMB-10		17		8.24	85	856.83
HEXADECAGONAL-COMB-11		11		12.73	55	802.83
HEXADECAGONAL-COMB-12		5.2		26.92	26	750.63
HEXADECAGONAL-COMB-13		9.5		14.74	47.5	789.33
HEXADECAGONAL-COMB-14		12.73		11	63.65	818.4
HEXADECAGONAL-COMB-15		8.75		16	43.75	782.58
HEXADECAGONAL-COMB-16		46.7		3	233.5	1124.13

Table A.16: Geometric Properties of Hexadecagonal (16-sided) Non-compact Sections Subjected to Combined Bending and Compression

Specimen	Element Width, b (mm)	Thickness, t (mm)	Compact Limit, λ_p (AASHTO)	Non-compact Limit, λ_r (AASHTO)	b/t	Inside Bend Radius, r_b (mm)	Mid-Surface Distance from Flat Side to Flat Side, D (mm)
HEXADECAGONAL-COMB-N-1	140	5.1	26.97	30.34	27.45	25.5	749.73
HEXADECAGONAL-COMB-N-2		5			28	25.4	748.83
HEXADECAGONAL-COMB-N-3		4.8			29.17	25.4	747.03
HEXADECAGONAL-COMB-N-4		4.65			30.11	25.4	745.68
HEXADECAGONAL-COMB-N-5		4.40503			31.78	25.4	743.47
HEXADECAGONAL-COMB-N-6		4.15331			33.71	25.4	741.21

Table A.17: Geometric Properties of Octagonal (8-sided) Compact Sections Subjected to Pure Torsion

Specimen	Element Width, b (mm)	Thickness, t (mm)	Compact Limit, λ_p (AASHTO)	b/t	Inside Bend Radius, r_b (mm)	Mid-Surface Distance from Flat Side to Flat Side, D (mm)
OCTAGONAL-TOR-1	100	6.5	26.97	15.38	32.5	299.92
OCTAGONAL-TOR-2		6		16.67	30	295.42
OCTAGONAL-TOR-3		5.5		18.18	27.5	290.92
OCTAGONAL-TOR-4		5		20	25.4	286.42
OCTAGONAL-TOR-5		4.6		21.74	25.4	282.82
OCTAGONAL-TOR-6		4		25	25.4	277.42
OCTAGONAL-TOR-7		3.71		26.95	25.4	274.81

Table A.18: Geometric Properties of Octagonal (8-sided) Non-compact Sections Subjected to Pure Torsion

Specimen	Element Width, b (mm)	Thickness, t (mm)	Compact Limit, λ_p (AASHTO)	Non-compact Limit, λ_r (AASHTO)	b/t	Inside Bend Radius, r_b (mm)	Mid-Surface Distance from Flat Side to Flat Side, D (mm)
OCTAGONAL-TOR-N-1	100	3.5	26.97	36.84	28.57	25.4	272.92
OCTAGONAL-TOR-N-2		3.3			30.3	25.4	271.12
OCTAGONAL-TOR-N-3		3			33.33	25.4	268.42
OCTAGONAL-TOR-N-4		2.72			36.76	25.4	265.9

Table A.19: Geometric Properties of Dodecagonal (12-sided) Compact Sections Subjected to Pure Torsion

Specimen	Element Width, b (mm)	Thickness, t (mm)	Compact Limit, λ_p (AASHTO)	b/t	Inside Bend Radius, r_b (mm)	Mid-Surface Distance from Flat Side to Flat Side, D (mm)
DODECAGONAL-TOR-1	95	6.5	26.97	14.62	32.5	413.04
DODECAGONAL-TOR-2		6		15.83	30	408.54
DODECAGONAL-TOR-3		5.5		17.27	27.5	404.04
DODECAGONAL-TOR-4		5		19	25.4	399.54
DODECAGONAL-TOR-5		4.6		20.65	25.4	395.94
DODECAGONAL-TOR-6		3.8		25	25.4	388.74
DODECAGONAL-TOR-7		3.524		26.96	25.4	386.26

Table A.20: Geometric Properties of Dodecagonal (12-sided) Non-compact Sections Subjected to Pure Torsion

Specimen	Element Width, b (mm)	Thickness, t (mm)	Compact Limit, λ_p (AASHTO)	Non-compact Limit, λ_r (AASHTO)	b/t	Inside Bend Radius, r_b (mm)	Mid-Surface Distance from Flat Side to Flat Side, D (mm)
DODECAGONAL-TOR-N-1	95	3.39	26.97	33.95	28.02	25.4	385.05
DODECAGONAL-TOR-N-2		3.25			29.23	25.4	383.79
DODECAGONAL-TOR-N-3		3			31.67	25.4	381.54
DODECAGONAL-TOR-N-4		2.8			33.93	25.4	379.74

Table A.21: Geometric Properties of Hexadecagonal (16-sided) Compact Sections Subjected to Pure Torsion

Specimen	Element Width, b (mm)	Thickness, t (mm)	Compact Limit, λ_p (AASHTO)	b/t	Inside Bend Radius, r_b (mm)	Mid-Surface Distance from Flat Side to Flat Side, D (mm)
HEXADECAGONAL-TOR-1	140	8	26.97	17.5	40	775.83
HEXADECAGONAL-TOR-2		7.5		18.67	37.5	771.33
HEXADECAGONAL-TOR-3		7		20	35	766.83
HEXADECAGONAL-TOR-4		6.5		21.54	32.5	762.33
HEXADECAGONAL-TOR-5		5.5		25.45	27.5	753.33
HEXADECAGONAL-TOR-6		6		23.33	30	757.83
HEXADECAGONAL-TOR-7		9.5		14.74	47.5	789.33

Table A.22: Geometric Properties of Hexadecagonal (16-sided) Non-compact Sections Subjected to Pure Torsion

Specimen	Element Width, b (mm)	Thickness, t (mm)	Compact Limit, λ_p (AASHTO)	Non-compact Limit, λ_r (AASHTO)	b/t	Inside Bend Radius, r_b (mm)	Mid-Surface Distance from Flat Side to Flat Side, D (mm)
HEXADECAGONAL-TOR-N-1	140	5.2	26.97	30.34	26.92	26	750.63
HEXADECAGONAL-TOR-N-2		5			28	25.4	748.83
HEXADECAGONAL-TOR-N-3		4.8			29.17	25.4	747.03
HEXADECAGONAL-TOR-N-4		4.65			30.11	25.4	745.68

Appendix B

Table B.1: FE Results of the Models subjected to Axial Compression

Specimen	P_{FEM} (KN)	Specimen	P_{FEM} (KN)	Specimen	P_{FEM} (KN)
OCTAGONAL-C-1	2137.42	DODECAGONAL-C-1	3019.37	HEXADECAGONAL-C-1	5985.71
OCTAGONAL-C-2	1663.09	DODECAGONAL-C-2	2665.59	HEXADECAGONAL-C-2	5495.11
OCTAGONAL-C-3	1491.45	DODECAGONAL-C-3	2305.82	HEXADECAGONAL-C-3	4529.20
OCTAGONAL-C-4	1066.80	DODECAGONAL-C-4	1643.11	HEXADECAGONAL-C-4	4061.47
OCTAGONAL-C-5	883.86	DODECAGONAL-C-5	985.83	HEXADECAGONAL-C-5	3689.01
OCTAGONAL-C-6	612.71	DODECAGONAL-C-6	809.19	HEXADECAGONAL-C-6	2870.32
OCTAGONAL-C-7	495.45	DODECAGONAL-C-7	679.04	HEXADECAGONAL-C-7	1674.40
OCTAGONAL-C-8	371.78	DODECAGONAL-C-8	1487.61	HEXADECAGONAL-C-8	7018.68
OCTAGONAL-C-9	2412.14	DODECAGONAL-C-9	1365.15	HEXADECAGONAL-C-9	6508.00
OCTAGONAL-C-10	1885.19	DODECAGONAL-C-10	1144.10	HEXADECAGONAL-C-10	3855.56
OCTAGONAL-C-11	780.28	DODECAGONAL-C-11	2081.41	HEXADECAGONAL-C-11	4249.72
OCTAGONAL-C-12	1250.04	DODECAGONAL-C-12	10272.50	HEXADECAGONAL-C-12	4992.32
OCTAGONAL-C-13	7493.98	DODECAGONAL-C-13	5960.11	HEXADECAGONAL-C-13	40229.94
OCTAGONAL-C-14	4036.46	DODECAGONAL-C-14	3721.95	HEXADECAGONAL-C-14	28530.02
OCTAGONAL-C-15	1143.83	DODECAGONAL-C-15	1746.83	HEXADECAGONAL-C-15	8649.75
OCTAGONAL-C-16	1315.94	DODECAGONAL-C-16	1924.71	HEXADECAGONAL-C-16	12593.68

Calculation of Elastic Moment Capacity (M_y) and Plastic Moment Capacity (M_p)

AASHTO has provided a sectional property table for common tubular shapes. Table B.2 shows the sectional property provided by AASHTO. In this study, this Table B.2 has been used to calculate Elastic Moment Capacity (M_y) and Plastic Moment Capacity (M_p) for the multi-sided tubes, as well as the rounded tubes.

Table B.2: Sectional Properties for Common Tubular Shapes (AASHTO 2015)

Property	Round Tube	Hexadecagonal Tube	Dodecagonal Tube	Octagonal Tube
Moment of Inertia, I	3.14 R'^3t	3.22R'^3t	3.29R'^3t	3.50R'^3t
Section Modulus, S	3.14R'^2t	3.22R'^2t	3.29R'^2t	3.50R'^2t
Area, A	6.28R't	6.37R't	6.43R't	6.63R't
Shape Factor, K_p=Z/S	1.27	1.27	1.26	1.24
Radius of Gyration, r	0.707R'	0.711R'	0.715R'	0.727R'

Elastic Moment Capacity (M_y) and Plastic Moment Capacity (M_p) Calculation for the Octagonal Sections

Calculations are shown for OCTAGONAL-B-1, which has the following properties,

Mid-surface Distance from Flat Side to Flat Side, D= 299.92 mm

Wall thickness, t= 6.5 mm

Yield Stress, F_y= 345 MPa

Radius Measured to the Mid-thickness of the wall, $R' = \frac{D}{2} = \frac{299.92}{2} = 149.96$ mm

Section Modulus, $S = 3.50 \times R'^2 \times t = 3.50 \times (149.96)^2 \times 6.5 = 511602.0364$ mm^4

Shape Factor, K_p=1.24

Plastic Section Modulus, $Z = S \times K_p = 511602.0364 \times 1.24 = 634386.5251$ mm^4

Plastic Moment Capacity, $M_p = Z \times F_y = 634386.5251 \times 345$ N-mm $= 218.86$ KN-m

Elastic Moment Capacity, $M_y = S \times F_y = 511602.0364 \times 345$ N-mm $= 176.50$ KN-m

Elastic Moment Capacity (M_y) and Plastic Moment Capacity (M_p) Calculation for the Dodecagonal Sections

Calculations are shown for DODECAGONAL-B-1, which has the following properties,

Mid-surface Distance from Flat Side to Flat Side, D= 413.04 mm

Wall thickness, t= 6.5 mm

Yield Stress, F_y= 345 MPa

Radius Measured to the Mid-thickness of the wall, $R' = \frac{D}{2} = \frac{413.04}{2} = 206.52$ mm

Section Modulus, $S = 3.29 \times R'^2 \times t = 3.29 \times (206.52)^2 \times 6.5 = 912081.1649$ mm^4

Shape Factor, K_p=1.26

Plastic Section Modulus, $Z = S \times K_p = 912081.1649 \times 1.26 = 1149222.268$ mm^4

Plastic Moment Capacity, $M_p = Z \times F_y = 1149222.268 \times 345$ N-mm $= 396.48$ KN-m

Elastic Moment Capacity, $M_y = S \times F_y = 912081.1649 \times 345$ N-mm $= 314.67$ KN-m

Elastic Moment Capacity (M_y) and Plastic Moment Capacity (M_p) Calculation for the Hexadecagonal Sections

Calculations are shown for HEXADECAGON-B-1, which has the following properties,

Mid-surface Distance from Flat Side to Flat Side, D= 775.83 mm

Wall thickness, t= 8 mm

Yield Stress, F_y= 345 MPa

Radius Measured to the Mid-thickness of the wall, $R' = \frac{D}{2} = \frac{775.83}{2} = 387.915$ mm

Section Modulus, $S = 3.22 \times R'^2 \times t = 3.22 \times (387.915)^2 \times 8 = 3876314.497$ mm^4

Shape Factor, K_p= 1.27

Plastic Section Modulus, $Z = S \times K_p = 3876314.497 \times 1.27 = 4922919.411$ mm^4

Plastic Moment Capacity, $M_p = Z \times F_y = 4922919.411 \times 345$ N-mm $= 1698.41$ KN-m

Elastic Moment Capacity, $M_y = S \times F_y = 3876314.497 \times 345$ N-mm $= 1337.33$ KN-m

Table B.3: FE Results and Code Suggested Resistances of Octagonal Compact Sections Subjected to Pure Bending

Specimen	M_{FEM} (KN-m)	M_p (KN-m)	M_y (KN-m)	M_{AASHTO} (KN-m)	M_{ASCE} (KN-m)	M_{Euro} (KN-m)	M_{EN} (KN-m)
OCTAGONAL-B-1	225	218.86	176.5	201.1	176.5	218.86	176.5
OCTAGONAL-B-2	200.6	196.01	158.07	180.1	158.07	196.01	158.07
OCTAGONAL-B-3	175.86	174.25	140.52	160.1	140.52	174.25	140.52
OCTAGONAL-B-4	153	153.54	123.82	141.08	123.82	153.54	123.82
OCTAGONAL-B-5	135.22	137.73	111.07	126.55	111.07	137.73	111.07
OCTAGONAL-B-6	110.26	115.24	92.93	105.88	92.93	115.24	92.93
OCTAGONAL-B-7	1557	1329.57	1072.23	1221.67	1072.23	1329.57	1072.23
OCTAGONAL-B-8	810	707.46	570.54	650.05	570.54	707.46	570.54
OCTAGONAL-B-9	452.61	411.16	331.58	377.79	331.58	411.16	331.58
OCTAGONAL-B-10	377.13	350.22	282.43	321.8	282.43	350.22	282.43
OCTAGONAL-B-11	280.6	267.92	216.06	246.18	216.06	267.92	216.06
OCTAGONAL-B-12	98.74	104.88	84.58	96.37	84.58	104.88	84.58
OCTAGONAL-B-13	128.63	131.97	106.43	121.26	106.43	131.97	106.43
OCTAGONAL-B-14	116.87	121.46	97.95	111.6	97.95	121.46	97.95
OCTAGONAL-B-15	177	189.29	152.65	173.92	152.65	189.29	152.65
OCTAGONAL-B-16	214.76	221.5	178.63	203.52	178.63	221.5	178.63

Table B.3: (Cont.) FE Results and Code Suggested Resistances of Octagonal Compact Sections Subjected to Pure Bending

Specimen	M_{FEM} (KN-m)	M_p (KN-m)	M_y (KN-m)	M_{AASHTO} (KN-m)	M_{ASCE} (KN-m)	M_{Euro} (KN-m)	M_{EN} (KN-m)
OCTAGONAL-B-17	282.51	282.98	228.21	260.02	228.21	282.98	228.21
OCTAGONAL-B-18	427.75	411.17	331.59	377.8	331.59	411.17	331.59
OCTAGONAL-B-19	934.65	834.46	672.95	766.74	672.95	834.46	672.95

Table B.4: FE Results and Code Suggested Resistances of Octagonal Non-compact Sections Subjected to Pure Bending

Specimen	M_{FEM} (KN-m)	M_p (KN-m)	M_y (KN-m)	M_{AASHTO} (KN-m)	M_{ASCE} (KN-m)	M_{Euro} (KN-m)	M_{EN} (KN-m)
OCTAGONAL-B-N-1	89.96	97.59	78.70	79.71	78.70	97.59	78.70
OCTAGONAL-B-N-2	81.38	90.8	73.23	73.66	73.23	90.8	73.23
OCTAGONAL-B-N-3	69.28	80.91	65.25	64.95	65.25	80.91	63.75
OCTAGONAL-B-N-4	74.95	84.99	68.54	68.53	68.54	84.99	67.6
OCTAGONAL-B-N-5	64.05	76.09	61.37	60.76	61.37	76.09	58.83
OCTAGONAL-B-N-6	59.84	71.83	57.93	57.07	57.77	57.93	54.48
OCTAGONAL-B-N-7	58.48	70.72	57.04	56.12	56.56	57.04	53.38
OCTAGONAL-B-N-8	55.68	68.12	54.94	53.68	53.72	54.94	50.91
OCTAGONAL-B-N-9	50.63	63.45	51.17	48.61	48.63	45.86	45.86
OCTAGONAL-B-N-10	53.23	65.71	52.99	51.05	51.09	48.57	48.57
OCTAGONAL-B-N-11	51.59	64.34	51.88	49.56	49.59	47	47
OCTAGONAL-B-N-12	47.51	61.35	49.47	46.32	46.33	43.41	43.41
OCTAGONAL-B-N-13	97.61	120.4	97.09	95.42	95.76	97.09	91.75
OCTAGONAL-B-N-14	102.87	127.38	102.73	101.43	102.73	102.73	98.02
OCTAGONAL-B-N-15	113.03	135.17	109.01	108.19	109.01	135.17	105.01
OCTAGONAL-B-N-16	145.36	163.71	132.03	133.34	132.03	163.71	132.03
OCTAGONAL-B-N-17	160.82	176.09	142.01	144.44	142.01	176.09	142.01

Table B.5: FE Results and Code Suggested Resistances of Dodecagonal Compact Sections Subjected to Pure Bending

Specimen	M_{FEM} (KN-m)	M_p (KN-m)	M_y (KN-m)	M_{AASHTO} (KN-m)	M_{ASCE} (KN-m)	M_{Euro} (KN-m)	M_{EN} (KN-m)
DODECAGONAL-B-1	403.24	396.48	314.67	381.42	314.67	396.48	314.67
DODECAGONAL-B-2	361.39	358.06	284.17	344.45	284.17	358.06	284.17
DODECAGONAL-B-3	320.76	321.03	254.79	308.82	254.79	321.03	254.79
DODECAGONAL-B-4	281.77	285.38	226.49	274.53	226.49	285.38	226.49
DODECAGONAL-B-5	251.09	257.84	204.64	248.04	204.64	257.84	204.64
DODECAGONAL-B-6	191.77	205.32	162.95	197.52	162.95	205.32	162.95
DODECAGONAL-B-7	2306.1	2043.25	1621.63	1965.57	1621.63	2043.25	1621.63
DODECAGONAL-B-8	1407.32	1285.29	1020.07	1236.42	1020.07	1285.29	1020.07
DODECAGONAL-B-9	739.09	706.57	560.77	679.71	560.77	706.57	560.77
DODECAGONAL-B-10	537.16	520.41	413.02	500.62	413.02	520.41	413.02
DODECAGONAL-B-11	445.96	436.34	346.3	419.75	346.3	436.34	346.30
DODECAGONAL-B-12	204.73	218.14	173.12	209.84	173.12	218.14	173.12
DODECAGONAL-B-13	170.94	187.98	149.19	180.84	149.19	187.98	149.19
DODECAGONAL-B-14	229.94	238.94	189.64	229.86	189.64	238.94	189.64
DODECAGONAL-B-15	318.34	347.56	275.84	334.35	275.84	347.56	275.84
DODECAGONAL-B-16	382.26	401.97	319.02	386.69	319.02	401.97	319.02
DODECAGONAL-B-17	539.15	541.18	429.51	520.6	429.51	541.18	429.51
DODECAGONAL-B-18	1151.36	1097.21	870.8	1055.5	870.8	1097.21	870.80
DODECAGONAL-B-19	1721.29	1603.51	1272.63	1542.55	1272.63	1603.51	1272.63

Table B.6: FE Results and Code Suggested Resistances of Dodecagonal Non-compact Sections Subjected to Pure Bending

Specimen	M_{FEM} (KN-m)	M_p (KN-m)	M_y (KN-m)	M_{AASHTO} (KN-m)	M_{ASCE} (KN-m)	M_{Euro} (KN-m)	M_{EN} (KN-m)
DODECAGONAL-B-N-1	150.18	171.16	135.84	139.72	135.84	171.16	135.84
DODECAGONAL-B-N-2	132.75	156.15	123.93	126.62	123.93	156.15	123.93
DODECAGONAL-B-N-3	119.08	144.37	114.58	115.16	114.58	144.37	109.85
DODECAGONAL-B-N-4	161.1	179.71	142.63	147.23	142.63	179.71	142.63
DODECAGONAL-B-N-5	145.91	165.72	131.52	134.95	131.52	165.72	131.52
DODECAGONAL-B-N-6	122.26	148.47	117.83	119.97	117.83	148.47	117.83
DODECAGONAL-B-N-7	114.53	139.78	110.93	110.07	109.5	110.93	105.85
DODECAGONAL-B-N-8	95.91	120.92	95.97	89.18	88.59	88.05	88.05
DODECAGONAL-B-N-9	104.95	129.67	102.91	98.87	98.29	102.91	96.31

Table B.6**:** (Cont.) FE Results and Code Suggested Resistances of Dodecagonal Non-compact Sections Subjected to Pure Bending

Specimen	M_{FEM} (KN-m)	M_p (KN-m)	M_y (KN-m)	M_{AASHTO} (KN-m)	M_{ASCE} (KN-m)	M_{Euro} (KN-m)	M_{EN} (KN-m)
DODECAGONAL-B-N-10	102.95	127.82	101.44	96.82	96.24	101.44	94.01
DODECAGONAL-B-N-11	99.87	126.02	100.02	94.83	94.25	92.22	92.22
DODECAGONAL-B-N-12	108.75	134.54	106.77	104.26	103.69	106.77	101.39
DODECAGONAL-B-N-13	291.71	325.67	258.47	267.25	258.47	325.67	258.47
DODECAGONAL-B-N-14	270.87	309.48	245.62	252.99	245.62	309.48	245.62
DODECAGONAL-B-N-15	242.16	285.59	226.66	232.08	226.66	285.59	226.66
DODECAGONAL-B-N-16	227.97	269.04	213.52	217.72	213.52	269.04	211.57
DODECAGONAL-B-N-17	198.86	243.36	193.15	190.18	189.15	193.15	184.29

Table B.7: FE Results and Code Suggested Resistances of Hexadecagonal Compact Sections Subjected to Pure Bending

Specimen	M_{FEM} (KN-m)	M_p (KN-m)	M_y (KN-m)	M_{AASHTO} (KN-m)	M_{ASCE} (KN-m)	M_{Euro} (KN-m)	M_{EN} (KN-m)
HEXADECAGONAL-B-1	1623.52	1698.41	1337.33	1656.19	1337.33	1698.41	1337.31
HEXADECAGONAL-B-2	1485.37	1573.82	1239.23	1534.72	1239.23	1573.82	1239.23
HEXADECAGONAL-B-3	1357.77	1451.81	1143.16	1415.74	1143.16	1451.81	1143.16
HEXADECAGONAL-B-4	1225.43	1332.33	1049.08	1299.23	1049.08	1332.33	1049.08
HEXADECAGONAL-B-5	969.51	1100.9	866.85	1073.55	866.85	1100.9	866.85
HEXADECAGONAL-B-6	1084.47	1215.37	956.98	1185.18	956.98	1215.37	956.98
HEXADECAGONAL-B-7	10929.2	10034.66	7901.3	9785.35	7901.3	10034.66	7901.30
HEXADECAGONAL-B-8	7249.01	6858.3	5400.23	6687.9	5400.23	6858.3	5400.23
HEXADECAGONAL-B-9	3394.17	3400.33	2677.42	3315.85	2677.42	3400.33	2677.42
HEXADECAGONAL-B-10	4485.79	4402.03	3466.16	4292.66	3466.16	4402.03	3466.16
HEXADECAGONAL-B-11	2441.29	2500.66	1969.02	2438.53	1969.02	2500.66	1969.02
HEXADECAGONAL-B-12	892.52	1033.40	813.70	1007.73	813.70	1033.40	813.70
HEXADECAGONAL-B-13	2006.82	2087.64	1643.81	2035.77	1643.81	2087.64	1643.81
HEXADECAGONAL-B-14	2979.35	3007.28	2367.94	2932.57	2367.94	3007.28	2367.94
HEXADECAGONAL-B-15	1819.43	1890.08	1488.25	1843.12	1488.25	1890.08	1488.25
HEXADECAGONAL-B-16	5715.58	5510.39	4338.89	5373.48	4338.89	5510.39	4338.89
HEXADECAGONAL-B-17	5902.33	5832.54	4592.55	5687.64	4592.55	5832.54	4592.55
HEXADECAGONAL-B-18	3368.21	3468.93	2731.44	3382.74	2731.44	3468.93	2731.44
HEXADECAGONAL-B-19	1535.34	1715.92	1351.12	1673.29	1351.12	1715.92	1351.12
HEXADECAGONAL-B-20	1717.5	1890.99	1488.97	1844.01	1488.97	1890.99	1488.97
HEXADECAGONAL-B-21	1388.01	1582.71	1246.23	1543.39	1246.23	1582.71	1246.23

Table B.8: FE Results and Code Suggested Resistances of Hexadecagonal Non-compact Sections Subjected to Pure Bending

Specimen	M_{FEM} (KN-m)	M_p (KN-m)	M_y (KN-m)	M_{AASHTO} (KN-m)	M_{ASCE} (KN-m)	M_{Euro} (KN-m)	M_{EN} (KN-m)
HEXADECAGONAL-B-N-1	869.39	1011.1	796.14	821.41	796.14	1011.1	796.14
HEXADECAGONAL-B-N-2	844.06	988.9	778.66	802.25	778.66	988.9	778.66
HEXADECAGONAL-B-N-3	792.7	944.78	743.92	764.32	743.92	944.78	743.92
HEXADECAGONAL-B-N-4	755.98	911.95	718.07	731.24	718.07	911.95	718.07
HEXADECAGONAL-B-N-5	585.11	746.11	587.49	544.66	541.61	560.56	560.56
HEXADECAGONAL-B-N-6	532.71	695.35	547.52	489.53	486.58	507.37	507.37
HEXADECAGONAL-B-N-7	607.47	762.81	600.63	562.80	559.71	600.63	578.61
HEXADECAGONAL-B-N-8	620.16	774.35	609.73	575.34	572.23	609.73	590.16
HEXADECAGONAL-B-N-9	699.58	858.81	676.23	667.12	663.83	858.81	676.23
HEXADECAGONAL-B-N-10	644.6	804.8	633.7	608.43	605.26	633.7	633.7
HEXADECAGONAL-B-N-11	1233.71	1446.02	1138.6	1171.60	1138.6	1446.02	1138.6
HEXADECAGONAL-B-N-12	1182.17	1385.74	1091.14	1119.86	1091.14	1385.74	1091.14
HEXADECAGONAL-B-N-13	1124.46	1349.81	1062.84	1069.59	1062.84	1349.81	1062.84
HEXADECAGONAL-B-N-14	1098.35	1317.46	1037.37	1034.41	1029.43	1317.46	1037.37
HEXADECAGONAL-B-N-15	1014.15	1249.81	984.1	960.88	956.04	984.1	984.1

Table B.9: FE Results and Code Suggested Bending Resistances of Octagonal Compact Sections Subjected to Combined Bending and Compression

Specimen	P_u/P_y	M_{FEM} (COMB) (KN-m)	M_{AASHTO} (COMB) (KN-m)	M_{ASCE} (COMB) (KN-m)	M_{Euro} (COMB) (KN-m)	M_{EN} (COMB) (KN-m)
OCTAGONAL-COMB-1	0.2	203.60	177.75	141.20	175.09	141.20
	0.3	187.10	153.91	123.55	153.21	123.55
	0.45	155.39	118.67	97.08	120.38	97.08
OCTAGONAL-COMB-2	0.2	180.89	159.10	126.46	156.81	126.46
	0.3	165.13	137.72	110.65	137.21	110.65
	0.45	136.30	106.12	86.94	107.81	86.94
OCTAGONAL-COMB-3	0.2	159.26	141.35	112.42	139.40	112.42
	0.3	144.95	122.31	98.36	121.97	98.36
	0.45	118.52	94.19	77.29	95.83	77.29
OCTAGONAL-COMB-4	0.2	138.07	124.48	99.06	122.83	99.06
	0.3	125.36	107.67	86.68	107.48	86.68
	0.45	99.79	82.86	68.10	84.45	68.10

Table B.9: (Cont.) FE Results and Code Suggested Bending Resistances of Octagonal Compact Sections Subjected to Combined Bending and Compression

Specimen	P_u/P_y	M_{FEM} (COMB) (KN-m)	M_{AASHTO} (COMB) (KN-m)	M_{ASCE} (COMB) (KN-m)	M_{Euro} (COMB) (KN-m)	M_{EN} (COMB) (KN-m)
OCTAGONAL-COMB-5	0.2	121.44	111.6	88.86	110.18	88.86
	0.3	110.4	96.51	77.75	96.41	77.75
	0.45	87.24	74.23	61.09	75.75	61.09
OCTAGONAL-COMB-6	0.2	95.63	93.3	74.35	92.19	74.35
	0.3	83.55	80.64	65.05	80.66	65.05
	0.45	68.6	61.97	51.11	63.38	51.11
OCTAGONAL-COMB-7	0.2	1398.17	1089.52	857.79	1063.65	857.79
	0.3	1307.35	948.34	750.56	930.7	750.56
	0.45	1139.82	738.12	589.73	731.26	589.73
OCTAGONAL-COMB-8	0.2	722.68	578.06	456.43	565.97	456.43
	0.3	672.28	502.31	399.37	495.22	399.37
	0.45	578.34	389.78	313.79	389.11	313.79
OCTAGONAL-COMB-9	0.2	404.01	335.02	265.26	328.93	265.26
	0.3	373.74	290.65	232.11	287.81	232.11
	0.45	316.17	224.88	182.37	226.14	182.37
OCTAGONAL-COMB-10	0.2	337.34	285.13	225.95	280.17	225.95
	0.3	311.24	247.24	197.7	245.15	197.7
	0.45	263.08	191.12	155.34	192.62	155.34
OCTAGONAL-COMB-11	0.2	253.03	217.82	172.85	214.34	172.85
	0.3	233.6	188.72	151.24	187.54	151.24
	0.45	195.11	145.67	118.84	147.36	118.84
OCTAGONAL-COMB-12	0.2	86.31	84.88	67.66	83.9	67.66
	0.3	75.98	73.35	59.21	73.42	59.21
	0.45	59.76	56.34	46.52	57.68	46.52
OCTAGONAL-COMB-13	0.2	115.34	106.91	85.14	105.58	85.14
	0.3	103.27	92.44	74.5	92.38	74.5
	0.45	82.36	71.09	58.54	72.58	58.54
OCTAGONAL-COMB-14	0.2	104.57	98.36	78.36	97.17	78.36
	0.3	93.63	85.03	68.57	85.02	68.57
	0.45	73.83	65.36	53.87	66.8	53.87

Table B.10: FE Results and Code Suggested Bending Resistances of Octagonal Non-compact Sections Subjected to Combined Bending and Compression

Specimen	P_u/P_y	M_{FEM} (COMB) (KN-m)	M_{AASHTO} (COMB) (KN-m)	M_{ASCE} (COMB) (KN-m)	M_{Euro} (COMB) (KN-m)	M_{EN} (COMB) (KN-m)
OCTAGONAL-COMB-N-1	0.2	76.75	70.19	62.96	78.07	62.96
	0.3	67.45	60.64	55.09	68.31	55.09
	0.45	52.57	46.56	43.28	53.67	43.28
OCTAGONAL-COMB-N-2	0.2	68.44	64.84	58.58	72.64	58.58
	0.3	60.5	56.01	51.26	63.56	51.26
	0.45	46.08	43.00	40.27	49.94	40.27
OCTAGONAL-COMB-N-3	0.2	56.91	57.15	52.2	64.73	49.72
	0.3	49.22	49.35	45.67	56.64	42.7
	0.45	38.72	37.87	35.89	44.5	32.17
OCTAGONAL-COMB-N-4	0.2	62.03	60.31	54.83	67.99	53.15
	0.3	52.93	52.09	47.98	59.49	45.93
	0.45	42.28	39.97	37.7	46.74	35.09
OCTAGONAL-COMB-N-5	0.2	51.79	53.45	49.09	60.87	45.61
	0.3	45.6	46.15	42.96	53.27	39
	0.45	35.53	35.40	33.75	41.85	29.09
OCTAGONAL-COMB-N-6	0.2	48.42	50.19	46.19	46.34	41.84
	0.3	42.01	43.34	40.39	40.55	35.53
	0.45	32.79	33.24	31.7	31.86	26.05
OCTAGONAL-COMB-N-7	0.2	47.57	47.80	45.16	45.63	40.87
	0.3	41.03	40.29	39.45	39.93	34.61
	0.45	32.33	29.24	30.9	31.37	25.23
OCTAGONAL-COMB-N-8	0.2	41.68	41.55	39.21	35.49	35.49
	0.3	35.48	34.60	34.03	29.73	29.73
	0.45	27.49	24.37	26.24	21.1	21.1

Table B.11: FE Results and Code Suggested Bending Resistances of Dodecagonal Compact Sections Subjected to Combined Bending and Compression

Specimen	P_u/P_y	M_{FEM} (COMB) (KN-m)	M_{AASHTO} (COMB) (KN-m)	M_{ASCE} (COMB) (KN-m)	M_{Euro} (COMB) (KN-m)	M_{EN} (COMB) (KN-m)
DODECAGONAL-COMB-1	0.2	369.55	338.03	251.74	317.19	251.74
	0.3	341.96	293.16	220.27	277.54	220.27
	0.45	284.18	226.68	173.07	218.07	173.07
DODECAGONAL-COMB-2	0.2	330.76	305.16	227.34	286.45	227.34
	0.3	305.57	264.6	198.92	250.64	198.92
	0.45	252.39	204.52	156.3	196.93	156.3
DODECAGONAL-COMB-3	0.2	293.08	273.51	203.83	256.82	203.83
	0.3	269.25	237.11	178.35	224.72	178.35
	0.45	218.71	183.2	140.13	176.57	140.13
DODECAGONAL-COMB-4	0.2	255.48	243.05	181.19	228.3	181.19
	0.3	234.09	210.65	158.54	199.77	158.54
	0.45	185.43	162.7	124.57	156.96	124.57
DODECAGONAL-COMB-5	0.2	225.94	219.53	163.71	206.27	163.71
	0.3	204.51	190.23	143.24	180.49	143.24
	0.45	162.9	146.88	112.55	141.81	112.55
DODECAGONAL-COMB-6	0.2	165.97	174.7	130.36	164.26	130.36
	0.3	144.48	151.34	114.07	143.73	114.07
	0.45	116.02	116.77	89.62	112.93	89.62
DODECAGONAL-COMB-7	0.2	2099.57	1752.89	1297.3	1634.6	1297.3
	0.3	1967.14	1525.72	1135.14	1430.28	1135.14
	0.45	1707.95	1187.46	891.9	1123.79	891.9
DODECAGONAL-COMB-8	0.2	1283.65	1100.69	816.06	1028.23	816.06
	0.3	1197.01	957.06	714.05	899.7	714.05
	0.45	1028.13	743.5	561.04	706.91	561.04
DODECAGONAL-COMB-9	0.2	675.84	603.68	448.62	565.26	448.62
	0.3	627.93	524.19	392.54	494.6	392.54
	0.45	529.87	406.22	308.42	388.61	308.42
DODECAGONAL-COMB-10	0.2	493.43	444.11	330.42	416.33	330.42
	0.3	457.14	385.38	289.11	364.28	289.11
	0.45	386	298.29	227.16	286.22	227.16

Table B.11: (Cont.) FE Results and Code Suggested Bending Resistances of Dodecagonal Compact Sections Subjected to Combined Bending and Compression

Specimen	P_u/P_y	M_{FEM} (COMB) (KN-m)	M_{AASHTO} (COMB) (KN-m)	M_{ASCE} (COMB) (KN-m)	M_{Euro} (COMB) (KN-m)	M_{EN} (COMB) (KN-m)
DODECAGONAL-COMB-11	0.2	410.19	372.14	277.04	349.07	277.04
	0.3	380.02	322.8	242.41	305.44	242.41
	0.45	317.8	249.68	190.47	239.99	190.47
DODECAGONAL-COMB-12	0.2	180.73	185.63	138.5	174.51	138.5
	0.3	159.54	160.82	121.19	152.69	121.19
	0.45	127.18	124.11	95.22	119.97	95.22
DODECAGONAL-COMB-13	0.2	144.73	159.91	119.35	150.39	119.35
	0.3	126.87	138.51	104.44	131.59	104.44
	0.45	98.56	106.84	82.06	103.39	82.06
DODECAGONAL-COMB-14	0.2	205	203.39	151.71	191.15	151.71
	0.3	183.31	176.23	132.74	167.26	132.74
	0.45	146.57	136.04	104.3	131.42	104.3

Table B.12: FE Results and Code Suggested Bending Resistances of Dodecagonal Non-compact Sections Subjected to Combined Bending and Compression

Specimen	P_u/P_y	M_{FEM} (COMB) (KN-m)	M_{AASHTO} (COMB) (KN-m)	M_{ASCE} (COMB) (KN-m)	M_{Euro} (COMB) (KN-m)	M_{EN} (COMB) (KN-m)
DODECAGONAL-COMB-N-1	0.2	124.66	123.52	108.67	136.93	108.67
	0.3	109.72	106.97	95.09	119.81	95.09
	0.45	86.41	82.50	74.71	94.14	74.71
DODECAGONAL-COMB-N-2	0.2	108.1	111.92	99.14	124.92	99.14
	0.3	93.7	96.91	86.75	109.3	86.75
	0.45	74.26	74.72	68.16	85.88	68.16
DODECAGONAL-COMB-N-3	0.2	97.78	101.77	91.66	115.49	85.9
	0.3	84.38	88.12	80.2	101.06	73.93
	0.45	63.57	67.93	63.02	79.4	55.97
DODECAGONAL-COMB-N-4	0.2	136.44	130.18	114.1	143.77	114.1
	0.3	120.09	112.75	99.84	125.8	99.84
	0.45	94.16	86.96	78.44	98.84	78.44
DODECAGONAL-COMB-N-5	0.2	118.38	119.30	105.22	132.58	105.22
	0.3	103.65	103.31	92.07	116	92.07
	0.45	82.39	79.67	72.34	91.15	72.34

Table B.12: (Cont.) FE Results and Code Suggested Bending Resistances of Dodecagonal Non-compact Sections Subjected to Combined Bending and Compression

Specimen	P_u/P_y	M_{FEM} (COMB) (KN-m)	M_{AASHTO} (COMB) (KN-m)	M_{ASCE} (COMB) (KN-m)	M_{Euro} (COMB) (KN-m)	M_{EN} (COMB) (KN-m)
DODECAGONAL-COMB-N-6	0.2	101.09	106.03	94.26	118.77	90.95
	0.3	87.95	91.81	82.48	103.93	78.59
	0.45	68.63	70.78	64.81	81.66	60.05
DODECAGONAL-COMB-N-7	0.2	92.2	96.16	87.31	88.75	82.31
	0.3	80.52	82.56	76.22	77.65	70.53
	0.45	62.95	62.45	59.58	61.01	52.88
DODECAGONAL-COMB-N-8	0.2	87.22	90.55	82.33	85.42	78.61
	0.3	77.85	77.41	71.65	74.74	67.21
	0.45	60.2	57.98	55.64	58.73	50.13

Table B.13**:** FE Results and Code Suggested Bending Resistances of Hexadecagonal Compact Sections Subjected to Combined Bending and Compression

Specimen	P_u/P_y	$M_{FEM\ (COMB)}$ (KN-m)	M_{AASHTO} (COMB) (KN-m)	M_{ASCE} (COMB) (KN-m)	M_{Euro} (COMB) (KN-m)	M_{EN} (COMB) (KN-m)
HEXADECAGONAL-COMB-1	0.2	1468.61	1473.88	1069.85	1358.71	1069.85
	0.3	1319.3	1281.3	936.12	1188.87	936.12
	0.45	1088.62	995.03	735.52	934.11	735.52
HEXADECAGONAL-COMB-2	0.2	1336.75	1365.6	991.38	1259.06	991.38
	0.3	1196.38	1187.07	867.46	1101.68	867.46
	0.45	966.66	921.73	681.58	865.6	681.58
HEXADECAGONAL-COMB-3	0.2	1195.29	1259.56	914.53	1161.45	914.53
	0.3	1052.43	1094.81	800.21	1016.27	800.21
	0.45	852.8	849.97	628.74	798.5	628.74
HEXADECAGONAL-COMB-4	0.2	1071.33	1155.74	839.27	1065.87	839.27
	0.3	943.97	1004.5	734.36	932.63	734.36
	0.45	754.91	779.74	577	732.78	577
HEXADECAGONAL-COMB-5	0.2	814.24	954.71	693.48	880.72	693.48
	0.3	715.24	829.64	606.79	770.63	606.79
	0.45	565.52	643.82	476.77	605.49	476.77

Table B.13: (Cont.) FE Results and Code Suggested Bending Resistances of Hexadecagonal Compact Sections Subjected to Combined Bending and Compression

Specimen	P_u/P_y	$M_{FEM\ (COMB)}$ (KN-m)	M_{AASHTO} (COMB) (KN-m)	M_{ASCE} (COMB) (KN-m)	M_{Euro} (COMB) (KN-m)	M_{EN} (COMB) (KN-m)
HEXADECAGONAL-COMB-6	0.2	937.73	1054.14	765.59	972.3	765.59
	0.3	825.28	916.11	669.89	850.76	669.89
	0.45	659.78	711.03	526.34	668.45	526.34
HEXADECAGONAL-COMB-7	0.2	10147.15	8744.21	6321.04	8027.73	6321.04
	0.3	9526.65	7619.84	5530.91	7024.26	5530.91
	0.45	8290.17	5943	4345.72	5519.06	4345.72
HEXADECAGONAL-COMB-8	0.2	6713.66	5970.49	4320.19	5486.64	4320.19
	0.3	6286.64	5199.84	3780.16	4800.81	3780.16
	0.45	5407.49	4051.43	2970.13	3772.06	2970.13
HEXADECAGONAL-COMB-9	0.2	3122.46	2955.05	2141.94	2720.26	2141.94
	0.3	2869.23	2571.05	1874.2	2380.23	1874.2
	0.45	2350.56	1999.61	1472.58	1870.18	1472.58
HEXADECAGONAL-COMB-10	0.2	4143.81	3827.92	2772.93	3521.62	2772.93
	0.3	3847.43	3331.68	2426.31	3081.42	2426.31
	0.45	3228.98	2592.84	1906.39	2421.11	1906.39
HEXADECAGONAL-COMB-11	0.2	2207.25	2171.72	1575.22	2000.53	1575.22
	0.3	2019.01	1888.77	1378.31	1750.46	1378.31
	0.45	1603.22	1467.94	1082.96	1375.36	1082.96
HEXADECAGONAL-COMB-12	0.2	740.58	896.1	650.96	826.72	650.96
	0.3	652.52	778.66	569.59	723.38	569.59
	0.45	516.38	604.21	447.54	568.37	447.54
HEXADECAGONAL-COMB-13	0.2	1823.08	1812.37	1315.05	1670.11	1315.05
	0.3	1657.92	1575.91	1150.67	1461.35	1150.67
	0.45	1320.47	1224.31	904.09	1148.2	904.09
HEXADECAGONAL-COMB-14	0.2	2718.25	2612.74	1894.35	2405.82	1894.35
	0.3	2496.18	2272.86	1657.56	2105.1	1657.56
	0.45	2027.28	1767.18	1302.37	1654	1302.37
HEXADECAGONAL-COMB-15	0.2	1648.67	1640.55	1190.6	1512.06	1190.6
	0.3	1483.45	1426.35	1041.78	1323.05	1041.78
	0.45	1203.9	1107.9	818.54	1039.54	818.54
HEXADECAGONAL-COMB-16	0.2	23313.72	18170.16	13111.48	16651.58	13111.48
	0.3	22074.93	15850.06	11472.54	14570.13	11472.54
	0.45	19704.16	12385.03	9014.14	11447.96	9014.14

Table B.14: FE Results and Code Suggested Bending Resistances of Hexadecagonal Non-compact Sections Subjected to Combined Bending and Compression

Specimen	P_u/P_y	M_{FEM} (COMB) (KN-m)	M_{AASHTO} (COMB) (KN-m)	M_{ASCE} (COMB) (KN-m)	M_{Euro} (COMB) (KN-m)	M_{EN} (COMB) (KN-m)
HEXADECAGONAL-COMB-N-1	0.2	719.35	730.41	636.91	808.88	636.91
	0.3	633.06	634.67	557.3	707.77	557.3
	0.45	499.88	492.46	437.88	556.1	437.88
HEXADECAGONAL-COMB-N-2	0.2	694.57	713.35	622.93	791.12	622.93
	0.3	607.77	619.84	545.06	692.23	545.06
	0.45	481.09	480.94	428.26	543.89	428.26
HEXADECAGONAL-COMB-N-3	0.2	647.94	679.57	595.14	755.82	595.14
	0.3	567.75	590.47	520.75	661.35	520.75
	0.45	433.97	458.12	409.16	519.63	409.16
HEXADECAGONAL-COMB-N-4	0.2	615.51	650.14	574.46	729.56	574.46
	0.3	539.31	564.88	502.65	638.37	502.65
	0.45	414.99	438.25	394.94	501.57	394.94
HEXADECAGONAL-COMB-N-5	0.2	565.7	597.02	528.59	687.05	540.98
	0.3	495.39	521.16	460.97	601.17	473.36
	0.45	392.97	408.50	359.53	472.34	371.92
HEXADECAGONAL-COMB-N-6	0.2	516.44	539.62	478.52	506.96	485.11
	0.3	456.32	468.04	415.15	443.59	416.63
	0.45	352.51	361.73	320.09	348.54	313.9

Table B.15: FE Results and Code Suggested Torsional Moments of Octagonal Compact Sections Subjected to Pure Torsion

Specimen	T_{FEM} (KN-m)	T_{AASHTO} (KN-m)	T_{ASCE} (KN-m)
OCTAGONAL-TOR-1	197.55	190.66	189.91
OCTAGONAL-TOR-2	175.16	170.30	170.31
OCTAGONAL-TOR-3	154.79	150.97	151.60
OCTAGONAL-TOR-4	135.75	132.84	133.78
OCTAGONAL-TOR-5	121.07	119.71	120.14
OCTAGONAL-TOR-6	100.61	100.86	100.70
OCTAGONAL-TOR-7	90.91	92.10	91.74

Table B.16: FE Results and Code Suggested Torsional Moments of Octagonal Non-compact Sections Subjected to Pure Torsion

Specimen	T_{FEM} (KN-m)	T_{AASHTO} (KN-m)	T_{ASCE} (KN-m)
OCTAGONAL-TOR-N-1	84.72	85.91	85.42
OCTAGONAL-TOR-N-2	78.63	80.12	79.53
OCTAGONAL-TOR-N-3	69.71	71.64	70.93
OCTAGONAL-TOR-N-4	61.74	63.95	63.17

Table B.17: FE Results and Code Suggested Torsional Moments of Dodecagonal Compact Sections Subjected to Pure Torsion

Specimen	T_{FEM} (KN-m)	T_{AASHTO} (KN-m)	T_{ASCE} (KN-m)
DODECAGONAL-TOR-1	353.91	346.66	351.22
DODECAGONAL-TOR-2	318.57	312.42	317.51
DODECAGONAL-TOR-3	284.77	279.53	284.97
DODECAGONAL-TOR-4	252.56	248.31	253.60
DODECAGONAL-TOR-5	227.60	225.51	229.33
DODECAGONAL-TOR-6	180.19	181.46	182.95
DODECAGONAL-TOR-7	164.61	166.75	167.61

Table B.18: FE Results and Code Suggested Torsional Moments of Dodecagonal Non-compact Sections Subjected to Pure Torsion

Specimen	T_{FEM} (KN-m)	T_{AASHTO} (KN-m)	T_{ASCE} (KN-m)
DODECAGONAL-TOR-N-1	156.82	159.69	160.28
DODECAGONAL-TOR-N-2	148.64	152.38	152.71
DODECAGONAL-TOR-N-3	134.79	139.48	139.40
DODECAGONAL-TOR-N-4	123.27	129.30	128.95

Table B.19: FE Results and Code Suggested Torsional Moments of Hexadecagonal Compact Sections Subjected to Pure Torsion

Specimen	T_{FEM} (KN-m)	T_{AASHTO} (KN-m)	T_{ASCE} (KN-m)
HEXADECAGONAL-TOR-1	1499.93	1475.69	1518.63
HEXADECAGONAL-TOR-2	1379.23	1365.92	1408.06
HEXADECAGONAL-TOR-3	1267.38	1258.59	1299.67
HEXADECAGONAL-TOR-4	1153.53	1153.68	1193.42
HEXADECAGONAL-TOR-5	929.07	951.05	987.32
HEXADECAGONAL-TOR-6	1035.50	1051.17	1089.31
HEXADECAGONAL-TOR-7	1852.77	1819.93	1863.49

Table B.20: FE Results and Code Suggested Torsional Moments of Hexadecagonal Non-compact Sections Subjected to Pure Torsion

Specimen	T_{FEM} (KN-m)	T_{AASHTO} (KN-m)	T_{ASCE} (KN-m)
HEXADECAGONAL-TOR-N-1	857.24	892.10	927.13
HEXADECAGONAL-TOR-N-2	804.74	854.44	887.42
HEXADECAGONAL-TOR-N-3	748.46	818.73	848.04
HEXADECAGONAL-TOR-N-4	699.03	792.03	818.73